DISSERTATION
submitted to the
Combined Faculties for the Natural Sciences and for Mathematics
of the Ruprecht-Karls-Universität Heidelberg, Germany
for the degree of
Doctor of Natural Sciences

presented by
M.Sc. Biology Gönül Simge Yüz
born in Antalya, Turkey
oral examination: 28.02.2018

Re-programming cell interactions with light dependent heterodimers

Referees: Prof. Dr. Ulrich Schwarz
Prof. Dr. Joachim P. Spatz

Re-programming cell interactions with light dependent heterodimers

Referees: Prof. Dr. Ulrich Schwarz
Prof. Dr. Joachim P. Spatz

Acknowledgements

I would like to thank Prof. Dr. Joachim P. Spatz for taking me as a PhD student in his research group and for his support, feedback and scientific discussions during these three years. I thank to Dr. Seraphine V. Wegner for her supervision and scientific discussions in this project. I want to thank to whole Spatz and Wegner groups for all the fun and scientific discussions.

The scientific discussions and feedbacks I got in my annual thesis advisory committee meetings were invaluable for me. I appreciate the input and support enormously and would like to thank to Prof. Dr. Ulrich Schwarz, Prof. Dr. Friedrich Frischknecht and Prof. Dr. Barbara Di Ventura for this.

A special thanks goes to Dr. Ada E. Cavalcanti-Adam for hosting me in her labs and to Dr. Rebecca Medda for scientific discussions, technical support and all the laughing. I would like to thank to Dr. Medhavi Wishwakarma for training me in traction force microscopy. I also would like to thank Stephan Schuhmacher for drawing the schematic pictures.

I want to thank to Julia Ricken for her co-operative work, scientific discussions, her support and for sharing all bad and good days we had together. I also thank to Saliha Erikci, Paulina Wysmolek, Siti Adam and Intango Family for making me laugh and calm especially during the non-working phase of the experiments.

Above all I thank to my mother Sıdıka Yüz and my father Asım Yüz, and also to Cemil Kadan, Nazik Kadan, Gül Kadan and Murat Kadan for always supporting and encouraging me.

Thank you!

Abstract

Cells interact with neighboring cells and the extracellular matrix forming cell-cell and cell-matrix contacts, which are mainly mediated by cadherins and integrins, respectively. These processes are dynamic and spatially and temporally tightly regulated during many biological events including embryogenesis, wound healing and cancer development. Dynamic control of cell interactions is a key to understanding many underlying cellular processes, to achieving the bottom-up assembly of single cells into tissues and to developing medical implants. The challenge lies in controlling specific cell-cell and cell-material interactions both dynamically and reversibly with high spatiotemporal control in a non-invasive way over a long period of time. The aim of this thesis is to generate platforms where these cell interactions are controlled spatially, temporally, dynamically and reversibly using visible light responsive proteins from plants.

The recent developments in the field of optogenetics provide powerful tools to overcome above-mentioned challenges and they have been employed to control many intracellular signaling pathways. Among others cryptochromes and phytochromes were used in this study. Cryptochrome 2 (CRY2) is a blue light photoreceptor and it heterodimerizes with CIBN upon blue light irradiation. This interaction can be reversed to the ground state passively in the dark. Phytochrome B (PhyB) is a red and far-red light sensing protein and upon red light illuminations it interacts and forms heterodimers with PIF6. This heterodimerization can be reversed under far-red light or passively in the dark.

To control cell-cell interactions with light, the blue light dependent heterodimers, CRY2 or CIBN were expressed on the surfaces of the cells, which do not form any native cell-cell contacts. In equally mixed cultures of CRY2 and CIBN expressing cells, these cells form cell-cell interactions upon blue light illumination, which provides high high spatial and temporal control. These photoswitchable interactions are reversible in the dark, and can be repeatedly and dynamically switched on and off. These genetically encoded interactions can be sustained over a long time as they are

genetically encoded and they respond to nontoxic low intensity blue light.

Towards controlling cell-material contacts of multiple cell types, one of the heterodimerization partners (CIBN or PIF6) was immobilized on non-adhesive glass surfaces. By expressing CRY2 or PhyB on the cell surfaces, their adhesion to CIBN and PIF6 functionalized substrates can be triggered under nontoxic low intensity blue and red light illumination, respectively. CRY2/CIBN and PhyB/PIF6 interactions are orthogonal to each other since they respond to only blue and red/far-red light, respectively. This orthogonality provides wavelength selective adhesion of one cell type to its complementary substrate in the presence of the other cell type. The ability of PhyB/PIF6 system to far-red light also makes orthogonal reversion of these adhesions possible while the other cell type (CRY2) remains adhered to its substrate. These photoswitchable cell-material interactions are reversible in the dark or under far-red light, and can be repeatedly and dynamically switched on and off.

Overall, this optogenetic approach to control cell interactions reflects the dynamic and reversible nature of cell-cell and cell-material interactions and provides the desired spatiotemporal control in a noninvasive manner. These blue and red/far-red light responsive proteins are genetically encodable; hence, they can be sustained over a long time. Finally, photoswitchable cell interactions will provide a new way of studying them and assembling cells into multicellular structures in the context of bottom-up tissue engineering.

Zusammenfassung

Zellen interagieren mit benachbarten Zellen und der extrazelluläre Matrix in dem sie Zell-Zell- und Zell-Matrix-Kontakte bilden, welche hauptsächlich durch Cadherine oder Integrine vermittelt werden. Diese Prozesse sind dynamisch und sowohl räumlich als auch zeitlich während vieler biologischer Ereignisse einschließlich Embryogenese, Wundheilung und der Entwicklung von Krebs. Die dynamische Kontrolle von Zellinteraktionen ist ein Schlüssel zum Verständnis vieler zugrundeliegender zellulärer Prozesse, zur Herstellung der Bottom-up-Anordnung einzelner Zellen in Gewebe und zur Entwicklung medizinischer Implantate. Die Herausforderung besteht darin, spezifische Zell-Zell- und Zell-Material-Interaktionen sowohl dynamisch als auch reversibel mit hoher raumzeitlicher Kontrolle auf nichtinvasive Weise über einen langen Zeitraum hinweg zu steuern. Das Ziel dieser Arbeit ist es, Plattformen zu konzipieren, in denen diese Zellinteraktionen räumlich, zeitlich, dynamisch und reversibel unter Verwendung von auf sichtbares Licht reagierenden Proteinen aus Pflanzen gesteuert werden.

Die jüngsten Entwicklungen auf dem Gebiet der Optogenetik bieten leistungsfähige Komponenten, welche bereits zur Kontrolle von intrazellulären Signalwegen angewedet wurden, um die oben genannten Herausforderungen zu überwinden. In dieser Studie wurden unter anderem Cryptochrome und Phytochrome verwendet. Cryptochrom 2 (CRY2) ist ein Blaulicht-Photorezeptor und heterodimerisiert mit CIBN unter blauem Licht. Diese Wechselwirkung kehrt im Dunkeln passiv in den Grundzustand zurück. Phytochrom B (PhyB) ist ein rotes und infrarotes Licht sensitives Protein und bildet unter Bestrahlung Heterodimere mit PIF6. Diese Heterodimerisierung kann unter infrarotem Licht oder passiv im Dunkeln umgekehrt werden.

Um die Zell-Zell-Wechselwirkungen mit Licht zu steuern, wurden die Blaulicht-abhängigen Heterodimere CRY2 oder CIBN auf den Oberflächen der Zellen exprimiert, die keine nativen Zell-Zell-Kontakte bilden. In gleichermaßen gemischten Kulturen von CRY2- und CIBN-exprimierenden Zellen bilden diese Zellen bei der Beleuchtung mit blauem Licht Zell-Zell Kontakte. Diese photoschaltbaren

Wechselwirkungen sind im Dunkeln reversibel und können mehrmals und dynamisch ein- und ausgeschaltet werden. Durch die genetische kodierung der vermittelnden Proteine, können die Interaktionen über eine lange Zeit aufrechterhalten werden, da sie zudem auf nichttoxisches blaues Licht mit niedriger Intensität reagieren.

Zur Steuerung von Zell-Material-Kontakten mehrerer Zelltypen, wurde einer der jeweiligen Heterodimerisierungspartner (CIBN oder PIF6) auf nicht-adhäsiven Glasoberflächen immobilisiert. Durch die Expression von CRY2 oder PhyB auf den Zelloberflächen kann deren Adhäsion an CIBN- und PIF6-funktionalisierte Substrate unter nichttoxischer Beleuchtung mit niedriger Intensität von blauem bzw. rotem Licht ausgelöst werden. CRY2 / CIBN- und PhyB / PIF6-Wechselwirkungen sind orthogonal zueinander, da sie nur auf blaues bzw. rotes bzw. infrarotes Licht ansprechen. Diese Orthogonalität sbefähigt zu eine wellenlängenselektive Adhäsion eines Zelltyps an sein komplementäres Substrat in Gegenwart des anderen Zelltyp. Die Fähigkeit des PhyB / PIF6-Systems zu weit rotem Licht macht auch eine orthogonale Reversion dieser Adhäsionen möglich, während der andere Zelltyp (CRY2) an seinem Substrat haften bleibt.Diese photoschaltbaren Zell-Material-Wechselwirkungen sind im Dunkeln oder im fernen Rotlicht reversibel und können wiederholt und dynamisch ein- und ausgeschaltet werden.

Insgesamt spiegelt dieser optogenetische Ansatz zur Kontrolle von Zellinteraktionen die dynamische und reversible Natur der Zell-Zell- und Zell-Material-Wechselwirkungen wider und liefert die gewünschte raumzeitliche Kontrolle auf nichtinvasive Weise. Die verwendeten blau und rot / weit-rot lichtempfindlichen Proteine sind genetisch codierbar; Daher können die durch sie vermittelten Interaktionen über eine lange Zeit aufrechterhalten werden. Schließlich werden photoschaltbare Zellinteraktionen eine neue Möglichkeit bieten, diese zu studieren und Zellen im Rahmen des Bottom-Up-Tissue Engineering zu mehrzelligen Strukturen zusammenzufügen.

List of abbreviations

A	absorbance
APC	adenomatous polyposis coli
BSA	bovine serum albumin
CAMs	cell adhesion molecules
cAMP	cyclic adenosine monophosphate
Cas9	CRISPR-associated protein 9
CCE	cryptochrome C-terminal extension domain
CFP	cyan fluorescent protein
CIBN	N-truncated Cry-interacting basic helix-loop-helix protein 1
CKI	casein kinase 1
COP1	constitutive photomorphogenesis protein1
Cph1	cyanobacterial phytochrome 1
CRISPR	clustered regularly interspaced short palindromic repeats
CRY2	cryptochrome 2
CSANs	chemically self-assembled nanorings
Da	dalton
DAH	differential adhesion hypothesis
DAPI	4',6-diamidino-2-phenylindole
DHFR	dihydrofolate reductase
DH-PH	Dbl homology-pleckstrin
DiI	1,1’-dioctadecyl-3,3,3’,3’- tetramethylindocarbocyanin perchlorate
DiO	3,3’-dioctadecyloxacarbocyanine perchlorate
DITH	differential interfacial tension hypothesis
DMEM	Dulbecco's Modified Eagle Medium
DMSO	dimethylsulfoxide
DNA	deoxyribonucleic acid
dNTP	deoxynucleoside triphosphates

DpnI	deoxyribonuclease I
DTT	dithiothreitol
EC	extracellular
E. coli	*Escherichia coli*
ECM	extracellular matrix
EDTA	ethylenediaminetetraacetic acid
EGF	epidermal growth factor
EMT	epithelial to mesenchymal transition
ERK	extracellular signal regulated kinase
FAD	flavine adenine dinucleoide
FAK	focal adhesion kinase
FBS	fetal bovine serum
FDA	Food and Drug Administration
FGF	fibroblast growth factor
FGFR	fibroblast growth factor receptor
FITC	fluorescein isothiocyanate
FKF	Kelch repeat F-box protein
FMN	flavin mononucleotide
FRET	Förster resonance energy transfer
GEF	Guanosine nucleotide exchange factor
GFP	green fluorescent protein
GSK3β	glycogen synthase 3β
GTP	guanosine triphosphate
HEK	human embryonic kidney
His_6	histidine tag
HPLC	high performance liquid chromatography
Hz	Hertz
Ig	immunoglobulin
ILK	integrin linked kinase
IPTG	isopropyl β-D-1-thiogalactopyranoside
LACE	light activated CRISPR-Cas9 effector
LB medium	Luria-Bertani medium

LEF	lymphoid enhancer factor
LOV	light-oxygen-voltage
LRP6	lipoprotein receptor related protein 6
MAPK	mitogen activated protein kinase
MET	mesenchymal to epithelial transition
MOPS	3-(N-morpholino)propanesulfonic acid
MTX	methotrexate
MTT	3-(4,5-Dimethylthiazol-2-yl)-2,5-Diphenyltetrazolium Bromide
NIR	near infrared
NTA	nitrilotriacetic acid
PAS	Per-ARNT-Sim domain
PBS	phosphate buffer saline
PCB	phycocyanobilin
PCR	polymerase chain reaction
PDGF	platelet derived growth factor
PDGFR	platelet derived growth factor receptor
PDMS	(poly)-dimethylsiloxane
PEG-N_3	polyethyleneglycol-azide
PFA	para-formaldehyde
PIF6	phytochrome interacting factor 6
PhyB	phytochrome B
PHR	photolyase region
PKB	protein kinase B
PM	plasma membrane
PMSF	phenylmethylsulfonyl fluoride
POI	protein of interest
P/S	penicillin/streptomycin
QCM-D	quartz crystal microbalance with dissipation
rpm	round per minute
RT	room temperature
RTK	receptor tyrosine kinase

SAM	self-assembled monolayers
SDS-PAGE	sodium dodecyl sulfide-polyacrylamide gel electrophoresis
ssDNA	single stranded DNA
TAE buffer	tris-acetate-EDTA buffer
TBS-T	tris buffer saline with tween 20
TCF	T cell factor
TGF	transforming growth factor
TM	transmembrane
TRIS	tris(hydroxymethyl)aminomethane
TRITC	tetramethylrhodamine
UCNPs	upconversion nanoparticles
UV	ultraviolet
Vis	visible light
VVD	vivid
YFP	yellow fluorescent protein

List of figures

List of tables

Contents

Chapter 1

Introduction

1. Introduction

1.1 Cell-cell interactions

Cadherins, a class of transmembrane glycoproteins, are calcium (Ca^{2+}) dependent cell adhesion molecules (CAMs) and they are the main mediators of cell-cell adhesions.[1-3] The classical cadherins (E-, N-, P-cadherins) consist of an N-terminal extracellular domain with five tandem repeats, a single-pass transmembrane domain and a C-terminal cytoplasmic domain **(Figure 1.1)**.[4] The extracellular domain of cadherins contains Ca^{2+}- binding pockets and the first N-terminal EC domain (EC1) is responsible for trans- interaction of cadherins of two neighboring cells.[2,4] The cytosolic domain is widely conserved in classical cadherins and interacts with cytosolic proteins, called catenins. The cadherin-catenin interaction is crucial for cadherins to interact with other cadherins on the neighboring cells and to stabilize these cadherin-cadherin interactions.[4] There are three major cytoplasmic binding partners of classical cadherins: α-catenin, β-catenin or γ-catenin and plakoglobin/p120.[2] β-catenin (and in some cases also γ-catenin) directly interacts with the cytoplasmic domain of classical cadherins, and then α-catenin binds to β-catenin. α-catenin has actin binding activity; hence, it links the cadherin/β-catenin complex to the actin cytoskeleton **(Figure 1.1)**.[2-4]

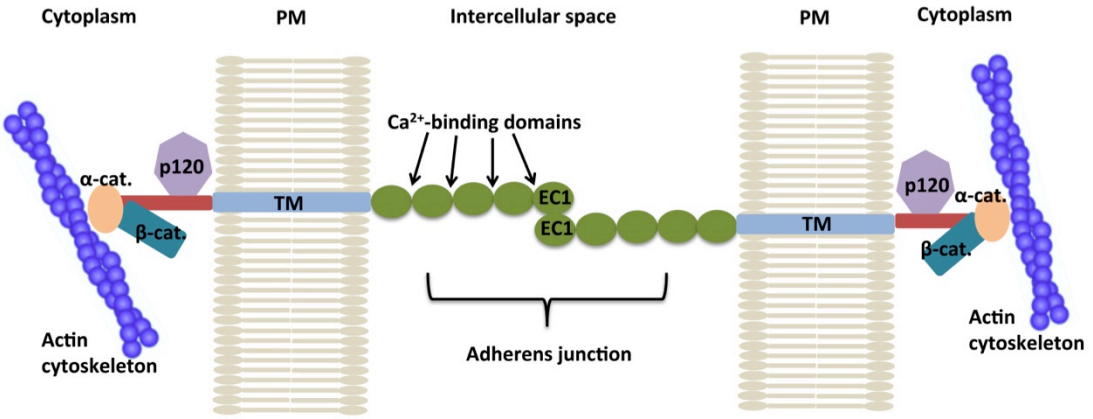

Figure 1.1 Schematic representation of homophilic cadherin interaction. Classical cadherins mediate calcium-dependent intercellular adhesion. They consist of an extracellular (EC) domain with five tandem repeats, a transmembrane (TM) domain and a cytoplasmic domain (in red). The cytoplasmic domain interacts with p120-catenin and β-catenin. β-catenin binds to α-catenin, which establishes a direct link between the cadherin-catenin complex and the actin cytoskeleton. PM: plasma membrane. Adapted from Gall *et al*.[5]

Cadherin mediated cell-cell adhesion is crucial in embryonic development and tissue organization.[4] Different cell types in a tissue express different cadherins and cadherin subtype-specific binding leads to formation and segregation of tissues during embryogenesis.[6] The spreading of the embryonic layers over each other and cell sorting was shown to be dependent on homophilic or heterophilic cadherin interactions and formulated for the first time by Malcolm Steinberg in 1963 in the Differential Adhesion Hypothesis (DAH).[6-8] The DAH states that in a population of different types of cells, the final configuration will favor minimal interfacial energy and maximum cell-cell binding strength.[6,7] Cell-cell interactions rearrange due to the repeated exchange of the weaker cohesive interactions for the stronger ones. This cell sorting behavior was shown experimentally by Duguay *et al*. with L-cells in 3D cell culture model **(Figure 1.2)**.[6] In that study, two populations of L-cells expressing the same amount of N-cadherin were mixed in equal proportions, the final configuration was a homogeneous mixture of these cells **(Figure 1.2A)**. When the N-cadherin expression was reduced to half in one of the sub-population, segregation took place; i.e, more adhesive cells (cells with high N-cadherin expression) were enveloped by the less adhesive cells (cells with low N-cadherin expression) **(Figure 1.2B)**. Finally, they showed that in a mixture of B- and R-cadherin expressing cells, two segregated assemblies were formed due to the poor interaction between those cadherins **(Figure 1.2C)**.

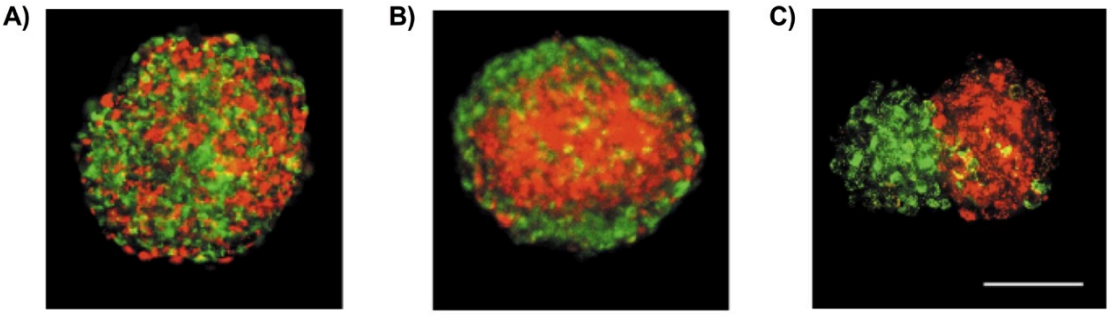

Figure 1.2 Cell sorting following DAH. Duguay *et al*.[6] showed cell sorting under equilibrium conditions of mixtures of red and green labeled cells having different number and kind of cadherins. Scale bar: 100 µm. **A)** Red and green cells express the same amount of N-cadherin; thus, they stay intermixed. **B)** Red cells express 50% more N-cadherin, which led to stronger interaction between them. Thus, they locate to the center of the assembly and are enveloped by green cells with weaker interactions. **C)**

Green cells express B-cadherin and red cells express R-cadherin. Since there is a weak interaction between these cadherins, the two cell types form two segregated assemblies.

The simplicity of DAH has provided a basis for bottom-up tissue engineering (See Section 1.3). After Steinberg's DAH, the Differential Interfacial Tension Hypothesis (DITH) was proposed, which can be regarded as both antagonist and complementary to DAH.[9-11] The DITH states that a cell's mechanical energy and the cortical tension contribute to the cell sorting, cell shape and migration during development.[9,12] The biophysics of cell sorting during development is still not fully understood and there are several experimental studies in order to understand the cohesive and mechanical forces driving this process.[12-14] For instance, Moore *et al*. used N- and E-cadherin knockout and wild type embryoid bodies from murine stem cells to understand the mechanism of cell sorting.[13] They showed that in undifferentiated state, the cells followed DAH when different cell types were mixed (for example, E-cadherin knockout and wild type cells). However, differentiated cells were sorted to the surface forming an enveloping layer (endoderm) independent of their adhesive strength; hence, they no longer followed DAH.[13] The reason for this is the apical polarity of these cells after differentiation was the determining factor in sorting and positioning.[13]

Since cadherins are linked to the actomyosin network inside the cell, it contributes to the formation and dissipation of the interfacial or cortical tension.[14-16] Borghi *et al*. has visualized the pulling forces of cells by using a cadherin-FRET sensor.[17] A later study from Ng *et al*. showed the measurement of cell-cell forces at the individual cell-cell junctions at a multicellular scale.[18] Both studies suggest that cadherins function as adhesion-dependent mechanosensors to respond both to extracellular mechanical stress and to the intracellular changes by corresponding signaling cascades, which are mediated by p120 catenin.[17-19]

p120 catenin is also an important mediator of β-catenin trafficking inside the cell. The phosphorylation of p120 catenin leads to dissociation of cadherin- α-,β- and p120 catenin complex and loss of cell-cell contacts.[20] As a result, β-catenin is released and

its cytosolic concentration increases. This cytosolic β-catenin has than two possible fates. It can be degraded by 26S proteasome consisting of the serine/threonine kinases casein kinase I (CKI), glycogen synthase 3β (GSK-3β), a scaffolding complex of protein axin and adenomatous polyposis coli (APC) protein **(Figure 1.3A)**.[20] When it is not degraded due to the presence of growth factors or the activation of the Wnt pathway, which inhibits GSK-3β activity, β-catenin is translocated into the nucleus to act as a transcription cofactor of T cell factor/lymphoid enhancer factor (TCF/LEF).[20,21] This induces the expression of Wnt target genes, which in turn induce cell migration **(Figure 1.3B)**.

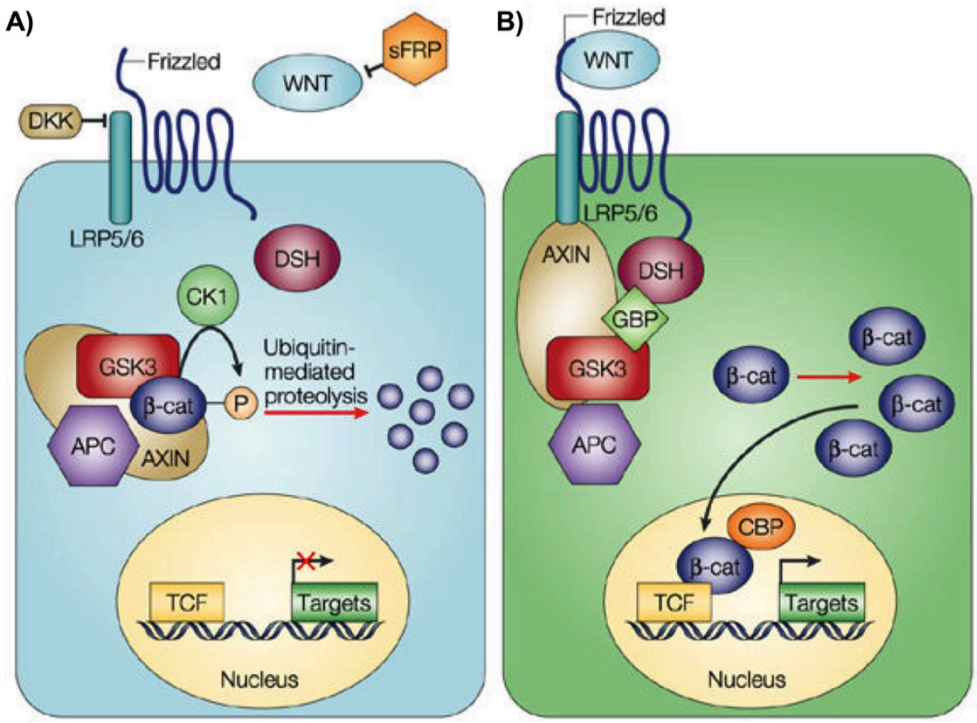

Figure 1.3 β-catenin/Wnt signaling pathway. A) In the absence of the Wnt ligand, cytosolic β-catenin is degraded by the proteasome complex; hence, the Wnt target genes are repressed. **B)** In the presence of the Wnt ligand, it binds to two receptors, frizzled proteins and lipoprotein receptor-related proteins 5 and 6 (LRP5/6). This activates another protein, disheveled (Dsh), which uncouples β-catenin from the proteasome complex. Then, β-catenin is translocated into the nucleus to activate the Wnt target genes. Adapted from Moon *et. al*.[22]

β-catenin/Wnt signaling is one of the pathways required for tissue segregation during development since the final products of Wnt pathway induces cell migration. For this to occur, cells disassemble adherens junctions and change their morphology in a process called epithelial-to-mesenchymal transition (EMT).[21] During EMT, cells lose

their epithelial phenotype, dissemble cell-cell contacts, reorganize their cytoskeleton and gain motility.[19] During the course of development, after the cells have reached their final differentiated state, they switch back to their epithelial phenotype through mesenchymal-to-epithelial transition (MET) in order to support the tissues **(Figure 1.4)**.[23] Other triggers of EMT include hypoxia, growth factors (eg. TGF-β, EGF, PDGF) or other initiating signals (eg. Wnt, Notch). Several transcription factors (eg. Snail, Zeb1/2, Twist), epigenetic regulators and non-coding mRNAs (miR200, miR34) mediate EMT-MET by repressing or activating expression of epithelial or mesenchymal markers.[24]

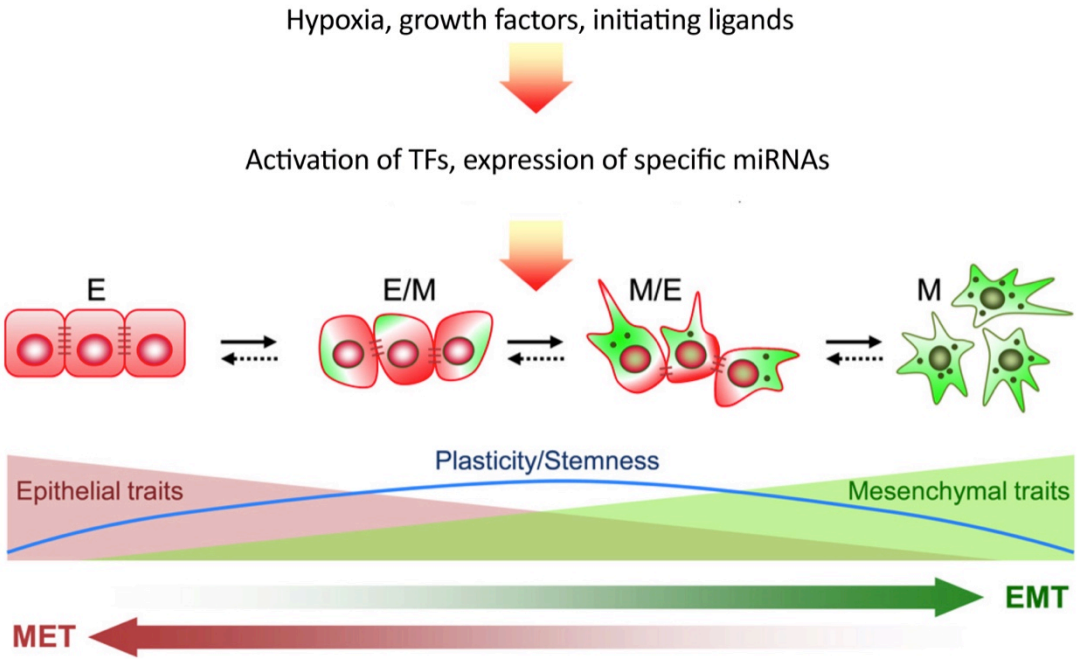

Figure 1.4 Epithelial to mesenchymal and mesenchymal to epithelial transitions (EMT-MET). EMT can be triggered by multiple mechanisms such as hypoxia, growth factors or initiating signals. Several intracellular signaling molecules that include transcription factors, epigenetic regulators and non-coding RNAs orchestrate the progress of EMT and MET. This progress involves many intermediary steps and through this EMT-MET spectrum where some cells may express both epithelial (E) and mesenchymal (M) markers. Adapted from Li *et. al*.[24]

EMT is not a binary process and includes several intermediary steps, where both epithelial and mesenchymal markers can be expressed simultaneously.[24] This plasticity in formation and dissociation of cell-cell contacts shows the dynamic and reversible nature of these contacts and involves complex signaling mechanisms,

which have to be regulated in space and time. In cases of aberrant regulation cancer develops and metastasis takes place.[19]

1.2 Cell-Extracellular Matrix (ECM) interactions

The interaction between cells and their extracellular matrix is also crucial for cell survival and tissue integrity. Cells attach to the basement membranes, which cover all epithelia, surfaces of muscle fibers and nerves.[3] There are two distinct layers of basements: the reticular lamina and the basal lamina. The reticular lamina is generated by fibroblasts that are present in the underlying connective tissue. The basal lamina is adjacent to the cells and has different adhesive ECM glycoproteins such as collagen IV, fibronectin, vitronectin, laminin.[3]

A family of cell-surface transmembrane glycoproteins, named integrins, mediates cell-ECM interactions. Integrins are heterodimers, which consist of an α and a β subunit **(Figure 1.5)**. There are 18 α and 8 β subunits in vertebrates.[25] Different combinations of the α and 8 β subunits can form 24 different integrins with different binding specificity to ECM proteins, signaling properties and distributions in different tissues.[25,26] Integrins can bind to large ECM proteins such collagen, laminin and fibronectin and some can recognize short peptide sequences within the large protein, such as RGD (Arg-Gly-Asp) that is found in fibronectin and vitronectin.[4]

Both integrin subunits are similar in structure: a large globular N-terminal extracellular domain, a single-pass transmembrane domain and a C-terminal cytoplasmic domain **(Figure 1.5)**.[27] The ectodomain of the α subunit consists of a seven-bladed β-propeller, a thigh and two calf domains. The lower side of the β-propeller contains Ca^{2+} binding pockets. The thigh and calf domains are similar in structure and they contain linkers for flexibility of the α subunits, which are also found in β subunits at similar position so that they can form a bent structure in the inactive state **(Figure 1.5, left)**.[25] The ectodomain of β subunit has also a β-I domain that is located in the hybrid domain. The hybrid domain is inserted in the plexin-semaphorin-integrin (PSI) domain. Four cysteine-rich epidermal growth factor (EGF) modules link to the PSI and the hybrid domains. EGF modules are followed by β-tail domain at the juxtamembrane.[25] The N-terminal domains of α and β subunits (β-

propeller and β-I, respectively) assemble non-covalently to form the ligand-binding site of the integrins **(Figure 1.5, right)**.[28,29]

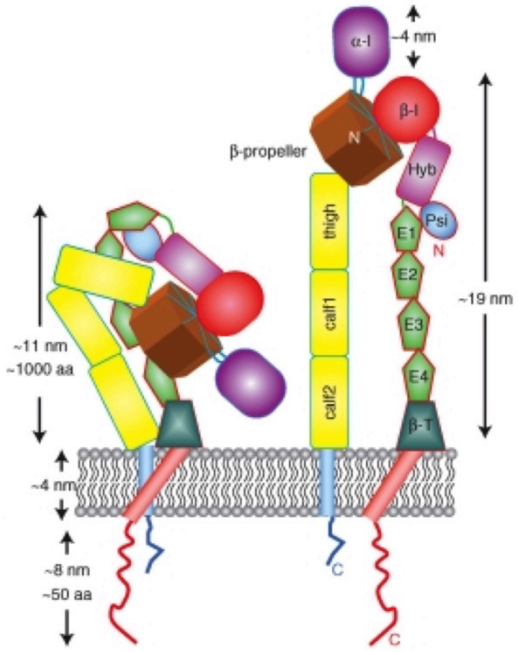

Figure 1.5 Integrin structure. Integrins are heterodimers composed of an α and a β subunit. Each subunit has an extracellular, a transmembrane and a cytosolic domain. β–propeller and β-I domains form the ligand-binding site of the integrins (right). The transmembrane domains of the α and β subunits are found to be associated in the resting or inactive state (left). Adapted from Campbell & Humphries.[25]

The cytosolic domain of integrins is associated with adaptor proteins, which connect integrins to the actin cytoskeleton forming focal adhesions **(Figure 1.6)**.[4] The activation of integrin takes place when talin, an adaptor protein, binds to the cytosolic tail of the β subunit and induces the separation of the cytosolic domains of both of the subunits.[30] Then, other integrin-associated proteins (FAK, Src, paxillin, ILK-Parvin complex) are recruited to the integrin-rich adhesion sites and this recruitment initiates the downstream signal transduction.[30] Phosphorylation of focal adhesion kinase (FAK) activates Src family kinases and activated FAK/Src complex can further phosphorylate other proteins such as paxillin at the adhesion site, which results in the activation of downstream signaling pathways (e.g mitogen activated protein (MAP) kinase pathway).[30] Integrin-linked kinase (ILK) and its binding partner, parvin, also form a bridge between the integrins and actin cytoskeleton. This complex

activates the downstream Akt/PKB (protein kinase B) pathway, which promotes cell survival and growth.[30]

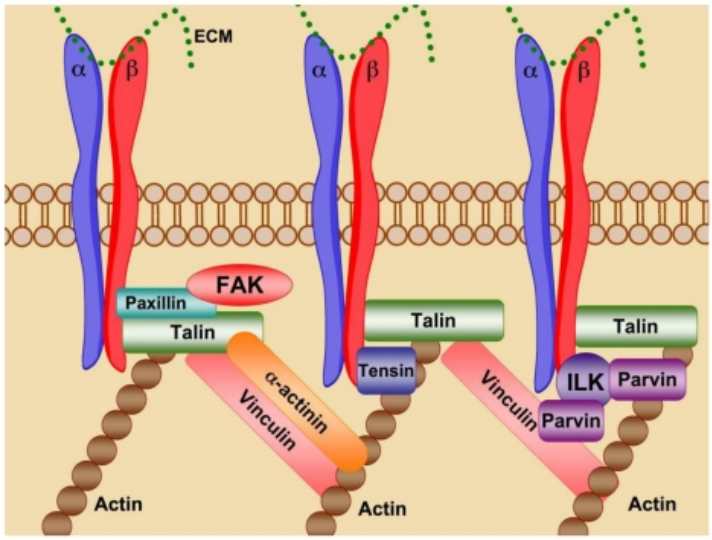

Figure 1.6 Integrin signaling. The initial contact between integrins and the actin cytoskeleton is formed by talin. Then other adaptor proteins are recruited to the integrin-rich adhesion sites. Vinculin crosslinks talin with actin to strengthen focal adhesions. This crosslinking is further stabilized by α – actinin, which interacts with integrin β-tails, vinculin, talin and actin**.** Phosphorylation of focal adhesion kinase (FAK) is a key event initiating Src family tyrosine kinase dependent signaling cascade. Integrin-linked kinase (ILK) can link to actin through its binding partner, parvin. Adapted from Millard *et. al*.[31]

Another important feature related to integrins is that they can change their confirmation depending on the presence of extracellular or intracellular signals. This implicates the bidirectional-signaling feature of the integrins **(Figure 1.7)**; i.e., the ECM binding activity is regulated from the inside of the cell (inside-out signaling) while, receiving and transmitting the signals upon ECM binding occurs through outside-in signaling.[26,28] The bidirectional signaling of integrins is important to control cell polarity, cytoskeletal structure, gene expression, cell survival and proliferation.[29] The variety of integrin subtypes provides versatility in cell adhesion. Their specificity for different kinds of ECM components and their dynamic nature is crucial for cells to attach at the right time and place.[28] A complex intracellular signaling mechanism underlies the specificity and dynamicity of integrin-ECM interactions, which indicates a tight spatiotemporal control as in all biological processes.

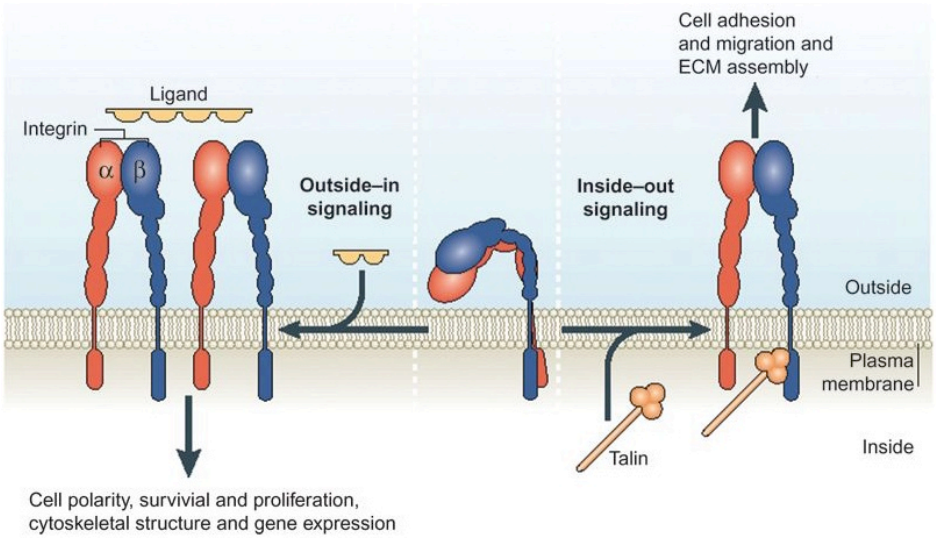

Figure 1.7 Bi-directional integrin signaling. Two directions of integrin signaling: inside-out and outside-in. During inside-out signaling, talin activates the integrins and triggers their binding to ECM. This allows cells to form strong cell-ECM contacts that are needed for cell migration. During outside-in signaling, ligand binding to integrins triggers conformational change leading to activation of intracellular signaling pathways. Adapted from Shattil *et. al.*[29]

1.3 Tissue engineering

Tissue engineering is an interdisciplinary field that combines the principles of molecular biology, material science, biomechanics and medicine in order to produce functional tissues *de novo* so that the defective or diseased tissues can be repaired or replaced.[32,33] There are two main approaches in tissue engineering: top-down and bottom-up approaches **(Figure 1.8)**.

1.3.1 Top-down tissue engineering

Traditional tissue engineering approach (also called as top-down approach) relies on biodegradable polymeric scaffold within which cells populate and produce their own extracellular matrix **(Figure 1.8A)**.[34] These cells are then cultured in a bioreactor, which provides microenvironmental control and required molecular and physical regulatory signals, such as growth factors or mechanical stimulation.[33,34]

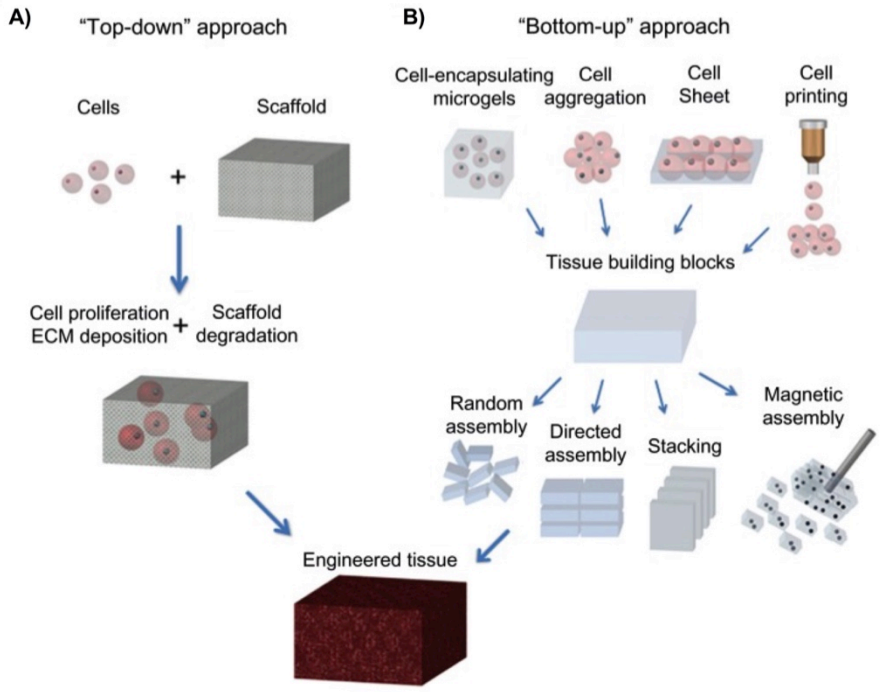

Figure 1.8 Top-down vs bottom-up tissue engineering. A) Top-down approach in tissue engineering combines cells and biodegradable scaffolds. The cells are cultured in a bioreactor until the cells fill the support structure and reach a desired developmental stage. **B)** In bottom-up tissue engineering, cells are used as building blocks to form individual subunits, which are then assembled into an engineered tissue by several methods such as directed assembly, stacking, etc. Adapted from Lu *et al.*[35]

Scaffold-based tissue engineering is attractive since scaffolds provide a 3-dimensional structure for the developing tissue and allow cells to adhere, proliferate, differentiate and produce ECM.[32,36] In addition to mechanical integrity, which is especially crucial for anchorage-dependent cells, scaffolds also provide precise control of surrounding microenvironment.[32] However, scaffold-base tissue engineering has some drawbacks. The scaffold material should be biodegradable after the production of ECM by the cells, which in itself may lead to toxicity or immunogenic responses in the host.[32,33] Furthermore, scaffolds may interfere with the normal organization of cells and obstruct mechanotransduction by stress shielding.[32,36] Finally, it is difficult to uniformly distribute high numbers of cells or introduce multiple cell types at specific positions.[33]

1.3.2 Bottom-up tissue engineering

Due to the above-mentioned limitations of top-down tissue engineering, many researchers have taken a scaffoldless approach (also called bottom-up tissue engineering) in which there is no requirement of cell seeding or adherence of cells to an exogenous scaffolds **(Figure 1.8B)**.[32] There are several advantages of bottom-up approach over the top-down. First, in the scaffoldless approach, cells show increased cell viability since they are not exposed to harsh processing conditions (spinning shear, elevated temperatures, toxic polymerizing chemicals).[32] There is high biocompatibility due to the absence of a scaffold: i.e., there is not any toxic by-products of scaffold degradation or any scaffold-dependent immunogenicity. Finally, the scaffoldless approach allows having a biomimetic environment, where maximum cell-cell communication is achieved leading to an increase in ECM production.[32] Hence, after implantation into the host, mechanotransduction and other signaling event can directly occur in the tissue.[32]

Scaffold-free tissue engineering is based on the self-assembly and self-organization of the cells into multicellular subunits such as spheroids, cell sheets or cylinders **(Figure 1.8B)**.[33] Self-organization in tissue engineering is a process where there is an external energy or force put into the system in order to produce tissues having different morphology and structure resembling the native tissues.[32] Self-assembly process

requires no external energy **(Figure 1.9)**.[32] The spontaneous organization in the self-assembling process occurs as a result of minimization of free energy by maximizing cell-cell contacts.[32]

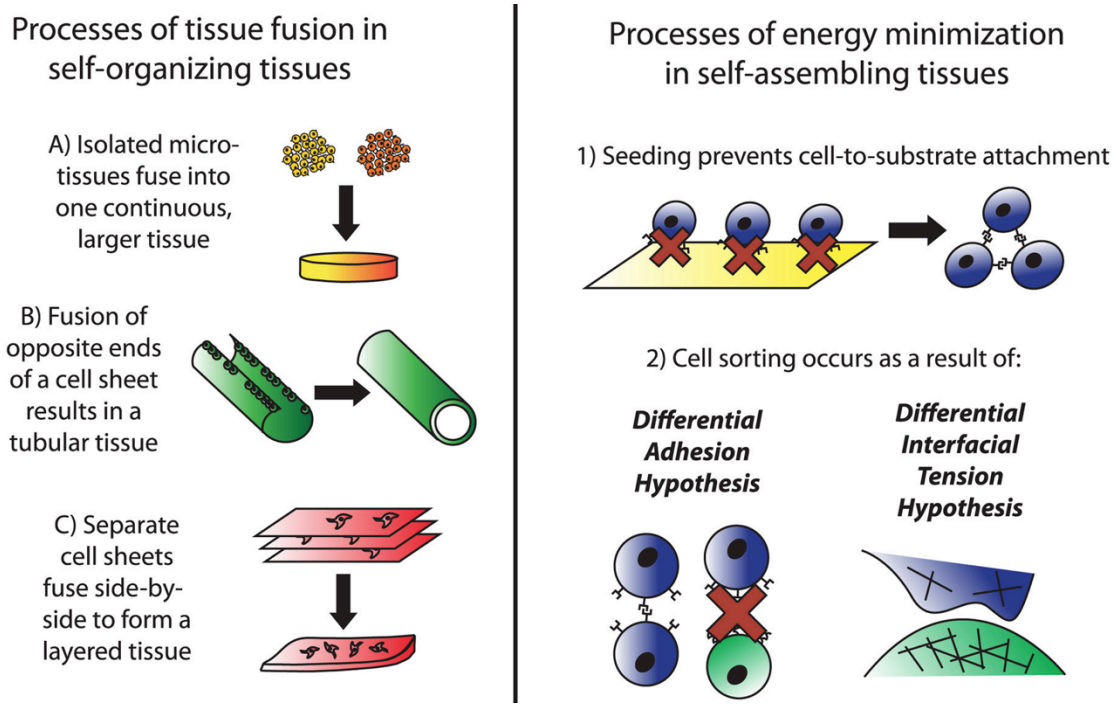

Figure 1.9 Self-organization and self-assembling processes in bottom-up tissue engineering. Tissue fusion takes place in both self-organizing and self-assembling processes. Tissue fusion includes cell-cell, cell-to-matrix and matrix-to-matrix contacts. Adapted from Athanasiou *et al*.[32]

Self-organization can be achieved by several techniques such as cell-encapsulating (or cell-laden) hydrogels (microgels), cell-sheet generation and cell printing **(Figure 1.8B)**.[32,35] Cell-laden hydrogels are used to create robust microtissues from the cells, which are not able to produce sufficient ECM. Commonly cells are embedded in photopolymerizable polymers such as polyethyleneglycol (PEG), temperature sensitive hydrogels or self-assembling peptide gels.[34] Cell-sheet technology involves the generation of sheets of cells under conditions that stimulate ECM production. Stacking these cell-sheets layer-by-layer leads to the formation of mechanically robust tissues.[34] In cell-printing technique, cells are deposited in small groups to engineer tissues with a variety of properties and geometries.[34]

Generation of cell aggregates is a self-assembly process. It involves use of a non-adherent substrate so that the cells will form aggregates or spheroids by minimizing the tissue free energy **(Figure 1.9)**.[32] This is achieved by maximizing cell-cell contacts,

a phenomena which is explained by differential adhesion and differential interfacial hypotheses.[32] The modular tissues generated by these self-organization or assembly processes can be further combined with random, directed and magnetic assembly or by stacking the modular tissues in order to engineer a macrotissue.[34,35]

Although bottom-up approach provides flexibility in tissue engineering, it still faces challenges in retaining the microarchitecture and cellular behavior while keeping robust mechanical properties for clinical implantation.[34] Hence, studies now integrate top-down and bottom-up approaches to create materials with biomimetic mechanical properties and functional microvasculature for nutrient and oxygen supply.[34] The examples include engineered hepatic microtissue, cardiac tissue, capillary networks and blood vessels[34]. With all these developments in the field of tissue engineering, it is now possible to create functional and suitable implants to repair failing tissues and organs such as skin, cartilage and bladder.[35] However, the major challenge in tissue engineering is precise control of spatial organization of cells at a given time.[34] It is also significant to control cell-cell and cell-ECM or cell-material interactions in the presence of different cell types since the response of cells upon these interactions affect their behavior and hence function within a tissue.[37] In addition, techniques to engineer a tissue also allows to study both physiology and pathology, and cell behavior and developmental processes in a controllable 3D environment.[33]

1.4 Controlling cell interactions

One of the fundamental questions in cell and developmental biology is how the composition or the physical organization of cells as building blocks of the body affects the function of tissues and organs.[38] Although controlling relative spatial positions of cells is challenging, bottom-up tissue engineering approaches provide additional means of controlling spatial organization of cells starting from cells or cell aggregates.[38,39] Engineering the surfaces of cells such that these cells can form interactions with neighboring cells and matrix components to mimic cadherins and integrins, respectively, are an attractive way to control cell adhesion.[37]

1.4.1 Controlling cell-cell interactions

There are two approaches in order to control cell-cell interactions: biological and chemical approaches. In the biological approach, the expression level of cadherins is manipulated by genetic methods such as knockdown, knockout, overexpression or mutations, and cell behavior is studied, as previously described in Section 1.1 **(Figure 1.2)**.[6,40,41] These interactions are genetically encoded, hence, sustained overtime and are biocompatible; however, it is problematic to alter these interactions locally and rapidly at a given time.

In the chemical approach, bio-orthogonal functional groups have been employed to chemically modify the surfaces of the cells. One example is the introduction of oxyamines or ketone groups to the cell surface by liposome fusion.[42,43] In this approach, a covalent bond is formed when oxyamines and ketone groups of the cells react resulting in a chemoselective and stable interaction between the cells **(Figure 1.10A)**. In another study, azide groups are inserted on the cell surface by metabolic glycoengineering, and tetrazine or *trans*-cyclooctane molecules are then attached to these azides on the cell surface.[44] When the cells are mixed together, they are glued together due to the covalent bond formation between tetrazine and *trans*-cyclooctane groups.

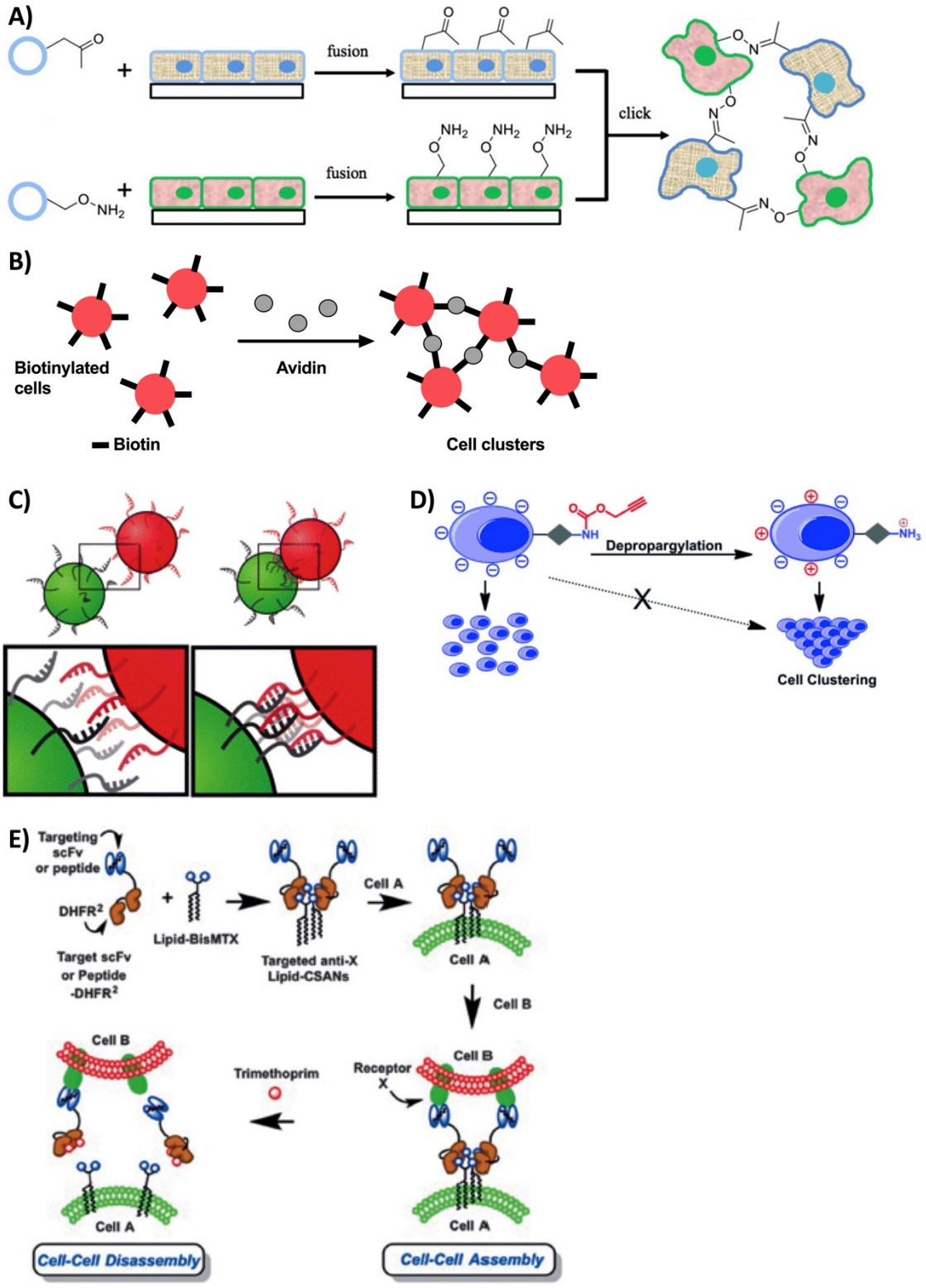

Figure 1.10 Engineering cell surface to induce cell-cell interactions. A) Cell-cell interactions by click chemistry.[43] **B)** Aggregation of biotinylated cells in the presence of avidin. Adapted from De Bank *et al*.[45] **C)** Cell-cell interactions by DNA hybridization.[46] **D)** Cell clustering induced electrostatically by modification of the charge of the cell surface.[47] **E)** Induction of cell-cell interaction by special lipids combined by specific ligand to target a receptor. This interaction can be reversed by trimethoprim.[48]

Cell surfaces have also been modified with non-covalent interaction partners, such biotin-avidin or biotin-streptavidin. De Bank *et al*. functionalized the cell surfaces with biotin by generating aldehyde groups at the sialic acid residues and then ligating biotin hydrazide by the formation of an hydrazone bond.[45] They showed the cross-linking of biotinylated cells in the presence of avidin into multicellular aggregates **(Figure 1.10B)**. In a similar approach, Wang *et al*. controlled induction of apoptosis of biotinylated Jurkat cells by inducing interactions with streptavidin-functionalized natural killer cells.[49]

Another strategy to induce non-covalent cell-cell interactions is modifying the surfaces of the cells with single stranded DNA (ssDNA) molecules so that the cells interact through sequence specific DNA hybridization **(Figure 1.10C)**.[46,50,51] There have been two strategies to modify the cell surface with ssDNA molecules. Teramura *et al*. used a DNA-polyethylene glycol conjugated with a lipid tail to insert the ssDNA on the cell surface by hydrophobic interaction.[50] Gartner *et al*. labeled the cells metabolically with *N*-azidoacetylmannosamine and the resulting cell surface azido sialic acid residues were ligated with phosphine conjugated ssDNA.[46] Gartner *et al*. was also able to engineer tissues in 3D through DNA hybridization and subsequently embedded these tissues in matrigel matrix, which combines bottom-up with top-down tissue engineering.[51]

The cell surface sialic acids have a versatile chemistry and a caged version of sialic acid has been used to control cell-cell interactions by altering electrostatic interactions. *N*-(propargyloxycarbonyl)mannosamine is an analogue of the naturally occurring sialic acids and can be metabolically inserted on the cell surface.[47] In the presence of palladium, which is a catalyst for cleavage of propargyl groups, a positive charge on the cell surface can be generated, which results in irreversible electrostatic cell clustering **(Figure 1.10D)**.[47]

Chemically self-assembled nanorings (CSANs) have been developed to induce high affinity dimerization to control cell-cell interactions reversibly **(Figure 1.10E)**.[48] Dihydrofolate reductase (DHFR) was recombinantly fused to another DHFR with a

peptide linker to form CSANs. Then, these CSANs were recombinantly fused to antibodies or other peptide to target cell surface receptors. It is known that DHFR can dimerize robustly with its inhibitor methotrexate (MTX). By fusing MTX to a lipid for insertion on the plasma membrane, these lipid-MTX-DHFR-peptide CSANs could be used for cell-cell assembly.[48] It was also shown in this study that the disassembly of the cells could be achieved in the presence of trimethoprim, which is an FDA (Food and Drug Administration) approved bacterial DHFR inhibitior.[48] Although the CSANs provide only reversible interaction of all above-mentioned approaches, the cell-cell assembly cannot be re-established due to the complete dissociation of DHFR-peptide molecules from the cell membrane in the presence of trimethoprim.

All the above-mentioned chemical modifications of the cell surface have limitations. Firstly, they can interfere unpredictably with other biological processes. Secondly, chemical modifications are difficult to sustain over longer periods since they are not embedded in any cellular machinery, and will diminish as cells divide and degrade them. In addition, apart from CSANs, none of the current platforms provide reversible interactions and hence, do not reflect the dynamic nature of cell-cell interactions. Most importantly, these chemical modifications do not provide spatiotemporal control over the cell-cell interactions.

1.4.1.1 Light controlled cell-cell interactions

Recently, light responsive chemical groups have been introduced to the cell surface to gain better spatiotemporal control over cell-cell interactions.[52,53] Luo *et al*. also used the click chemistry between oxyamines and ketone groups, which were inserted on the cell membrane by liposome fusion. In addition, a photocleavage site between the oxyamines and the lipid was also inserted in order to irreversibly break the covalent bond formed between the cells by UV light **(Figure 1.11A)**.[54] In another study, cell surfaces were labeled with β-cyclodextrin either through lipid insertion or through the combination of metabolic glycan labeling and bio-orthogonal click reactions. Subsequently, the host-guest interactions between azobenzenes and β-cyclodextrin were used to render the cell-cell interactions light responsive. Azobenzenes are photoswitchable molecules and have two confirmations: the *cis*-

confirmation under UV light illumination, which cannot bind to β-cyclodextrin and *trans*- confirmation under visible light, which can bind to β-cyclodextrin. An azo-PEG-azobenzene linker served as homobifunctional guest molecule to induce cell-cell interactions under visible light and break them under UV light **(Figure 1.11B)**.[52,53] Although this approach is the first to achieve high spatiotemporal and reversible control over cell-cell interactions, these interactions respond to UV light, which is toxic for cells and the general problems associated with the chemical modification of cell surfaces still hold true.

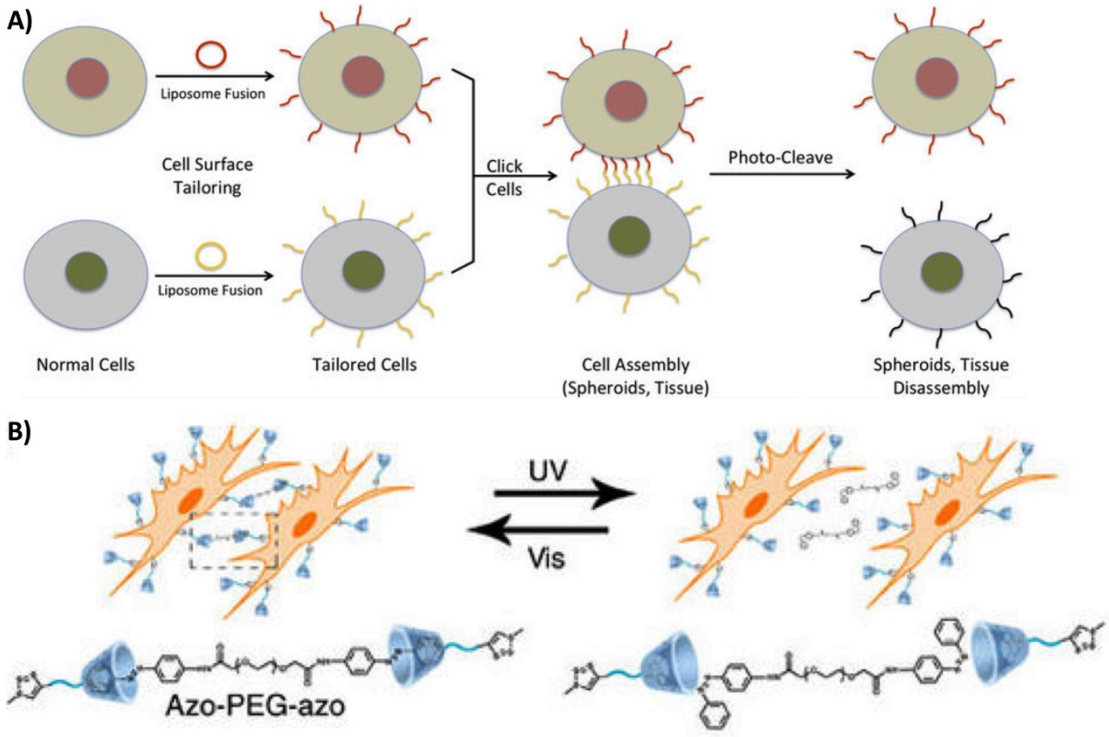

Figure 1.11 Light controlled cell-cell interactions. A) Cell-cell interaction is induced by clicking oxyamines and ketone groups present on the cell surface. This interaction is irreversibly broken by UV light illumination.[54] **B)** Light induced cell-cell interactions based on host-guest recognition of azobenzene and β-cyclodextrin. β-cyclodextrin is presented on the cell surface (in blue) and cell-cell contacts can be switched on and off by UV/VIS illumination.[53]

Overall, a platform is still missing in order to control cell-cell interactions dynamically, reversibly and with high spatial and temporal resolution in a noninvasive, sustainable and bio-orthogonal way. The design and development of photoswitchable cell-cell interactions that fulfill these requirements is the first aim of this PhD thesis and this would enable us to study cell-cell interactions and to build-up complex multicellular architectures.

1.4.2 Independently controlling multiple cell-material interactions

Cells respond to their immediate environment by interacting with different components of the ECM. Different ligands presented in the ECM, which are recognized by integrins, regulate cellular processes such as adhesion, migration, growth, secretion, gene expression and apoptosis.[55] Mimicking cell-ECM interactions and controlling them with molecular approaches are of central importance in the fields of tissue engineering, medical implantation and immunology.[55,56] Hence, it is crucial to achieve dynamic control over the interface between the cells of different types and the artificial substrates.[55]

One approach to selectively control cell-material interactions of two different cell types is to modify substrates (e.g. glass, gold or titanium dioxide surfaces) with peptidomimetics, which are selective for either integrin $\alpha_v\beta_3$ or $\alpha_5\beta_1$.[57,58] With this strategy it is possible to differentially adhere cell types expressing different integrins and to study the role of specific integrins in biological events such as migration and proliferation.[57,58] In a similar approach, antibody functionalized biomaterials have been used to isolate and recruit specific cell types, namely human adipose stem cells and osteoblast-like cells.[59] In this study, chitosan, a linear polymer of glucosamine and N-acetyl glucosamine, was used to immobilize different antibodies since chitosan is known to be biocompatible, biodegradable and nontoxic.[59] With this approach, selective cell attachment from a co-culture was achieved and it was spatially controlled.

Another strategy to control the adhesion of multiple cell types independently is to modify the surfaces of cells with synthetic orthogonal interaction partners such as ssDNAs to selectively bind these cells to substrates with complementary DNA strands.[60,61] As described above, ssDNA molecules were conjugated to the cell surface combining metabolic labeling with the click reaction between azide and phosphine groups (Staudinger ligation).[60] The complementary DNA strand was immobilized on a microfluidic channel of (poly)-dimethylsiloxane (PDMS) such that cells can bind to the surfaces of the microfluidic device **(Figure 1.12A)**.[60,61] This strategy allowed different cells to be immobilized in a DNA sequence specific manner and has been used to co-

pattern multiple cell types[61] as well as to construct 3D-tissues.[51] Leroy *et al*. have combined DNA hybridization and antibody-specific cell adhesion approaches to design a biochip where cells can be removed from their substrate with a photothermal effect **(Figure 1.12B)**.[62] Immunoglobulins (Ig) specific for B and T lymphocytes were covalently conjugated with ssDNA molecules and immobilized on ssDNA based biochip. The primary lymphocytes could then be captured by recognition of these Ig molecules with specific receptors. These lymphocytes could be released by laser induced local heating.[62] Although this approach is gentle and non-invasive, it does not reflect the reversible nature of cell-material interactions.

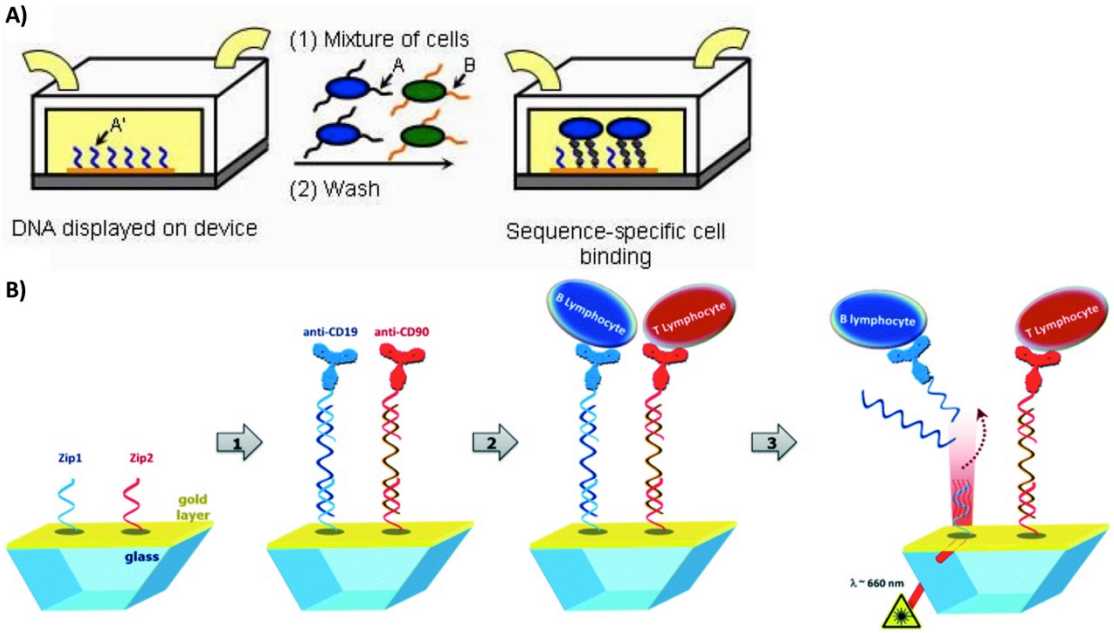

Figure 1.12 Cell-capture strategies from co-culture of cells. A) Sequence specific cell attachment by DNA hybridization.[60] **B)** Immobilization of immunoglobulins by DNA hybridization for antibody specific cell adhesion and detachment of cells by laser induced local heating.[62]

For improved spatial control of cell adhesion of multiple cell types and prompt different cells to adhere to specific positions on substrates, adhesion molecules have been immobilized to preformed micro- and nano- patterns.[63,64] For example, chitosan membranes have been functionalized with *o*-nitrobenzyl caged biotin. Light-triggered binding of streptavidin coupled antibodies led to specific cell adhesion of cells with different cell surface receptors.[63] Another strategy is orthogonal immobilization of different combinations of peptidomimetics, which are selective for either integrin $\alpha_v\beta_3$ or $\alpha_5\beta_1$, onto a micropatterned gold-metal oxide substrates.[64] This orthogonally

functionalized and micropatterned substrates provide an insight to localize integrin specific focal adhesions and quantification of spatial organization of integrins, which affects cell adhesion and migration.[64]

Although these above-mentioned strategies provide selective adhesion of multiple cell types to functionalized materials, they do not capture the reversibility of native cell adhesions and only provide limited spatiotemporal control. To mimic this dynamic nature of cell-matrix adhesion with synthetic materials, stimuli-responsive surfaces can be used to alter cell adhesion with light, temperature, pH and biochemical signals.[55] Of all, light responsive cell-material interactions provide the highest spatiotemporal control.

1.4.2.1 Light controlled cell-material interactions

A general strategy for light controlled cell adhesion is caging RGD peptides with photolabile caging groups like nitrobenzyl.[65,66] The caging group leads to steric hindrance, conformational constrain or alterations in the charge distribution of the RGD peptide; hence, prevent recognition by the integrins.[67] The caging group can be removed with UV light (350 nm) to render the RGD peptide active resulting in an adhesive substrate **(Figure 1.13A)**. The disadvantages of this approach are that photodecaging is achieved by UV light, which is damaging for the cells and it is irreversible; thus, the cell adhesion can only be altered once.

Another strategy is to fuse RGD to reversible photoisomerization units such as azobenzenes to make the cell attachment and detachment reversible.[68-70] Azobenzenes undergo *trans* to *cis* isomerization upon UV light irradiation and *cis* to *trans* isomerization under visible light illumination.[68] Hence, when immobilized on a non-adhesive substrate, the RGD peptide is only presented to the cells in when azobenzenes are in *trans* configuration whereas under UV light in the *cis* configuration the azobenzenes orients the RGD peptide towards the substrate and prevent the cell adhesion **(Figure 1.13B)**.[70] Although azobenzenes provides fast and reversible switching, the drawback of these approaches is the constant exposure of cells to UV light, which is damaging to cells.

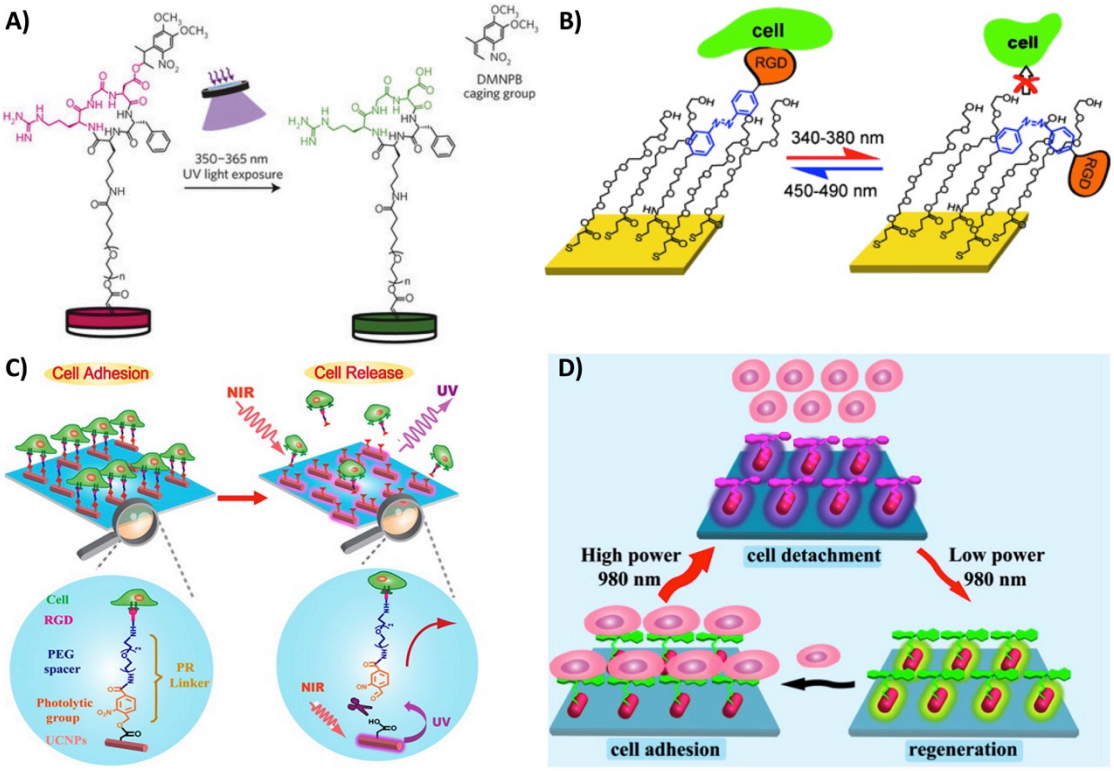

Figure 1.13 Light controlled cell-material interactions. A) RGD peptides are caged with photolabile nitrobenzyl groups, which can be cleaved by UV light illumination.[65] **B)** RGD peptide is fused to azobenzene molecules, which undergo *trans* to *cis* isomerization upon UV light irradiation and *cis* to *trans* isomerization under visible light illumination.[70] **C)** Modification of UCNPs with a photocleavable linker and an RGD peptide.[71] **D)** Combination of UCNPs with fibronectin coated photochromic spiropyran molecules, which also has two confirmations under UV and visible light.[72]

One of the most promising approaches is to combine the above-mentioned systems with lanthanide-doped upconversion nanoparticles (UCNPs), which can absorb near infrared (NIR) light (980 nm) and emit UV or visible light depending on the power of the NIR light.[71,72] One strategy is to modify UCNPs with a photocleavable linker and an RGD peptide.[71] Upon illumination with NIR light, the UV light emission from UCNPs resulted in cleavage of the photolytic group and the RGD peptide, which led to irreversible cell-detachment from the substrate **(Figure 1.13C)**.[71] The other strategy is combining UCNPs with fibronectin coated photochromic spiropyran molecules.[72] Spiropyrans have two conformations: the spiro form (under visible light) and the merocyanine form (under UV light). This isomerization of spiropyrans was used for reversible control of cell attachment and detachment **(Figure 1.13D)**.[72] Although promising, there is no system that allows to independently control the adhesion of

multiple cell types with light as none of these present orthogonal cell adhesion ligands to the cells. In addition exposing the cells to UV light remains a problem.

Overall, none of these light responsive strategies provides bio-orthogonal, noninvasive and independent control over multiple cell-material interactions in multicellular mixtures. This is due to the lack of photoswitchable cell adhesion ligands that specifically interact with different cell types and that can be addressed orthogonally with different wavelengths of light. This summarizes the second aim of this PhD project.

1.5 Non-neuronal optogenetics

Light is fundamental to life on earth and crucial for organisms of all kingdoms. Thus, there are a number of light-responsive proteins evolved over time, which have different biochemical and biophysical properties.[73,74] These photoreceptors respond to a specific wavelength and they undergo a reversible conformational change upon photon absorption, which affects their binding affinities for interacting proteins.[73] These natural resources have been used in the emerging field of optogenetics, which provides genetically encodable light responsive proteins as synthetic biology tools.[74] The major advantage of the optogenetic tools is that addition of photo-responsive chemical inducers or introduction of caged aminoacids, which can interfere with and perturb the mammalian systems, is not needed.[74]

The use of Channelrhodopsin-2, an algal blue light sensitive cation channel from *Chlamydomonas reinhardtii*, in mammalian neurons marked the beginning of the neuronal optogenetics era.[73,75] This development was followed by employing other microbial and animal opsins to control neural and muscle activity by activating these channels for specific ions.[76-78] These opsins utilize retinal as their chromophore and induce ion flux upon blue or orange light illumination.[74] Hence, they act as potential channels and their activity can be blocked in the dark.[74]

The other light sensitive proteins found in plants, fungi and microbes change conformation in response to light or interact with other proteins forming homo- or heterodimers **(Figure 1.14)**.[79,80] The prime example of an ultraviolet sensing photoreceptor is UVR8 from *Arabidopsis thaliana.* Its light perception is dependent on intrinsic tryptophan residues; hence, this protein does not need a cofactor. In dark UVR8 is a homodimer and upon illumination with UV-B light (280-315 nm), it interacts with constitutive photomorphogenesis protein 1 (COP1).[73] This tool has been used to control protein-protein interactions and gene expression in mammalian cells.[81]

A class of optogenetic building blocks are light-oxygen-voltage (LOV) domains, which are blue light sensing proteins conserved in prokaryotes, fungi and plants.[74] LOV domains have a conserved Per-ARNT-Sim (PAS)- core flanked by α-helices. The C-terminal α-helix is unwinded upon blue light illumination due to a covalent bond formation between a cysteine residue and its chromophore flavin mononucleotide (FMN).[74] The hydrolysis of the cysteinyl-flavin bond occurs in dark so that the α-helix turns back to the LOV core in its resting state.[73,74] Three versions of LOV domains were developed as optogenetic tools: FKF1-GI heterodimers from *Arabidopsis thaliana*, AsLOV2 which is based on unwinding of the Jα-helix from *Avena sativa* and VVD which homodimerizes under blue light from *Neurospora crassa*.[73] These domains have been used to control important processes including gene transcription[82,83], cell signaling[84] and protein-protein interactions.[85]

A couple of fluorescent proteins such as DRONPA from the stone coral *Pectiniidae* have also been used as optogenetic tools. This green photoswitchable fluorescent protein is found as a fluorescent tetramer or dimer in dark and upon cyan light illumination (500 nm) it forms monomers.[86,87] This system has been used for super resolution imaging[86] and control of enzyme activities.[88,89]

Blue and red light dependent CRY2/CIBN and PhyB/PIF6 heterodimers were used in this study and explained in more detail below.

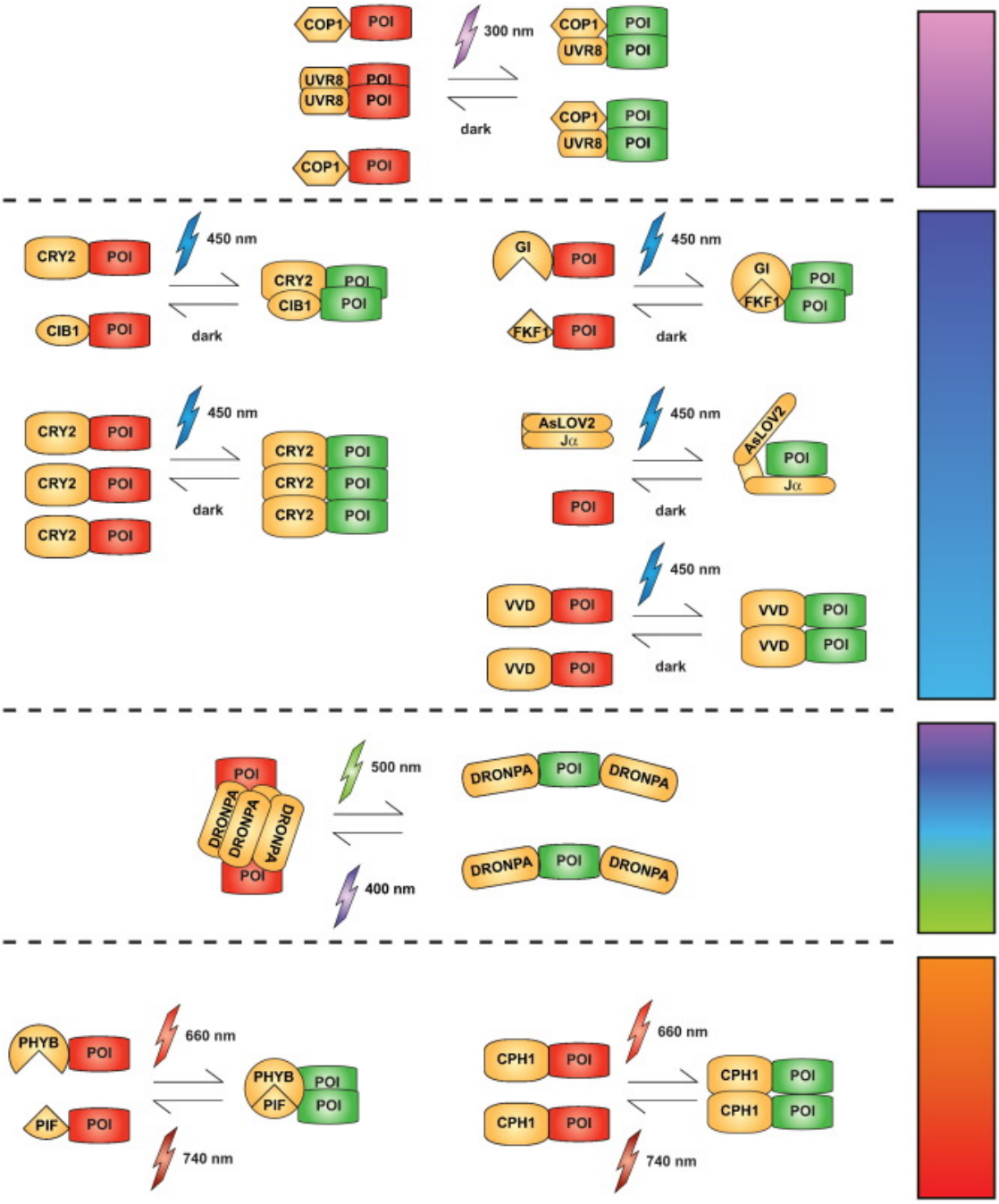

Figure 1.14 Chimeric photoreceptors as optogenetic tools. The photoswitchable proteins are groups based on their absorption peaks. AsLOV2: *Avena sativa* light-oxygen-voltage domain 2, CRY2: cryptochrome 2, CIB1: cryptochrome interacting basic helix-loop-helix 1, COP1: constitutive photomorphogenesis protein 1, Cph1: cyanobacterial phytochrome 1, FKF1: Kelch repeat F-box protein, GI: GIGANTEA, PhyB: phytochromes B, PIF6: phytochromes interacting factor 6, UVR8, ultraviolet B receptor, VVD: vivid, POI: protein of interest. Adapted from Mühlhäser *et. al.*[73]

1.5.1 Cryptochromes (CRY)

Cryptochromes are blue light sensing photoreceptors that regulate growth and development in plants and the circadian clock in both plants and animals.[90] Cryptochromes were first identified and best studied in *Arabidopsis thaliana* and there are three members of cryptochromes in *Arabidopsis*, CRY1-3.[73,90] There are two domains in CRY apoprotein: and N-terminal photolyase homology region (PHR) and a cryptochrome C-terminal extension (CCE) domain.[90] The PHR domain is the chromophore binding domain of cryptochromes and they non-covalently interact with flavin adenine dinucleotide (FAD).[90] In the dark, FAD is in its oxidized state and upon absorption of blue light, the flavin chromophore is reduced leading to a conformational change in the cryptochromes.[73,90] This is the biologically active form of the cryptochromes and they can either form homooligomers or heterodimers by interacting with cryptochrome-interacting basic helix-loop-helix 1 (CIB1) proteins.[73,74,80] CIB1 is a transcription factor and has a nuclear localization sequence, which is deleted for optogenetic studies in mammalian cells.[73,91]

Cryptochrome 2 (CRY2) was first used as an optogenetic building block in mammalian cells in 2010 by Kennedy *et al*. In this study, the activity of CRY2-CIB1 heterodimerization was investigated for full length CRY2 and only the PHR domain of CRY2 (CRY2PHR) together with full length CIB1 and an N-terminal truncated version of CIB1 (CIBN), which lacks DNA binding domain.[91] It was shown that CRY2-CIB1 and CRY2-CIBN were equally active under blue light. CRY2PHR expression was shown to be higher due to its smaller size, hence showed higher activity than full length CRY2 but with a higher dark background.[91] In the same study, CIBN was localized to the plasma membrane of the human embryonic kidney (HEK) cells and the blue light dependent reversible membrane recruitment of CRY2 from the cytosol was demonstrated. The authors further showed that CRY2-CIBN heterodimerization takes place within seconds and the complex dissociates within 12 min. The advantage of this blue light dependent system is that CRY2 does not need an exogenously added chromophore since FAD is found in mammalian cells.[92] Taslimi *et al*. improved versatility and tenability of the CRY2-CIB heterodimerization for specific applications by single mutations within the proteins or truncations.[93] For instance CRY2-CIBN

heterodimerization was used to control DNA recombination by induction of dimerization splitted Cre recombinase under blue light.[91,93]

Che *et al*. systematically characterized the two blue light dependent responses of CRY2 under different conditions.[94] They proposed that there are two independent binding sites of CRY2 for CRY2-CRY2 and CRY2-CIBN interactions, and CRY2-CIBN interaction sterically hinders the CRY2 oligomerization. The blue light dependent homooligomerization of CRY2 has been used for optogenetic control of intracellular signaling events. For instance, Bugaj *et al*. used the blue light dependent homooligomerization of CRY2 to control Wnt/β-catenin pathway and Rho GTPases in mammalian cells.[95] In this study CRY2 was fused to lipoprotein receptor-related protein 6 (LRP6), which oligomerizes in the presence of Wnt ligand and activates β-catenin signaling. In the absence of the Wnt ligand, β-catenin expression was turned on and off depending on the blue light illumination and a higher transcriptional response was achieved compared with that of induced by the natural Wnt ligand. Further, CRY2 was fused to Rho GTPase Rac1, which is involved in cytoskeletal reorganization. By activating Rac1 with blue light, its direct effect on actin dynamics was studied.[95] CRY2 homooligomerization was also used by Kim *et al*. to control fibroblast growth factor receptors (FGFRs) to control actin dynamics and cell polarization, and to induce directed cell migration.[96] Later an improved variant of CRY2, CRY2olig, which homooligomerizes more robustly, was developed by Taslimi *et al*. and used to control clathrin mediated endocytosis.[97]

CRY2-CIBN heterodimerization has also been used to control a variety of intracellular signaling events. Idevall-Hagren *et al*. used the blue light dependent CRY2-CIBN heterodimerization to control the phosphoinositide metabolism in mammalian cells.[98] In this study, CIBN was localized to the plasma membrane and CRY2 was fused to 5-phosphatases. The cellular mechanisms dependent on dephosphorylation phosphoinositides at the plasma membrane were tested by CRY2 recruitment to the plasma membrane upon blue light illumination. In a later study, the same group provided a more detailed insight on the regulation of membrane lipid metabolism by blue light illumination.[99] Xu *et al*. used CRY2-CIBN heterodimerization to unravel the

contributions of the phosphoinositide-3-kinase and Akt in the translocation of the glucose transporter 4 in response the insulin in adipocytes.[100] CRY2-CIBN system was also used to study the roles of proteins and transcription factors in the cellular forces with high spatiotemporal resolution.[101] Hence, it is now possible to study the direct effects of the players of different signaling cascades in cellular response and function.

A variety of different cellular events were also controlled by CRY2-CIBN heterodimerization. For instance, Duan *et al*. used blue light dependent CRY2-CIBN heterodimerization to reversibly control organelle distribution, which is important in a variety of cellular functions including cell survival and apoptosis.[102] By fusing CRY2 to an organelle (mitochondria, peroxisomes and lysosomes) and CIBN to motor proteins (dynein or kinesin), light controlled organelle distribution was achieved and can be used to study the effect of organelle distribution on cellular functions.[102] Sinnen *et al*. used CRY2-CIB1 heterodimerization in neurons in order to control the composition of the postsynaptic densities, which are protein dense regions bringing receptors and other proteins for neurotransmitter release in neuronal communication.[103] Deb Roy *et al*. employed CRY2-CIB1 heterodimerization in order to study the repulsion between osteoblasts and osteoclasts upon contact formation with high spatiotemporal resolution.[104] Polstein and Gersbach have developed a light activated CRISPR-Cas9 (clustered regularly interspaced short palindromic repeats-CRISPR associated protein 9) effector (LACE) system to control transcription of endogenous genes.[105] They fused CRY2 and CIB1 to the transactivation domain and catalytically inactive Cas9, respectively, and induced endogenous gene expression under blue light illumination.

The CRY2-CIBN optogenetic system has been used to gain insight into developmental and aging processes. Choudhury *et al*. investigated the epigenetic regulatory mechanisms of telomere length maintenance by using blue light dependent CRY2-CIB1 heterodimerization.[106] CRY2 and CIB1 were fused to human DNA methyltransferase 3A and telomere-associated protein telomere repeat binding factor-1, respectively, and methylation at the subtelomeric sites was increased under blue light illumination, resulting in the increase in the telomere length.[106] In another

study from Krishnamurthy *et al*., blue light dependent CRY2-CIBN pair was employed to control cell differentiation in mammalian cells and in developmental stages of *Xenopus* embryos by targeting Raf/MEK/Erk signaling cascades to study the effect of these signaling events in development.[107]

Recently more mechanistic insight for CRY2 homooligomerization and heterodimerization has emerged.[108] Duan *et al*. showed the effect of the charged residues at the N- and C- terminal of CRY2 on heterodimerization with CIBN homooligomerization of CRY2, respectively. General protocols based on blue light dependent CRY2-CIB1 heterodimerization for studying and analyzing the protein kinases[92], membrane lipid metabolism[99] and embryonic development[109] are also available.

In summary, all these studies show that CRY2-CIBN heterodimerization and CRY2 homooligomerization are powerful optogenetic tools to control and study a variety of cellular functions from gene transcription to neuronal communication with high spatiotemporal resolution.

1.5.2 Phytochromes (Phy)

The phytochromes are red and far-red light absorbing photoreceptors in plants, fungi and bacteria.[74] There are five members of phytochromes (PhyA-E) in *Arabidopsis thaliana* and they regulate seed germination, seedling de-etiolation and shade avoidance response.[110] They are covalently linked to an open chain tetrapyrrole chromophore, phytochromobilin (PϕB) and they exist in two reversible confirmations with different spectroscopic and functional properties.[111] The red light absorbing form (Pr form) is biologically inactive and red light absorption switches Pr to biologically active far-red light absorbing form (Pfr form). The Pfr form can interact to form heterodimers with the basic helix-loop-helix transcription factor superfamily, phytochrome interacting factors (PIFs).[111] Upon far-red light illumination the Phy- PIF heterodimer dissociates back to the ground state.[73]

The phytochromobilin chromophore is synthesized in chloroplasts of plants and then exported to the cytosol, where it is bound to phytochromes through a thioether linkage.[110] Since biosynthesis of phytochromobilin does not take place in mammalian systems, phycocyanobilin (PCB), a derivative of phytochromobilin, which can be extracted from cyanobacterium *Spirulina* and must be added exogenously to the cell culture medium for optogenetic control.[73,74,112] The biosynthesis pathway of PCB can also be genetically implemented in mammalian cells by encoding the necessary enzymes.[113,114]

The PhyB-PIF6 and PhyB-PIF3 heterodimerization have been engineered as an optogenetic tool in mammalian systems. The first study with red light dependent PhyB-PIF3/6 heterodimers in mammalian systems was done by Levskaya *et al*. in 2009.[115] In this study, different truncated versions of PhyB were anchored to the plasma membrane and a YFP-fused PIF3 and PIF6 protein was tested for reversible membrane recruitment under red and far-red light. It was shown that only PIF6 was recruited to the plasma membrane under red light and this interaction was reversible under far-red light provided that C-terminal PAS domain of the phytochrome is intact.[115] After showing precise and reversible recruitment of PIF6 to the plasma membrane under red light illumination, this PhyB/PIF6 interaction was used to modulate the upstream activators of Rho family GTPases under red light, which control actin cytoskeleton, thereby cell morphology. For this, PhyB was localized on the plasma membrane and PIF6 was fused to the Dbl homology-pleckstrin homology (DH-PH) domains of either Tiam or intersectin, which are Rho guanine nucleotide exchange factors (GEFs) and are responsible for activation of Rho family GTPases.[115] Depending on which PIF6-RhoGEF was recruited to the plasma membrane upon red light illumination, filopodia or lamellipodia protrusions were observed indicating the activation of the downstream GTPase signaling.[115]

Although PhyB/PIF3 heterodimerization has been used for controlling gene expression[116-118] and intein splicing[119] in yeast, this system was not successful to control interactions in mammalian systems.[120] Pathak *et al.* compared the activities of PhyB/PIF3 and PhyB/PIF6 systems using a yeast transcriptional assay.[120] This study

revealed that to control transcription in yeast, compared to PhyB/PIF6 system, PhyB/PIF3 system was activated more robustly with a low background and reversible under far-red light; however, extra light care had to be taken as it was quite sensitive to the ambient light.[120] Hence, PhyB/PIF6 heterodimers has been mainly used to control protein interactions and other intracellular signaling events in the mammalian cells.

The red light dependent PhyB-PIF6 interaction has been used to control signaling inside the cell. Toettcher *et al*. used red light dependent PhyB-PIF6 heterodimers to follow the flow of information in signaling cascade from Ras to Erk.[121] PhyB-PIF6 system was also used in a study by Yu *et al*. to regulate the second messenger molecules, Ca^{2+} and cAMP, by fusing PhyB and PIF6 to the subunits of heterotrimeric G proteins.[122] Juillot *et al*. designed a synthetic signaling cascade starting from the plasma membrane to the nucleus and combined PhyB-PIF3 heterodimerization with small molecules to sequentially control the protein localization.[123] These approaches in controlling intracellular signaling based on red/far-red light dependent photoswitch provide insights about the role of each step in the signaling cascade in the cellular response and function.

The PhyB-PIF6 interaction has also been used in the context of gene expression and gene delivery. Müller *et al*. used PhyB-PIF6 heterodimerizers to control gene transcription in mammalian cells by fusing PhyB and PIF6 to splitted transcription factors.[124] Gomez *et al*. used PhyB-PIF6 heterodimerization to improve viral gene delivery to the mammalian cells.[125] In this study, adeno-associated viruses were engineered to display PIF6 on their capsids. A nuclear localization sequence, which was linked to PhyB, allowed modulating the efficiency of the viral gene delivery by changing the red/far-red light ratio. This approach provided enhanced, tunable and spatiotemporally regulated viral gene delivery into the cells.[125]

Finally, red light dependent interaction between PhyB and PIF6 was used *in vivo* to study the roles of the key signaling events in the embryonic development by using model organisms. Müller *et al*. also applied this red/far-red light switch to control and

modulate angiogenesis in chicken embryos.[124] This PhyB-PIF6 mediated Ras/Erk signaling pathway was further developed and characterized[126] and also implemented in *Drosophila* embryos to follow the effects of Erk signaling in morphogenesis.[127] Further, Buckley *et al*. used the light induced heterodimerization of PhyB-PIF6 to rapidly and reversibly recruit proteins to specific regions within specific cells in zebrafish embryo.[128] In this study, they optimized the expression of PhyB and PIF6 in zebrafish embryo and also delivered PCB deep in the embryo without toxic effects. Hence, PhyB-PIF6 system was suitable to study developmental stages noninvasively and with high spatiotemporal resolution.

Not only plant PhyB but also cyanobacterial phytochrome 1 (CPH1) has recently taken its place in the optogenetic tool kit. Like PhyB, CPH1 also utilizes PCB as its chromophore; however, in contrast to PhyB, CPH1 homodimerizes under red light and dissociates under far-red light irradiation.[73] Reichhart *et al*. used red light dependent CPH1 homodimerization to trigger mitogen activated protein kinase/extracellular signal regulated kinase (MAPK/ERK) pathways through receptor tyrosine kinase (RTK) activation.[129]

All these studies show that PhyB-PIF3 and PhyB-PIF6 heterodimerization have been powerful optogenetic tools to control a variety of cellular functions raging from cell signaling to gene delivery and development with high spatiotemporal resolution. The advantage of this red/far-red light responsive system is that it provides an orthogonal fast switching within seconds. PCB chromophore has to be added exogenously, which was considered as a disadvantage; however, it brings an advantage of handling without extra light safety in the absence of PCB. Furthermore, the genetic implementation of PCB biosynthesis pathway can overcome this disadvantage.[73]

Chapter 2

Results and Discussion

2. Results and Discussion

2.1 Part 1: Blue light induced reversible cell-cell interactions

The interactions between cells is crucial for formation and function of tissues and organs; hence, controlling the arrangement of cells with respect to each other provides an insight into underlying cellular processes in development and allow the generation of functional tissues *de novo*.[4,38] The current genetic approaches[6,40,41] or covalent[42-44] and non-covalent[45-51] modifications of cell surfaces to control cell-cell interactions are neither sustainable nor reversible and do not provide spatiotemporal resolution. Although recently developed light controlled methods[52-54] provide reversible control in space and time, the sustainability of the cell surface properties still remains challenging. Furthermore, use of UV light in these systems is phototoxic for cells. Therefore, a platform to control cell-cell interactions dynamically, reversibly and with high spatial and temporal resolution in a noninvasive, sustainable and bio-orthogonal way is needed. The aim of the first part of this thesis deals with the reversible control of cell-cell interactions in space and time by using CRY2/CIBN heterodimerization as an optogenetic tool. Towards this aim, the photoswitchable proteins CRY2 or CIBN were stably expressed on the surfaces of MDA-MB-231 cells to switch on cell-cell interactions under blue light. The hypothesis is that when CRY2 and CIBN expressing cells are mixed in equal proportions, they would form cell-cell contacts under blue light illumination and these contacts would reverse in the dark **(Figure 2.1)**.

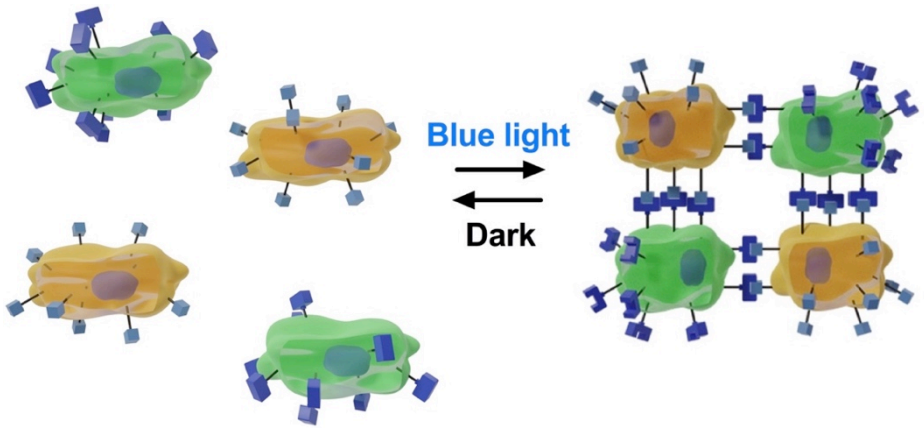

Figure 2.1 Schematic representation of blue light induced cell-cell contacts. Cells that express CRY2 (green) and CIBN (yellow) form cell-cell interactions under blue light and dissociate from each other in the dark.

2.1.1 Generation and characterization of stable cell lines

In order to control cell-cell interactions with blue light, the first step is to display the blue light dependent heterodimers, CRY2 and CIBN, on the surfaces of the cells. To maintain the expression of these proteins over longer periods, stable cell lines were generated. The human breast cancer line, MDA-MB-231, was chosen as host cell line since MDA-MB-231 cells lack E-cadherin expression and do not form any native cell-cell contacts.[41] To express these proteins on the cell surface, CRY2-mCherry and CIBN-GFP were inserted into a plasmid (pDisplay) having an N-terminal Igκ leader sequence to lead the proteins into the secretory pathway and a C-terminal transmembrane domain of the platelet derived growth factor receptor (PDGFR) **(Figure 2.2A)**. Subsequently, MDA-MB-231 cells were transfected with either pDisplay-CRY2-mCherry or pDisplay-CIBN-GFP plasmids to yield MDA-CRY2-mCherry and MDA-CIBN-GFP stable cell lines that constantly express these proteins on the their surfaces. For detection of mCherry and GFP signals from the transfected stable cell lines, confocal imaging was done, which showed the expression of the CRY2 and CIBN fused to fluorescent proteins in the cells **(Figure 2.2B)**.

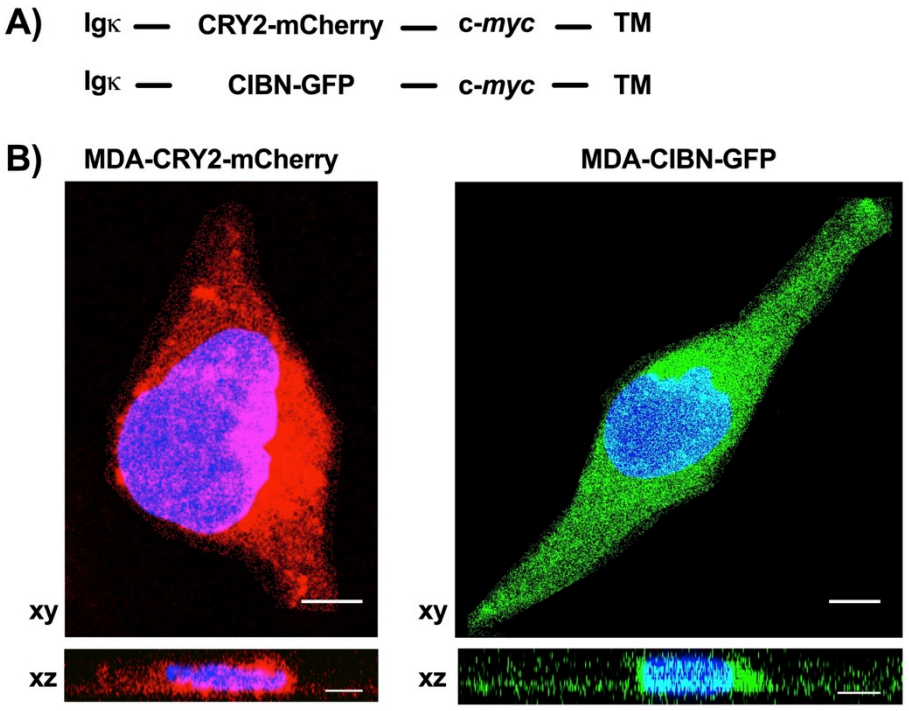

Figure 2.2 Generation of MDA-CRY2-mCherry and MDA-CIBN-GFP stable cell lines. A) Protein domains of pDisplay. **B)** Confocal images of MDA-CRY2-mCherry (left) and MDA-CIBN-GFP (right). Red: mCherry, Green: GFP, Blue: DAPI. The discontinuous signal of mCherry and GFP observed from xz-view indicates the presence of the proteins on the plasma membrane. Scale bar: 5 µm.

To further confirm that the CRY2 and CIBN proteins were expressed in the stable cell lines, the cells were immunostained for the *c-myc* epitope, which is located between the transmembrane domain of PDGFR and the protein of interest (CRY2-mCherry and CIBN-GFP) in pDisplay plasmids **(Figure 2.3)**. To detect the protein in the whole cell, cells were first permeabilized with Triton-X-100 before the addition of anti-*c-myc* antibody **(Figure 2.3A)**. To detect the protein expression only from the cell surface, cells were incubated with anti-*c-myc* antibody without permeabilization so that the antibody could only bind to the proteins on the plasma membrane **(Figure 2.3B)**. An Alexa 488 conjugated secondary antibody was used to visualize the proteins and z-stack images were acquired from both permeable and impermeable cells. In the permeabilized cells, where the whole cell proteins were detected, the side view (yz axes) showed a continuous green signal, which indicates the proteins were expressed in the cells and could be found both in the cytosol and on the plasma membrane **(Figure 2.3A)**. This was expected since the transmembrane domain fused to these proteins can localize the protein to all membranes in the cells via vesicular trafficking. The side view (yz axes) of impermeable cells showed a discontinuous green signal, which indicates that the proteins were on the plasma membrane **(Figure 2.3B)**. Hence, immunostainings confirmed that CRY2 and CIBN proteins were expressed and localized on the cell membrane.

The constant expression of CRY2 and CIBN on the cell surface provides maintenance for longer periods. Compared to other approaches in which cell surfaces are chemically modified, the use of genetically encodable proteins is an advantage. The chemical modifications of cell surfaces may lead to decrease in cell viability and cannot be sustained over longer periods of time because they are not genetically implemented.

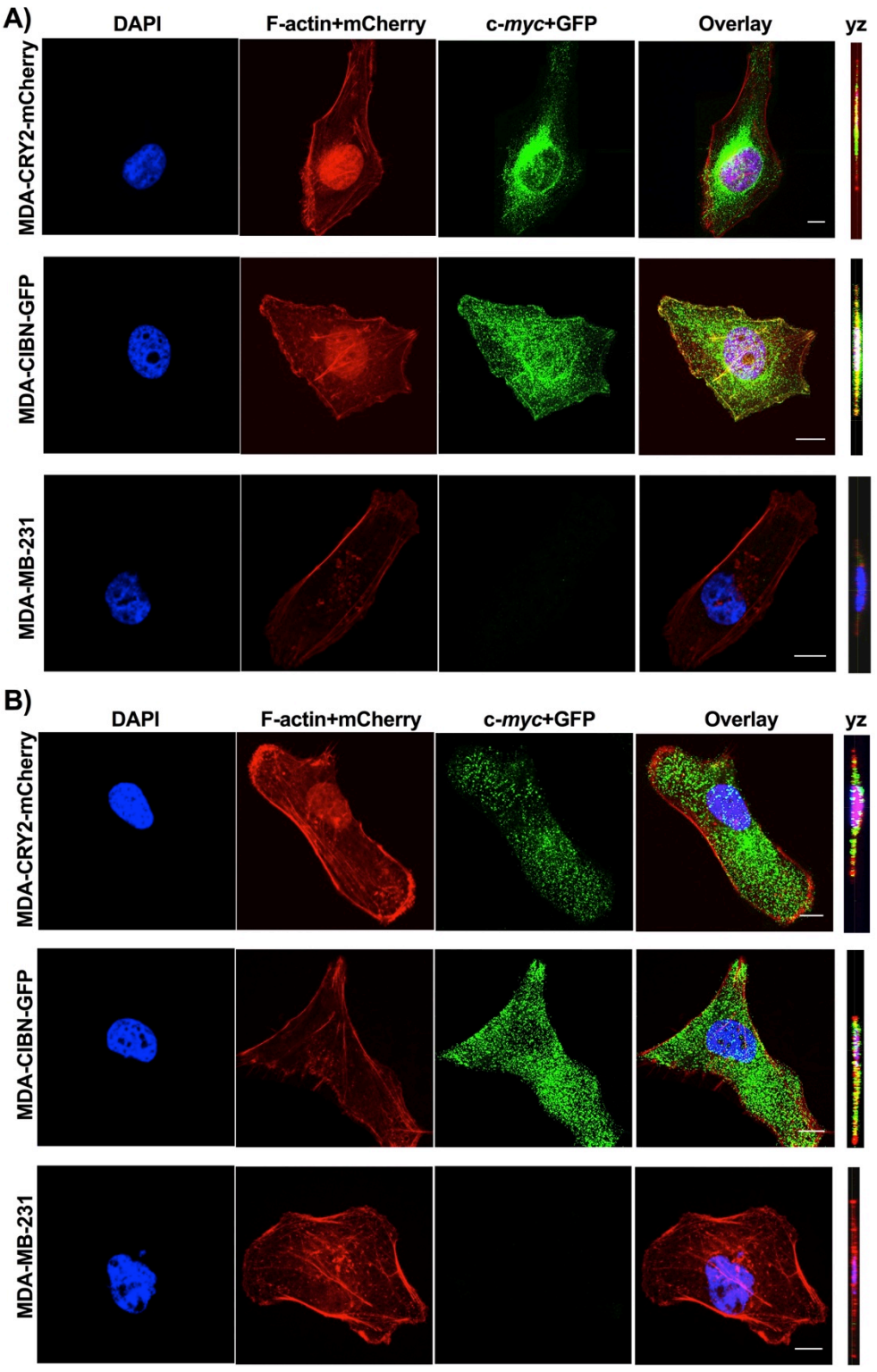

Figure 2.3 Immunostaining for c-*myc* epitope showing the expression of CRY2 and CIBN on the cell surface. The c-*myc* epitope was used to detect protein expression **A)** in the whole cell (permeable) and **B)** on the cell surface (impermeable). MDA-MB-231 cells were used as negative control. Blue: Nuclear stain (DAPI), Red: F-Actin stain (phalloidin-TRITC)+mCherry, Green: c-*myc* epitope (goat anti-Mouse Alexa Fluor 488)+GFP. The discontinuous green signal in the yz-axis is due to the proteins on the plasma membrane. Scale bar: 5 µm.

2.1.2 Blue light induced heterophilic cell-cell interactions

It was hypothesized that upon blue-light illumination cells expressing the blue light sensitive complementary interaction partners, CRY2 and CIBN, will interact and form cell clusters **(Figure 2.1)**. In order to test this hypothesis, MDA-CRY2-mCherry and MDA-CIBN-GFP cells were mixed in equal proportions and incubated in dark and under blue light (480 nm, 80 µW/cm^2) for 4 hours. After incubation, the cells were fixed and bright field microscopy images were obtained **(Figure 2.4A)**. The bright field images showed clusters of cells in the cultures that were incubated under blue light illumination and mostly single cells in cultures kept in the dark. This demonstrates that the blue light dependent interactions between cells expressing CRY2 and CIBN on the cell surface is suitable to induce cell-cell interactions.

In order to quantify these interactions, the actin cytoskeleton was stained with phalloidin-TRITC and the nucleus with DAPI. Fluorescence images of a total area of 1 cm^2 were obtained in the TRITC and DAPI channels **(Figure 2.4B)**. The actin staining was used to visualize the cell boundaries and measure the spreading area of cells, which allowed to separate single cells from cells in clusters. Based on that, the area occupied by clusters having more than 3 cells (objects with an area > 10000 µm^2) and by single cells (objects with an area of 300-3000 µm^2) were calculated in dark and under blue light from the TRITC channel. The % area was then calculated by normalizing the total area of clusters to that of all cells as follows:

$$\%\ area = \frac{\Sigma\ area\ occupied\ by\ clusters\ \geq\ 3\ cells}{\Sigma\ area\ occupied\ by\ all\ cells}\ x\ 100$$

DAPI staining was used to determine the total number of cells in the cultures in order to confirm that the increase in cell clustering under blue light was not due to differences in cell seeding. The total number of cells was calculated for the objects between 50-5000 µm^2 from the DAPI channel by using the analyze particles tool in ImageJ.

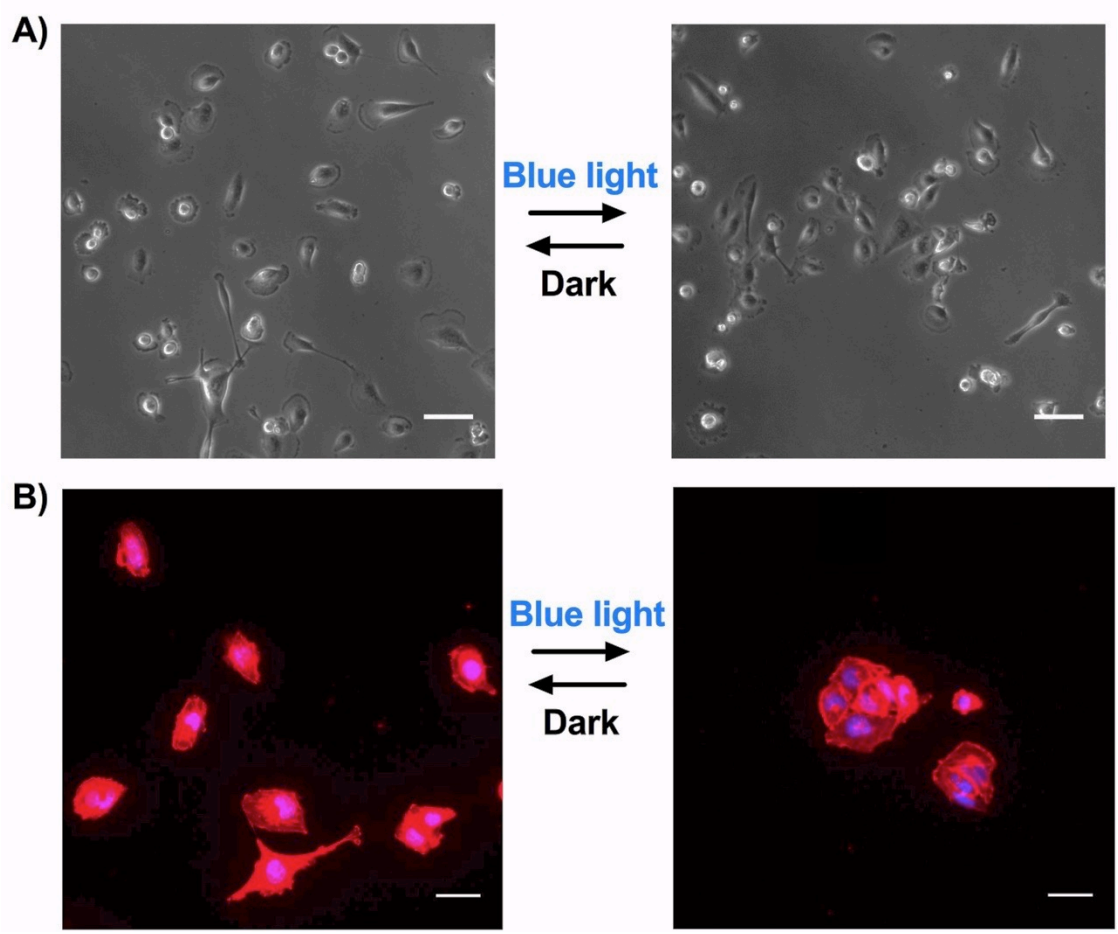

Figure 2.4 Blue light induced cell-cell interactions. A) Bright field images of MDA-CRY2 and MDA-CIBN co-culture in dark and under blue light illumination. Scale bar: 80 µm **B)** Fluorescence images of MDA-CRY2 and MDA-CIBN co-culture in dark and under blue light illumination. Cells cultured in the dark remained as single cells but cells cultured under blue light formed cell clusters due to CRY2-CIBN heterodimerization. Red: actin stain, Blue: nuclear stain. Scale bar: 50 µm.

To quantify the light dependent clustering, cell density in the co-cultures of CRY2 and CIBN expressing cells was adjusted depending on their clustering behavior under blue light illumination and in the dark **(Figure 2.5)**. The two cell types were mixed in a 1:1 ratio, seeded at densities of 2000, 5000, 10 000, 20 000 and 50 000 cells/cm^2 and were cultured under blue light illumination or in the dark for 4 hours. Quantification of the cluster formation in terms of % area and the total number of cells was performed as described above. The DAPI count showed that there was not any significant difference in the total number of cells between the cultures incubated in dark and under blue light illumination **(Figure 2.5A)**.

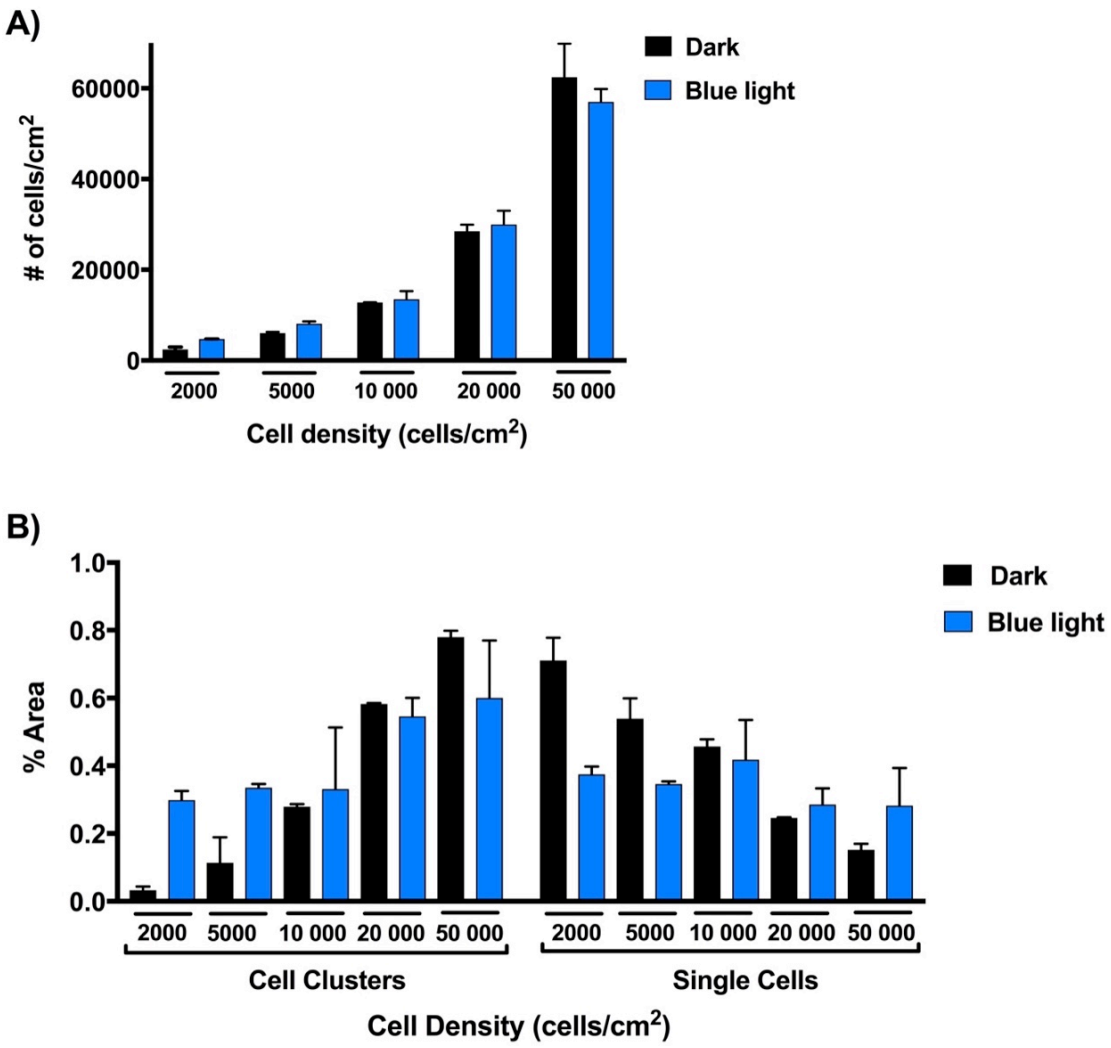

Figure 2.5 Cell number optimization for blue light induced cell-cell interactions. MDA-CRY2-mCherry and MDA-CIBN-GFP cells were seeded in equal proportions at different cell densities. **A)** Total cell number after 4 hours incubation, which was calculated from the DAPI staining. **B)** % area occupied by cell clusters and single cells at the different cell densities. The error bars are the standard error of the mean of two technical replicates.

The occupied % area analysis showed that at higher cell densities (>10 000 cells/cm^2), the light dependent cell-cell interactions were not distinguishable from general crowding in the cell culture and at very low cell densities (2000 cells/cm^2) the cells were too sparse to efficiently interact with each other **(Figure 2.5B)**. Hence, the optimal cell density was determined as 5000 cells/cm^2.

A potential error source is the phototoxicity caused by blue light illumination since some cell lines are known to be sensitive to photostress.[130] In order to detect whether the blue light illumination used in these experiments caused phototoxicity

and to determine the range of non-toxic blue light intensity, the cell viability was checked for the parent cell line MDA-MB-231 using the MTT assay at three different light intensities **(Figure 2.6)**. In the host cell line (MDA-MB-231), no phototoxicity at 80 µW/cm^2 after 4 hours incubation was observed, which were the parameters used in all experiments. It was also observed that cell viability was not lowered even at a 100-fold higher light intensity in the given incubation period (8000 µW/cm^2, 4 h illumination). This also demonstrates that the here used light intensities were not harmful and that this approach is non-hazardous for cells. Therefore, blue-light dependent CRY2/CIBN heterodimerization provides a platform to control cell-cell interactions non-invasively, as opposed to for the UV light controlled systems.[52-54]

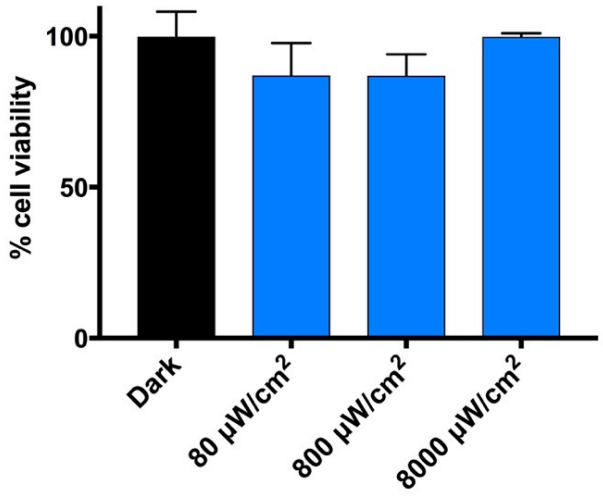

Figure 2.6 Cell viability under blue light illumination. MDA-MB-231 cells were incubated under three different intensities of blue light and in dark for 4 hours. Subsequently, cell viability was measured by MTT assay. The absorbance values were normalized to the dark value to determine % cell viability. 80 µW/cm^2 blue light illumination was used in all other cell experiments. The measurements were done in duplicates and the error bars are standard error of the mean.

After confirming that the blue light intensity (80 µW/cm^2) was non-hazardous and obtaining the optimal cell density (5000 cells/cm^2), the co-cultures of CRY2 and CIBN expressing cells were incubated under blue light and in dark and cluster formation was quantified as described above. The area occupied by cell clusters increased 6-fold under blue light illumination compared to dark **(Figure 2.7A)**. Similarly, the area occupied by single cells was higher in the dark in the co-culture. In the same co-cultures, number of clusters with ≥3 cells was also calculated. There were 180

clusters/cm^2 in the co-culture incubated under blue light illumination whereas only 20 clusters/cm^2 could be detected in the co-culture that was kept in dark (**Figure 2.7B**)

CRY2 has been shown to homodimerize to some extent under blue light.[94] In order to exclude the effect of homodimerization of CRY2 on cell clustering, the same experimental conditions were used for the monocultures of CRY2 and CIBN expressing cells. It was observed that CRY2 and CIBN expressing cells were found mainly as single cells both in dark and under blue light **(Figure 2.7A)** with low number of clusters **(Figure 2.7B)**, resembling the co-cultures kept in the dark. Again, there was no significant difference in the total number of cells in all cultures **(Figure 2.7C)**. Hence, these data demonstrates that the blue light dependent cell-cell interactions are heterophilic and mediated by specific CRY2-CIBN heterodimerization.

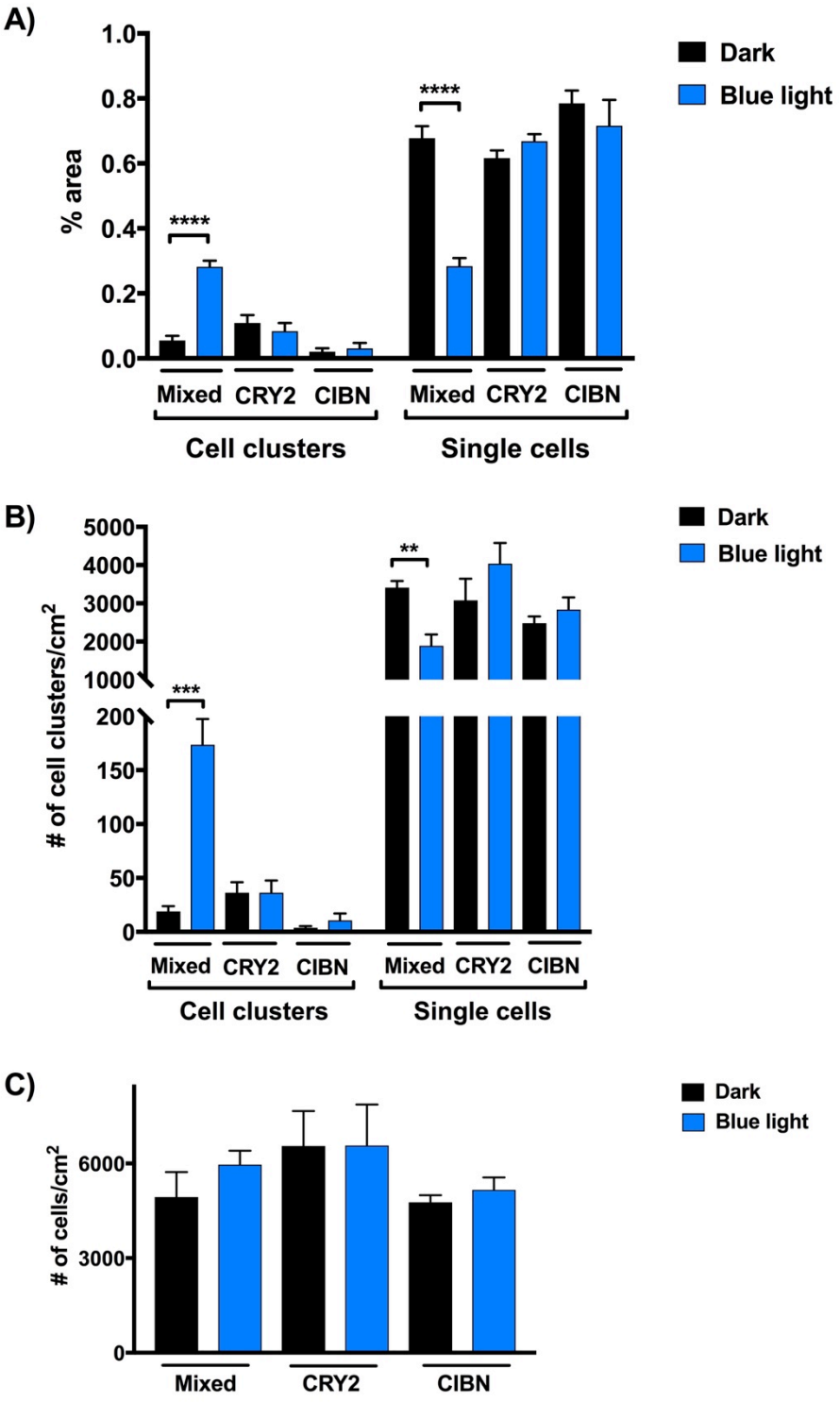

Figure 2.7 Quantification of cell-cell interactions between CRY2 and CIBN expressing cells in dark and under blue light. A) % Area of cells that grow in cell clusters and as single cells. The cells kept in dark primarily stayed isolated, whereas cells grown under blue light showed a higher number of cell clusters. MDA-CRY2-mCherry and MDA-CIBN-GFP cells formed heterophilic and not homophilic interactions since in monocultures cells grew as single cells. **B)** The number of cell clusters having ≥3 cells and single cells in the dark and under blue light. **C)** The number of cells in the co- and monocultures of MDA-CRY2-mCherry and MDA-CIBN-GFP cells were measured to prevent any errors

due to cell number. There was not any significant difference between the number of cells, which may affect the size or amount of the clusters. The error bars are the standard error of the mean from technical duplicates with 2 replicates each. Unpaired parametric t-test was used for statistical significance (p value <0.0001 (****), p value < 0.001 (***), p value<0.01 (**)).

2.1.3 Reversible control of blue light dependent cell-cell interactions

A critical merit of the CRY2-CIBN based cell-cell interactions is that these interactions are reversed in the dark, which reflects the dynamic and reversible nature of cell-cell interactions. The interaction between CRY2 and CIBN has been reported to turn on in a few seconds with blue light when the protein is located directly towards each other and to turn off in a couple of minutes in the dark.[91] To show the reversibility of blue light dependent cell-cell interactions, MDA-CRY2-mCherry cells were seeded on adhesive circular patterns with 20 µm in diameter, such that isolated MDA-CRY2-mCherry cells grew on an otherwise non-adhesive background. Subsequently, MDA-CIBN-GFP cells were added and their interactions with the MDA-CRY2-mCherry cells were monitored under blue light and in the dark and a time-lapse movie was recorded in light/dark cycles (**Figure 2.8A**). CIBN cells were seeded on top of the CRY2 expressing cells under blue light illumination and the first time interval was set as 30 min to allow CIBN cells to settle and interact with the CRY2 cells. Then the blue light was switched off and imaging time intervals were shortened to 20 min which allowed to monitor many cells at one time point and also to follow the fast interaction and dissociation of the proteins that were reported to take place within several minutes.[91] It was observed that under blue light illumination MDA-CIBN-GFP cells stayed close to MDA-CRY2-mCherry cells showing a reduced mobility upon interacting with MDA-CRY2-mCherry cells. When the blue light was switched off, the MDA-CIBN-GFP cells gained mobility in dark due to the dissociation from the MDA-CRY2-mCherry cells. This cycle was performed twice and each time under blue light the two cells interacted with each other and dissociated from each other in the dark. Hence, these blue light dependent cell-cell interactions are reversible and can be switched on and off repeatedly.

Based on this time-lapse movie, the distance between CIBN and CRY2 expressing cells was calculated at each minute for the repeated light/dark cycles (**Figure 2.8B**). The boundaries of the CRY2 and CIBN expressing cells were marked with red and green

circles, respectively. It was observed that the distance between the CRY2 and CIBN expressing cells increased to a maximum of 15 µm in the dark within 1 min. This distance completely disappeared also within 1 min when the blue light was switched on. This is a similar time range to what was observed with the photoswitchable protein interactions based on this pair.[91]

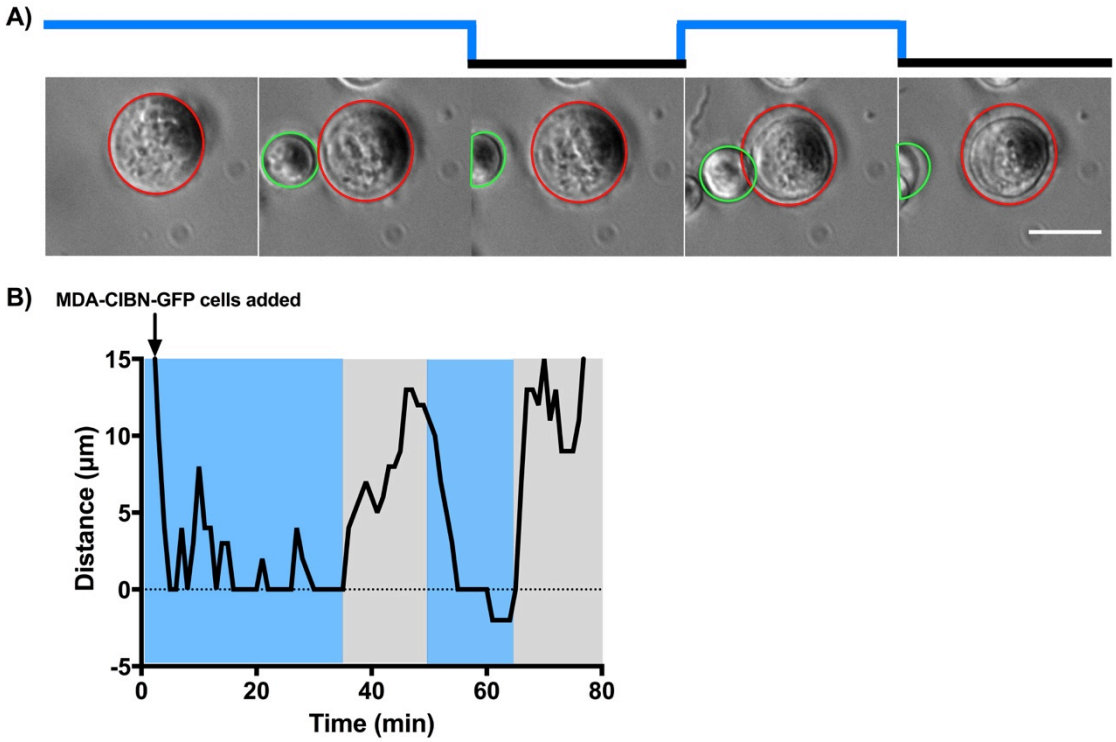

Figure 2.8 Reversible control of cell-cell interactions. A) Phase contrast images from the time-lapse movie showing the binding of a MDA-CIBN-GFP cell (green circle) to an MDA-CRY2-mCherry cell (red circle) under blue light and its dissociation in the dark. Scale bar: 25 µm. **B)** Distance between the MDA-CRY2-mCherry and MDA-CIBN-GFP cells over time. The distance between the two cells decreased under blue light due to the CRY2/CIBN heterodimerization and increased in dark due the CRY2/CIBN dissociation.

Up-to-date there are few studies showing reversible control of cell-cell interactions. The first one was based on modifications of the plasma membranes with the chemically self-assembled nanorings (CSANs) targeting specific receptors on neighboring cells **(Figure 1.10E)**.[48] Cell-cell assembly triggered by CSANs could be reversed by a competitor molecule for DHFRs, trimethoprim. However, in the presence of trimethoprim, CSANs dissociated completely from the plasma membrane; hence, cell-cell assembly could not be re-established. Additionally, this approach does not provide spatial control over cell-cell interactions.

Light is a powerful tool to achieve spatiotemporal control over these interactions since the stimulus can be delivered at the speed of light. Recently, light responsive small molecules were also introduced on the plasma membrane to control cell-cell interactions.[52-54] One approach was to introduce either oxyamines or ketone groups on the plasma membrane by liposome fusion and a photocleavage site between the oxyamines and the lipid bilayer **(Figure 1.11A)**.[54] When oxyamines and ketone bearing cells were mixed, a covalent bond was formed between the cells and due to the presence of the photocleavable linker, this bond would be irreversibly broken by UV light. Again, the cell-cell contacts could not be re-established due to the irreversibility of loss of covalent bonds between the chemical groups. Furthermore, UV light is invasive and can damage the cells.

Shi *et al.* controlled cell-cell interactions reversibly and dynamically by labeling the plasma membranes with β-cyclodextrin and used host-guest interactions between β-cyclodextrin and azobenzenes **(Figure 1.11B)**.[52,53] In this study, formation of cell-cell interactions was triggered by visible light and cell disassembly was achieved by UV light illumination, and assembly-disassembly cycle could be repeated. Apart from the continuous UV exposure of cells, β-cyclodextrin/azobenzene association and dissociation have slower kinetics compared to the blue light dependent CRY2/CIBN heterodimerization.

While cell assembly and disassembly mediated by azobenzenes took place in 10 minutes,[53] this was achieved within 2 minutes with CRY2/CIBN system **(Figure 2.8B)**. Thus, blue light dependent CRY2/CIBN heterodimerization provides a sustainable, non-invasive, reversible and rapid control of cell-cell interactions.

2.1.4 Layer-by-layer tissue formation by blue light illumination

For tissue engineering and artificial organ research, a big challenge is to construct three-dimensional tissues consisting of multiple cell types.[131] Recently, two studies showed 3D tissue formation with the bottom-up approach by ssDNA hybridization[51], which was then combined with a matrigel, and oxime ligation,[42,43] in which the ECM secreted by the cells was used as mechanical support. In this thesis, CRY2 and CIBN expressing cells were used to constitute a defined microtissue from the bottom-up by seeding the cells layer-by-layer. Pre-stained CIBN cells (in green) were seeded on a glass bottom dish and grown to confluency overnight. Then, pre-stained CRY2 expressing cells (in red) were seeded on top of CIBN cells. This co-culture was incubated under blue light and in the dark for 8 hours. Then, the cells were fixed and stained for nuclei. In order to obtain z-stack images of the micro-tissue, confocal microscopy was used **(Figure 2.9)**. In the dark, there was only a monolayer of CIBN expressing cells and no CRY2 cells were found to form a second layer on top of CIBN cells **(Figure 2.9A)**. For the cells cultured under blue light illumination, formation of two layers was observed at many different positions **(Figure 2.9B)**.

Two complete monolayers on top of each other throughout the surface could not be observed. This could be because CIBN expressing cells could not form a firm monolayer due to lack of native cell-cell contacts and lack of homodimerization of CIBN. This led CRY2 expressing cells also adhere to glass surface, in between CIBN expressing cells. However, absence of any layer formation in the co-culture in the dark but only under blue light shows that the layers were formed through CRY2-CIBN heterodimerization. This system can be further optimized and utilized to obtain scaffold-free multicellular *in vitro* tissue formation defined by blue light illumination.

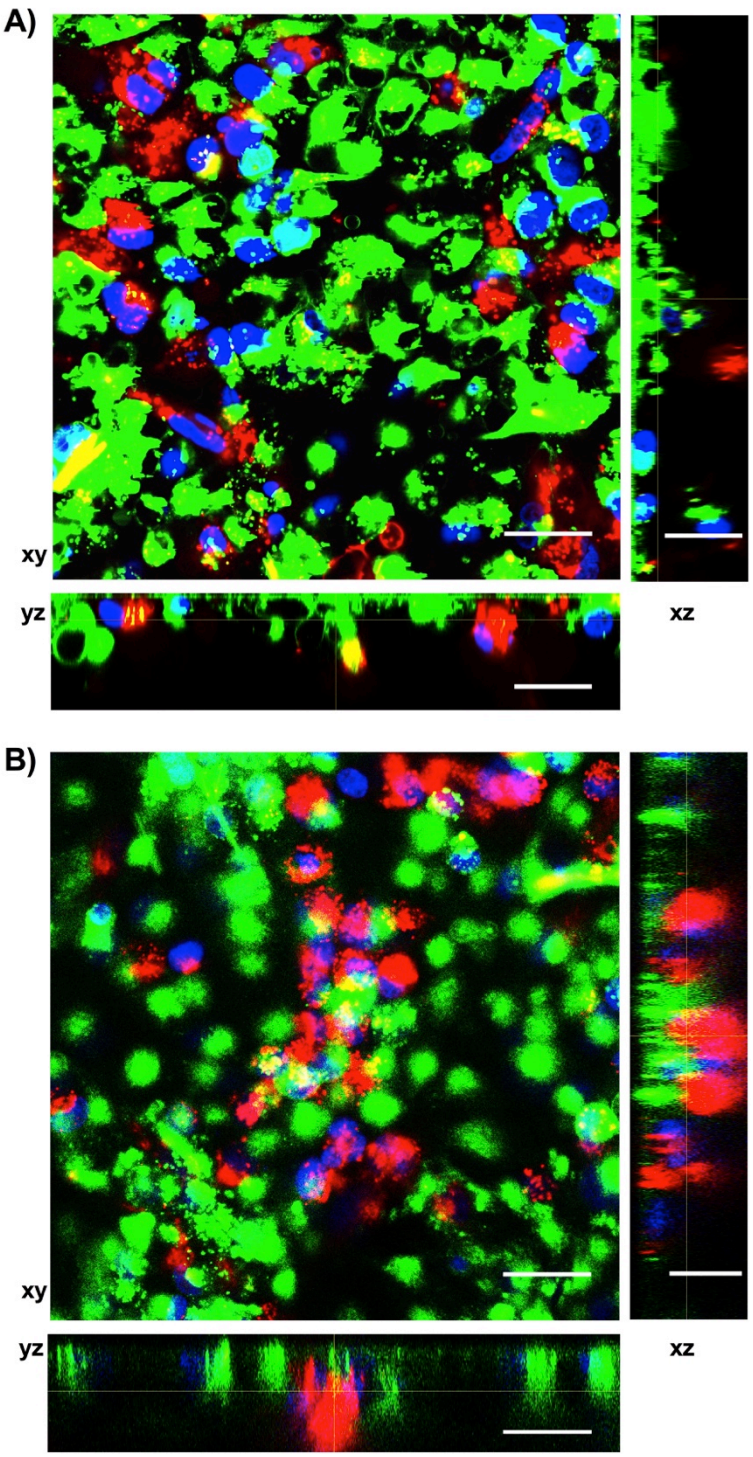

Figure 2.9 Layer-by-layer tissue formation under blue light illumination. A) in the dark. Stack number is 8 of 44 slices for the xy view. **B)** under blue light illumination. Stack number is 23 of 54 slices for the xy view. Side views (yz and xz) shows that **A)** there is only a monolayer of CIBN expressing cells in the dark whereas **B)** under blue light, CRY2 expressing cells interacted with CIBN cells to form a second layer. Blue: nuclear stain, green: MDA-CIBN-GFP cells, red: MDA-CRY2-mCherry cells. Scale bar: 30 µm.

2.2 Part 2: Blue and red light controlled cell-substrate interactions

Cells respond to their immediate environment by interacting with different components of ECM and this interaction regulates cellular processes such as adhesion, migration and apoptosis.[55,56] Different ligands presented in the ECM are recognized by different cells and independent control of the interactions of different cell types with different matrices is of central importance for tissue engineering and medical implantation.[55,56] Current approaches to control cell-material interactions with multiple cell types involve modification of substrates with peptidomimetics as ligands for different integrins,[57,58] antibodies for specific cell surface markers,[59,62] ssDNA molecules,[60,61] and preformed micro- and nano-patterns.[63,64] These strategies provide selective adhesion of multiple cell types to functionalized materials; however, they do not capture the reversibility of native cell adhesions and only provide spatiotemporal control. Light responsive functional molecules such as caging groups,[65-67] azobenzenes[68-70] and UCNPs[71,72] have been employed to achieve the spatiotemporal control over cell-material interactions. Although azobenzenes and UCNPs provide reversible control, they are invasive due to the exposure of cells to UV light. The major drawback of these platforms is that none of them provides independent and spatiotemporal control over cell-material interactions in a multicellular environment. Hence, a platform that provides reversible and spatiotemporal control over cell-material interactions and that allows cell adhesion ligands to specifically interact with different cells is needed. The aim of the second part of this thesis is to reversibly control cell-material interactions of multiple cell types in space and time by using CRY2/CIBN and PhyB/PIF6 heterodimers as optogenetic tools. Towards this aim, the photoswitchable proteins CRY2 or PhyB were expressed on the surfaces of MDA-MB-231 cells to turn on the cell binding on the substrates with the complementary interaction partners -CIBN or PIF6- under blue or red light, respectively. It was hypothesized that by incubating the CRY2 and PhyB expressing cells on CIBN and PIF6 functionalized substrates in the dark and under blue and/or red light, different cell-material interactions can be turned on and off orthogonally in a wavelength-dependent manner **(Figure 2.10)**.

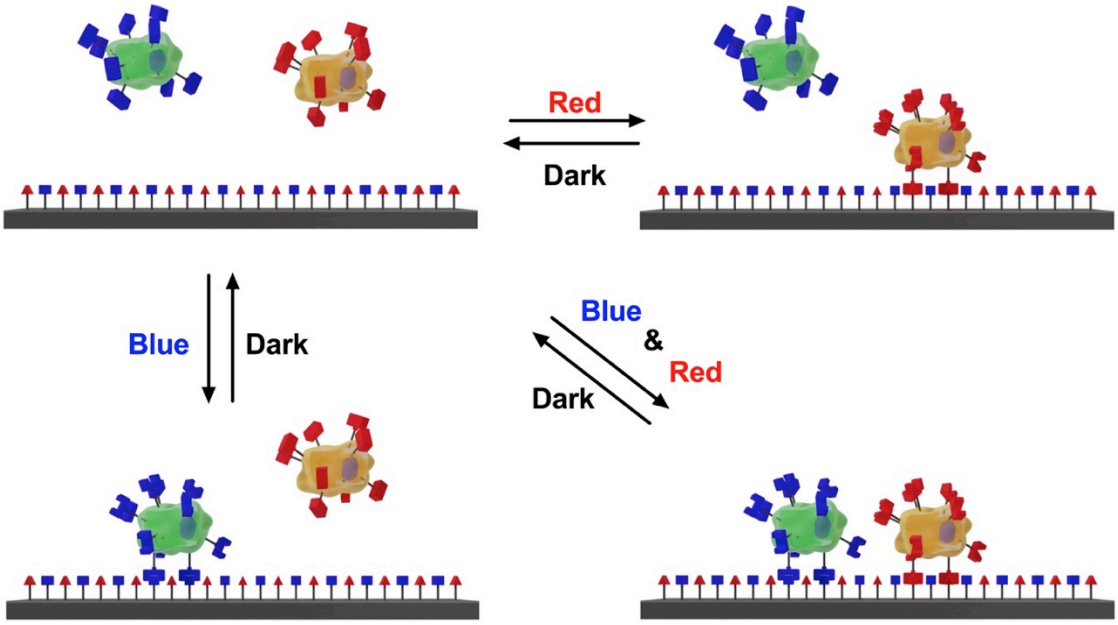

Figure 2.10 Schematic representation of orthogonal and reversible control of cell-material interactions. Cells that express CRY2 (green cell) or PhyB (orange cell) on their surfaces orthogonally bind to substrates presenting CIBN and PIF6 under blue or red light, respectively. In the dark neither of the cells binds to the substrate. Under blue light only CRY2 cells and under red light only PhyB cells bind to the substrate. Both CRY2 and PhyB cells bind to the substrate under co-illumination with blue and red light. All binding events are reversible in the dark.

2.2.1 Cell lines, protein purification and characterization

To achieve blue and red light controlled-cell material interactions, one of the complementary heterodimers is displayed on the cell surface (CRY2 or PhyB) while the other partner (CIBN or PIF6) is presented on a functionalized non-adhesive substrate **(Figure 2.10)**. In order to display CRY2 and PhyB on the surfaces of the cells, the genes encoding these proteins were inserted into a plasmid (pDisplay) having an N-terminal Igκ leader sequence to lead the proteins into the secretory pathway and a C-terminal transmembrane domain of the platelet derived growth factor receptor (PDGFR). Subsequently, MDA-MB-231 cells were transfected with pDisplay-CRY2-mCherry and pDisplay-PhyB-YFP plasmids to yield MDA-CRY2 and MDA-PhyB stable cell lines that constantly express these proteins on their surfaces. The fluorescence from the fused mCherry and YFP proteins in the stable cell lines was detected in confocal imaging. This showed the expression of the CRY2 and PhyB fused to fluorescent proteins inside and on the surfaces of the cells **(Figure 2.11A)**. Meanwhile, PIF6 and CIBN were cloned into a pET21b vector, which includes an N-

terminal His_6 sequence. After bacterial expression of CIBN and PIF6 in *E. coli*, these proteins were purified by affinity and size exclusion chromatography. The purified proteins were characterized with SDS-PAGE **(Figure 2.11B)**, which showed that the bands for CIBN-GFP-His_6 and PIF6-CFP-His_6 were at 50 and 40 kDa, respectively, corresponding to their molecular weight and that both proteins were pure after two-step purification indicated by the presence of single bands for each. For immobilization of CIBN and PIF6, a glass surface was functionalized with azide terminated poly(ethylene glycol) (PEG-N_3) through silanization reaction to obtain a non-adhesive area. Subsequently, an alkyne with an NTA group was clicked through copper catalyzed azide alkyne cycloaddition (CuAAC) reaction (Section 6.2).[132] Then, these surfaces were incubated first with 100 mM $NiCl_2$, then with 10 µM CIBN and/or PIF6 to achieve His_6-Ni^{2+}-NTA coordination for immobilization.

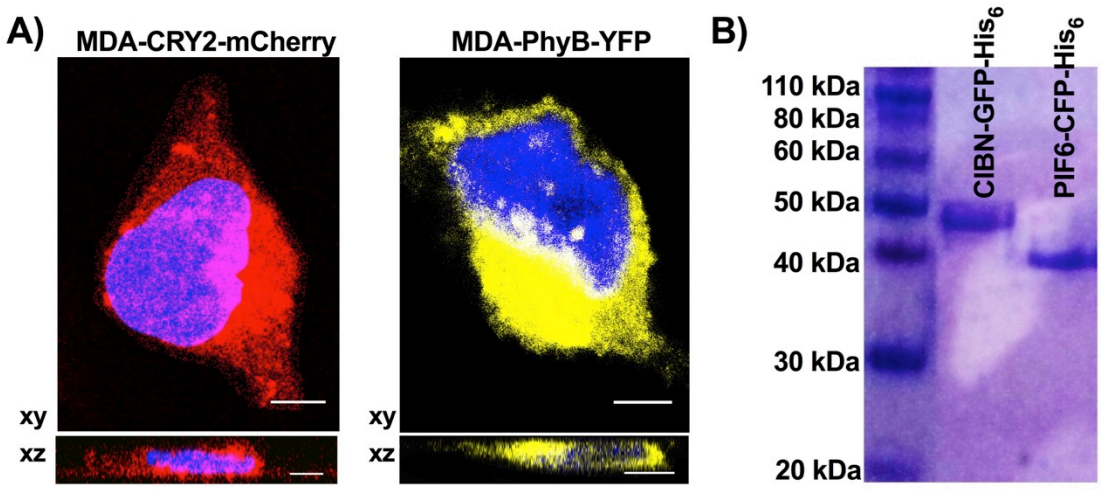

Figure 2.11 Characterization of stable cell lines and purified proteins. A) Confocal images of MDA-CRY2 and MDA-PhyB stable cell lines. Red: mCherry, Yellow: YFP, Blue: nuclear stain. Scale bar: 5 µm. **B)** SDS-PAGE of the purified CIBN-GFP-His_6 (50 kDa) and PIF6-CFP-His_6 (40 kDa) shows that both of the proteins were obtained purely after two-step purification.

In order to show these proteins are immobilized specifically through this coordination, their binding was measured with QCM-D as a change in the frequency **(Figure 2.12)**. SiO_2 QCM-D sensors were functionalized in the same way as described before for the glass surfaces. The sensors were washed with a buffer containing 300 mM NaCl, 50 mM TRIS at pH 7.4 (Buffer A) until the baseline was reached. Then, the proteins were flushed on the sensors and incubated approximately for 15 min until a plateau was reached. The sensors were washed once again with Buffer A to remove

unspecifically bound proteins. The net frequency change was 13 Hz for CIBN and 15 Hz for PIF6. His_6-Ni^{2+}-NTA coordination can be broken in the presence of competitive ligands as imidazole. Hence, the sensors were washed with Buffer A containing 250 mM imidazole (Buffer B) and the frequency increased since all the protein was washed off from the surfaces of the sensors. The sensors were washed further with Buffer A until the frequency was back to its baseline. The big change in frequency during this last washing step was due to the removal of imidazole.

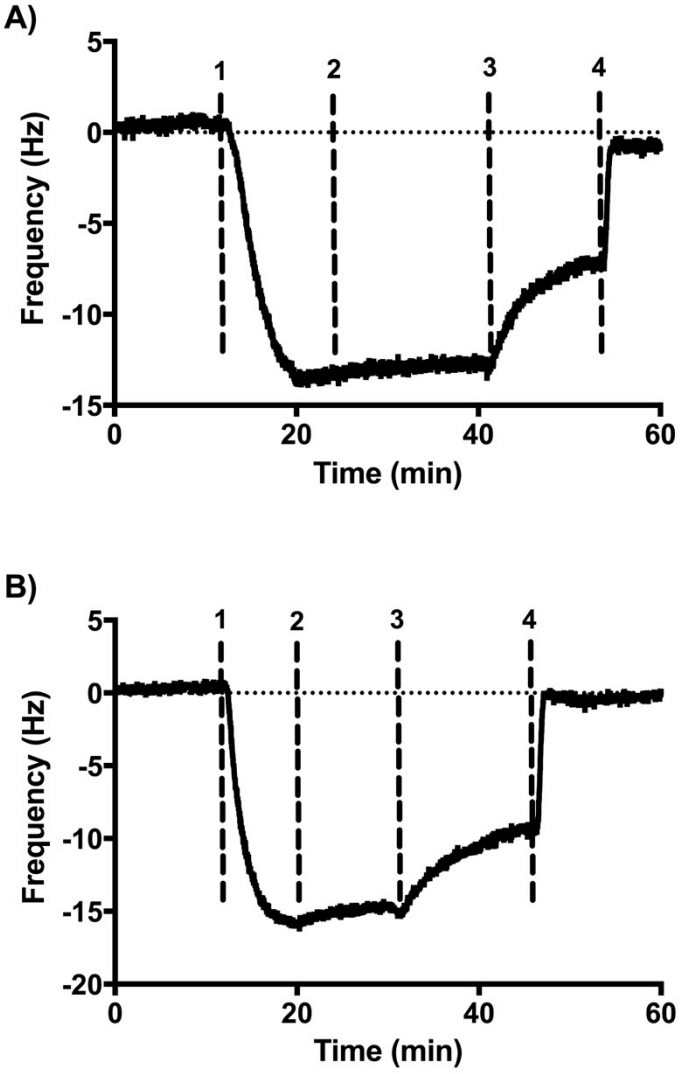

Figure 2.12 Frequency vs Time plots from QCM-D measurements to show protein immobilization through His_6-Ni^{2+}-NTA coordination. A) CIBN-GFP-His_6 showed a net frequency change of 13 Hz **B)** PIF6-CFP-His_6 showed a net frequency change of 15 Hz. Both of the proteins could be immobilized through His_6-Ni^{2+}-NTA coordination and this coordination was broken in the presence of imidazole. 1: protein, 2: Buffer A, 3: Buffer B, 4: Buffer A.

2.2.2 Blue and red light induced cell adhesion

After it was confirmed that the proteins could be immobilized to the NTA-functionalized glass surfaces specifically through His_6-Ni^{2+}-NTA coordination, CIBN and PIF6 were immobilized first separately on the Ni^{2+}-NTA functionalized glass surfaces. The cells expressing CRY2 and PhyB were seeded on CIBN and PIF6 functionalized substrates, respectively, and incubated in dark and under blue (480 nm) or red light (673 nm) illumination for 2 hours. Then, the cells were fixed and the nuclei were stained with DAPI. Then, the fluorescence images from DAPI channel were obtained from a total area of 1 cm^2. The number of cells (object with an area between 50-5000 μm^2) was calculated in dark and under light illumination by the analyze particles tool in ImageJ **(Figure 2.13)**. A PEGylated surface without any protein immobilization was used as a negative control. The number of CRY2 cells adhered to the CIBN functionalized substrates was calculated as 250 cells/cm^2 under blue light illumination, which is 5-fold more compared to the dark. It was observed that there was no significant difference in the number of cells cultured in dark and on the negative control (PEG). Similarly, the number of PhyB expressing cells was calculated as 300 cells/cm^2, also 5-fold higher compared to the dark.

In order to test whether these two systems are orthogonal to each other, CRY2 cells were illuminated with red light and PhyB cells with blue light **(Figure 2.13)**. In both cases, the number of cells that attached to the surfaces was similar to the dark and the negative control. That is, MDA-CRY2-mCherry cells did not interact with CIBN functionalized substrates under red light and MDA-PhyB-YFP cells were not found to interact with PIF6 functionalized substrates under blue light. This demonstrates that these systems are exclusively responsive to their corresponding wavelengths, which provides an orthogonal and selective system to control cell-material interactions with two different wavelengths of visible light.

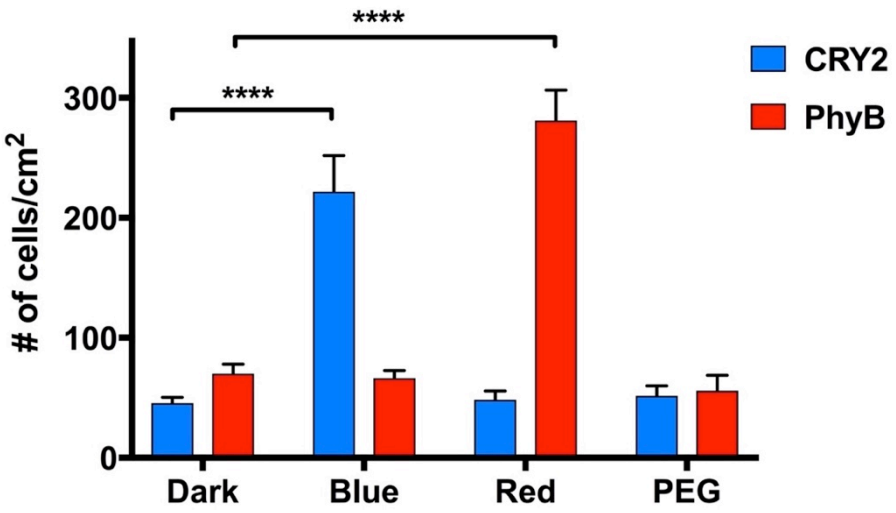

Figure 2.13 Quantification of light controlled cell-material interactions. MDA-CRY2 cells bound to CIBN functionalized substrates only under blue light but not in the dark or under red light. Likewise, MDA-PhyB cells attached to PIF6 functionalized substrates only under red light but not in dark or under blue light. The error bars are the standard error of three technical replicates with three biological replicates in each (n = 9), unpaired t-test is used as statistical test (p value <0,0001 (****)).

2.2.3 Cell spreading by photoswitchable interactions

In order to see whether the synthetic photoswitchable interactions are strong enough to induce cell spreading like in the integrin mediated adhesions, the adhesion area of cells on their complementary partners was compared to that of on the bare glass. For this, MDA-CRY2-mCherry cells were seeded on CIBN functionalized substrates and MDA-PhyB-YFP cells were seeded on PIF6 functionalized substrates. At the same time, these cells were cultured on bare glass substrates. Phalloidin-TRITC was used to stain actin cytoskeleton and Cell Outliner in ImageJ was used to determine the spreading area of randomly selected cells (n=30) **(Figure 2.14A)**. It was observed that there was no significant difference in spreading area of the cells on their complementary proteins and on glass **(Figure 2.14B)**.

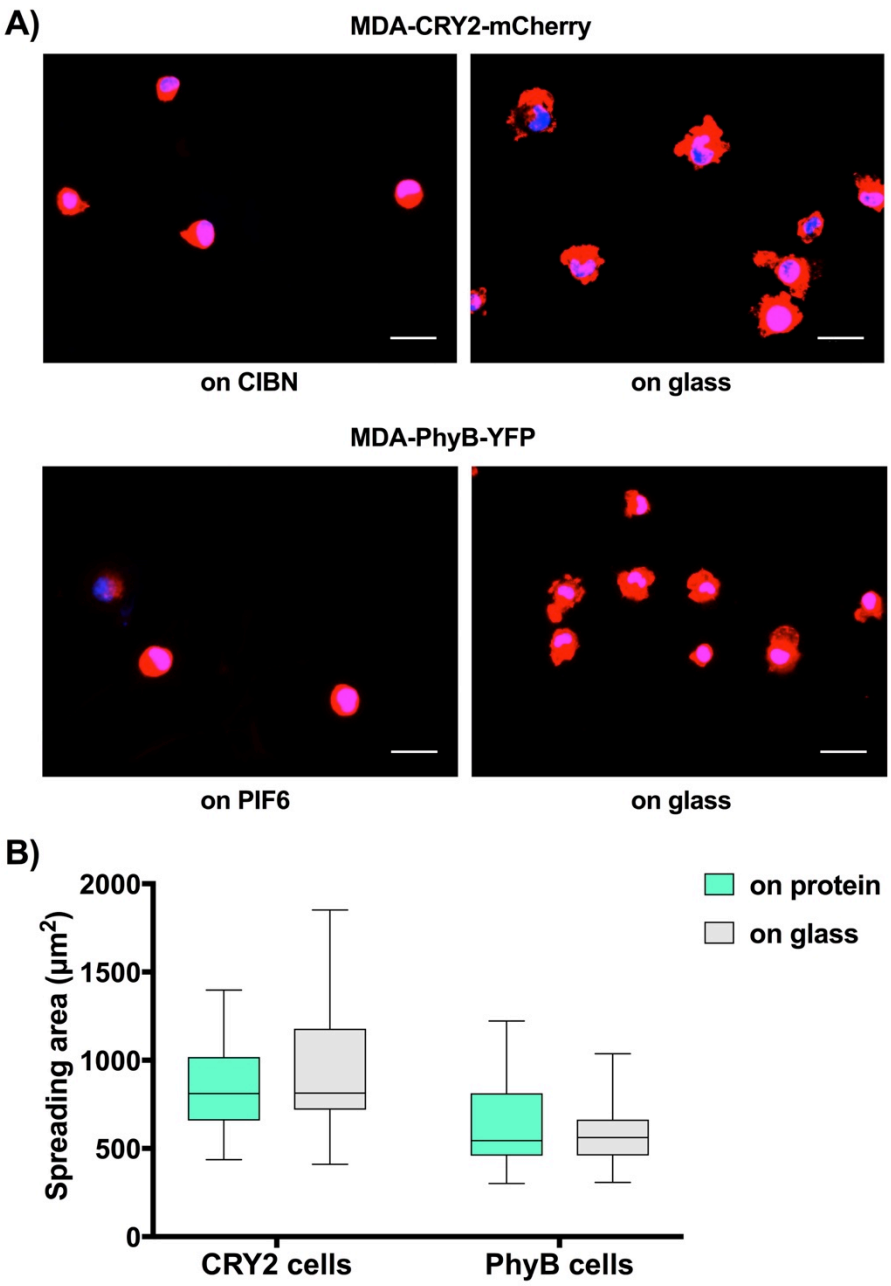

Figure 2.14 Spreading area of CRY2 and PhyB expressing cells. A) Fluorescence images of MDA-CRY2 and MDA-PhyB cells on their complementary substrates under light illumination and on glass. Red: actin, Blue: nuclear stain. Scale bar: 40 μm. **B)** Quantification of spreading area of PhyB and CRY2 expressing cells on their complementary proteins and on bare glass. For both cell types, there was no significant difference between their spreading area when they adhered to protein functionalized substrates or to the glass. The error bars are the standard error of the mean of the area measurements from 30 cells.

Then, confocal imaging was done to monitor the morphology of the cells adhered on the protein functionalized substrates and on the glass. The main difference between the light dependent cell adhesion and the integrin-mediated adhesions on the glass

substrates is the structure of the actin network **(Figure 2.15)**. While the native integrin mediated adhesions link to the actin network and lead to the formation of actin fibres, the artificial photoswitchable cell adhesions are not connected to the actin network and actin remains homogenously distributed in the cell.

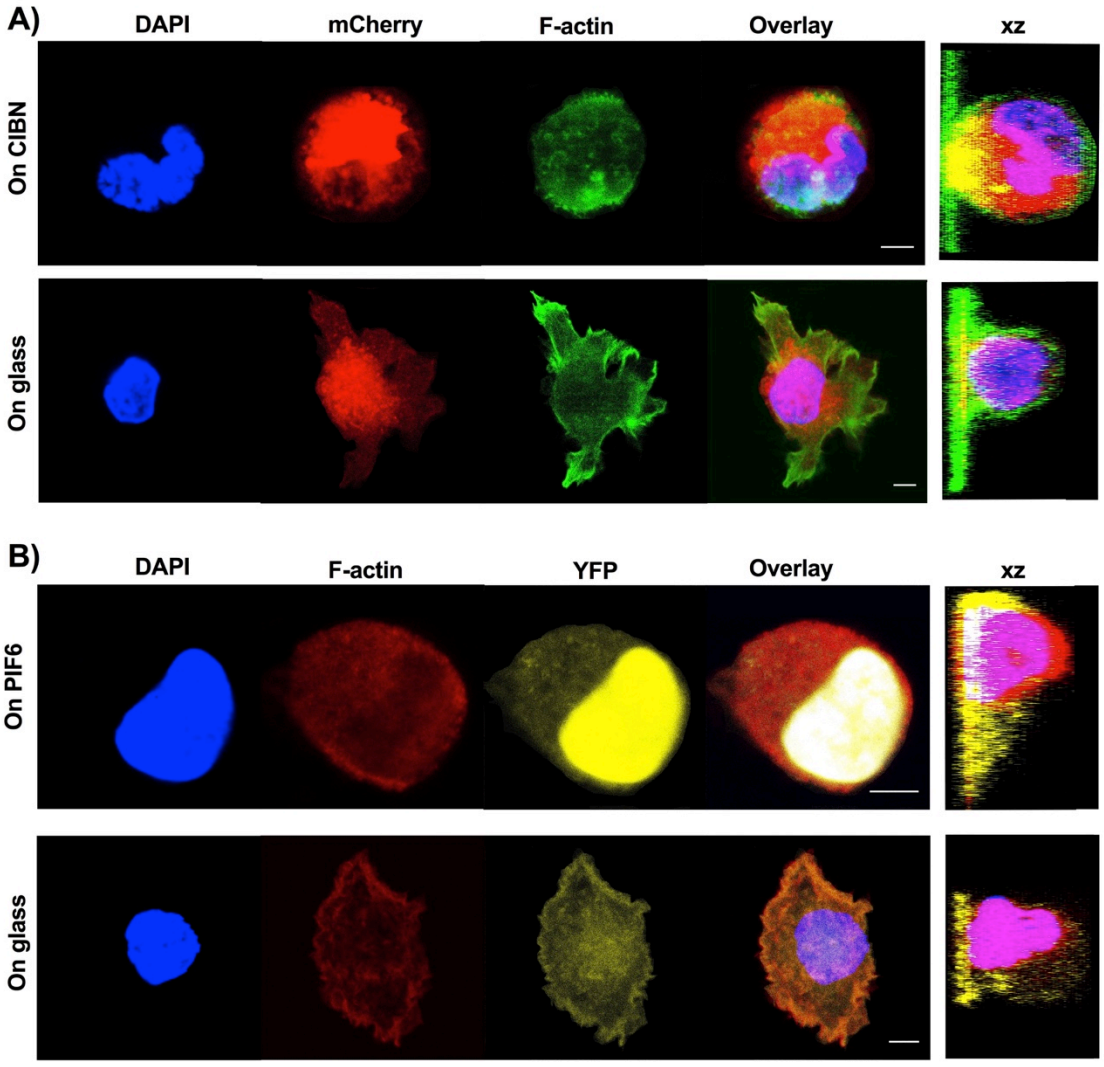

Figure 2.15 Confocal images for comparison of morphology of CRY2 and PhyB expressing cells on protein and glass substrates. A) MDA-CRY2-mCherry cells on CIBN functionalized substrates under blue light and on glass. Red: mCheery, green: actin (phalloidin-FITC), blue: nuclear stain. **B)** MDA-PhyB cells on PIF6 functionalized substrates under red light and on glass. Red: actin (phalloidin-TRTIC), yellow: YFP, blue: nuclear stain. The cells were stained for their nucleus and actin cytoskeleton and fluorescence signal from the stable cell lines was also detected. Scale bar: 5 µm.

2.2.4 Adhesion and reversion kinetics

For further characterization of light-dependent cell adhesion, a kinetic study was done to determine the time needed for cell adhesion to the surface and for reversion **(Figure 2.16)**. For adhesion kinetics, the CRY2 and PhyB cells were seeded on the CIBN and PIF6 functionalized surfaces (t=0), respectively, and incubated for 30, 60, 90 and 120 min under blue or red light and in the dark. At each time point, three samples were fixed, stained with DAPI and the total cell number/cm^2 was determined. It was observed that MDA-CRY2-mCherry cells reached saturation after 30 min incubation, while PhyB expressing cells showed slower kinetics and reached saturation after 60 min **(Figure 2.16A)**. It was observed that the number of CRY2 and PhyB expressing cells that adhere under blue and red light are about the same.

For reversion kinetics, the CRY2 and PhyB expressing cells were first incubated under blue and red light, respectively, for 1 hour on their complementary substrates and then they were taken in the reversion conditions. CRY2-CIBN interaction can only be reversed in the dark and PhyB-PIF6 heterodimerization can reverse both in dark and under far-red light (750 nm) illumination. After 1 h blue or red light illumination, both of the cell types were incubated in dark for 30, 60, 90 and 120 min. In addition, substrates with PhyB expressing cells were also incubated under far-red light illumination for 5, 15 and 30 min **(Figure 2.16B)**. CRY2 and PhyB cells were also incubated only in the dark and on PEG (negative control) in order to see whether the reversions would be complete. For both CRY2-CIBN and PhyB-PIF6 interactions, a complete reversion could be achieved after 2 hours incubation in the dark. With far-red illumination PhyB-PIF6 interaction could be reversed completely in 30 min **(Figure 2.16B)**. These findings confirm that these cell-material interactions based on the blue and red light switchable proteins are reversible and that the PhyB/PIF6 mediated interactions can be turned off orthogonally.

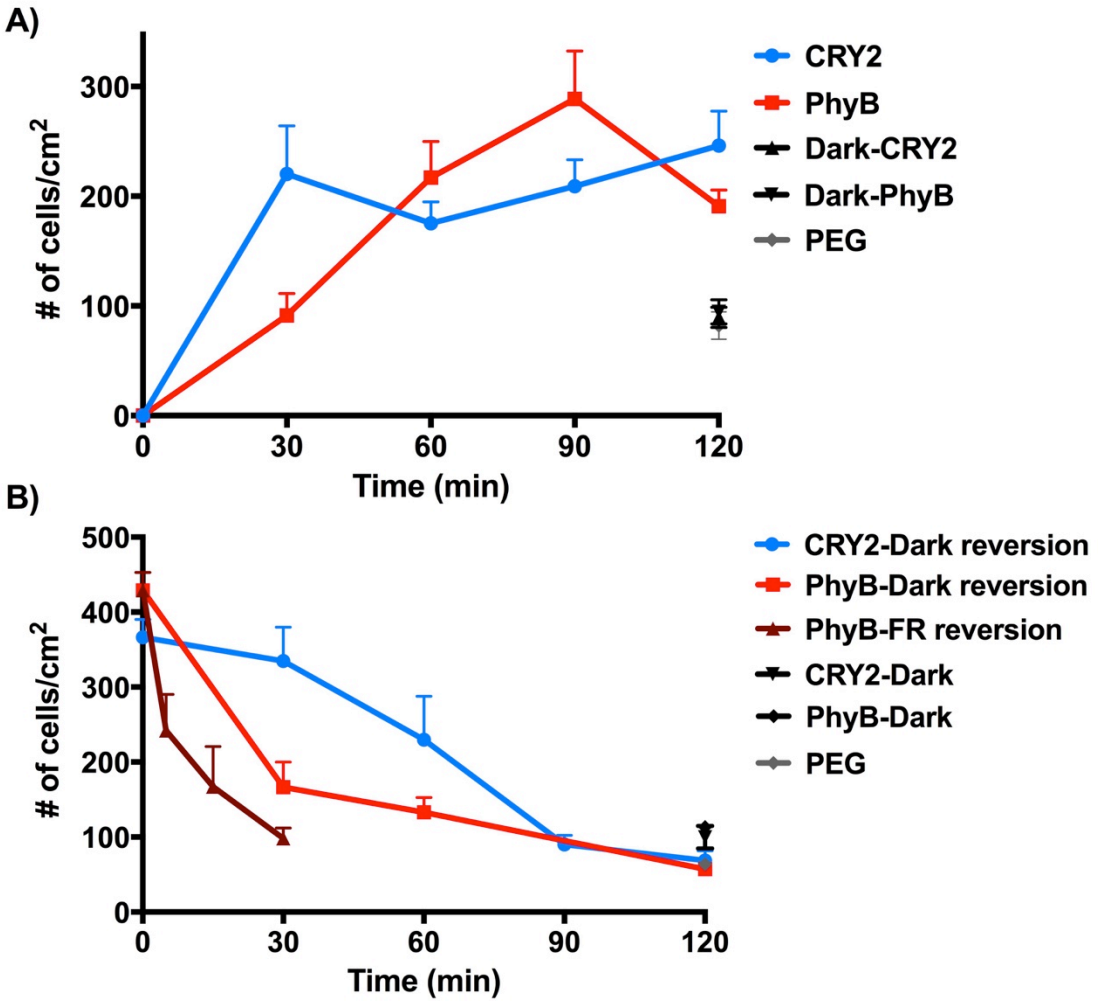

Figure 2.16 A) Adhesion kinetics **B)** Reversion kinetics of light controlled cell-material interactions. The error bars are the standard error of three technical replicates with three biological replicates in each (n = 9), unpaired t-test is used as statistical test.

3.2.5 Orthogonal switching of cell adhesion

The main goal of this study is to control the adhesion of two cell types to a substrate orthogonally in space and time. Hence, the orthogonal interaction pairs, CRY2/CIBN and PhyB/PIF6, were used for orthogonal switching. For this, the glass surfaces were functionalized with Ni^{2+}-NTA groups as described above. Then, 10 µM CIBN and PIF6 proteins were premixed and incubated with the Ni^{2+}-NTA functionalized glass surfaces for co-immobilization. In order to distinguish the cell types on the substrates, CRY2 and PhyB expressing cells were pre-stained with red (DiI) and green (DiO) membrane intercalating fluorescent dyes, respectively. Again, a PEGylated nonadhesive glass substrate without protein immobilization was used as a negative

control. The cells were co-cultured under only blue, blue and red (co-illumination), only red light illumination and in dark for 2 hours. In the co-illuminated samples, PhyB and CRY2 cells were homogeneously distributed on the substrate **(Figure 2.17A)** and equally attached to it **(Figure 2.17B)**. On the other hand, none of the cell types adhered to the substrates in the dark and the number of cells in dark was comparable to that of on negative control. It was observed that when there was only red light, only PhyB cells bound to the substrate. Similarly, when there was only blue light illumination, only CRY2 cells attached. This demonstrates that this dual visible light responsive photoswitch provides an orthogonal control over cell-material interactions of multiple cell types and can be used to mimic real tissues, where cells can secrete and interact with different ECM components.

Although selective adhesion of multiple cell types to functionalized materials could be achieved with the current strategies such as modification of substrates with peptidomimetics as ligands for different integrins,[57,58] antibodies for specific cell surface markers,[59,62] ssDNA molecules,[60,61] and preformed micro- and nano-patterns, [63,64] these approaches do not provide spatiotemporal and reversible control. To achieve the spatiotemporal control over these interactions, light responsive functional molecules such as caging groups,[65-67] azobenzenes[68-70] and UCNPs[71,72] have been employed. Although azobenzenes and UCNPs provide reversible control with high spatiotemporal control, these platforms do not provide independent control over cell-material interactions in a multicellular environment. Additionally, these systems are responsive to UV light, which is invasive for the cells. Hence, CRY2/CIBN and PhyB/PIF6 mediated photoswitchable cell-material interactions provide a platform where cell-material interactions of multiple cell types can be controlled noninvasively, reversibly, independently and in a wavelength selective manner with high spatiotemporal resolution.

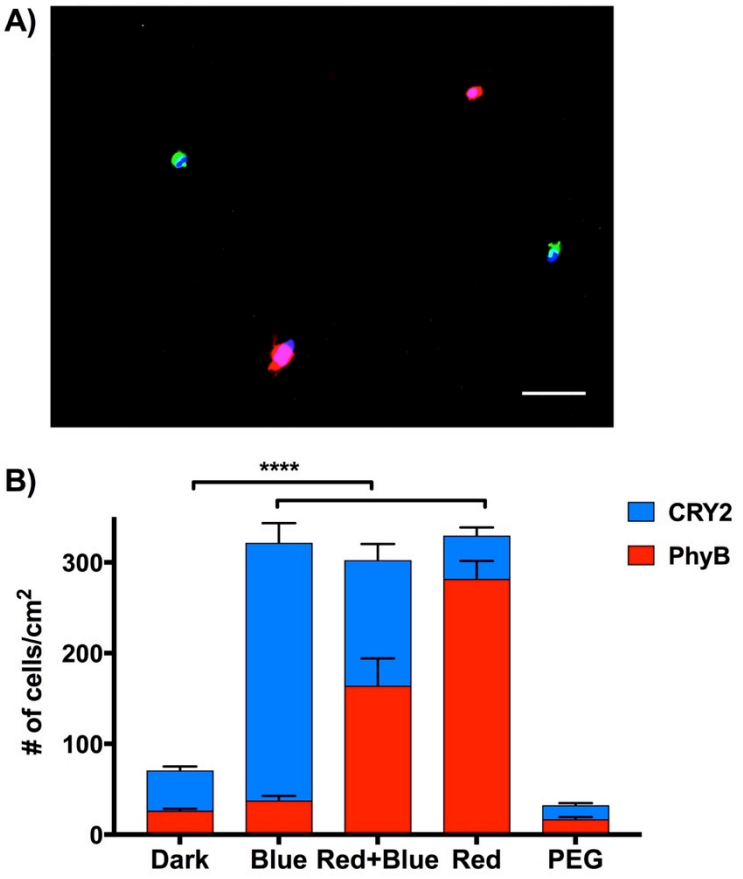

Figure 2.17 Orthogonal blue and red light switchable cell adhesions. A) Fluorescence image of MDA-CRY2-mCherry (in red) and MDA-PhyB-YFP (in green) cells on CIBN and PIF6 co-immobilized substrates under co-illumination with blue and red light. Both cell types equally adhered to the substrate. Scale bar: 75 µm. **B)** Quantification of the number of MDA-CRY2-mCherry and MDA-PhyB-YFP cells in dark, under red and blue co-illumination, only red or only blue light illumination. Number of cells were calculated from red (MDA-CRY2-mCherry) and green (MDA-PhyB-YFP) fluorescence channels. The error bars are the standard error of three technical replicates with three biological replicates in each (n=9), unpaired t-test is used as statistical test (p value <0,0001 (****)).

Chapter 3

Summary and Outlook

3. Summary and Outlook

Cells interact with the extracellular matrix and neighboring cells forming cell-cell and cell-matrix contacts, which are mainly mediated by cadherins and integrins, respectively. These processes are dynamic and are both spatially and temporally tightly regulated during many biological events including embryogenesis, wound healing and cancer development. Controlling these interactions is crucial for both understanding the biochemical machinery and for several applications in biomedicine such as bottom-up tissue engineering, medical implantation and developing cell-based screening devices. Current approaches for controlling cell-cell or cell-matrix contacts are limited in terms of dynamicity, reversibility, sustainability, bio-orthogonality, high spatiotemporal resolution and noninvasiveness. In this thesis, genetically encodable blue and red light switchable cell contacts were developed to overcome all the above-mentioned limitations.

In the first part of this project, blue light switchable cell-cell interactions by using the blue light-dependent heterodimerization of CRY2 and CIBN was developed. Cell-cell contact formation was induced between MDA-CRY2-mCherry and MDA-CIBN-GFP cells under blue light. This interaction was reversed by simply switching the blue light off. It was also shown in this study that blue light dependent CRY2-CIBN heterodimerization could be further developed to form microtissues layer-by-layer in the direction of bottom-up tissue engineering.

The CRY2-CIBN mediated photoswitchable cell-cell interactions have key features of native cell-cell interactions; hence, provide unmatched advantages over the current platforms. First of all, the control with light makes it possible to induce these interactions with unmatched precision in space and time. The low intensity blue light that triggers these cell-cell interactions is noninvasive for the cells. These interactions are dynamic and reversible, which enables manipulation of cell-cell interactions over time. Additionally, these protein-based photoswitches are well-suited to sustainably control the cell-cell interactions over a long period of time because they are genetically encodable and new proteins are expressed in the cells as they degrade

and the cell divides. Finally, the high specificity of the CRY2-CIBN heterodimerization provides specific induction of heterophilic interactions but not homophilic ones.

In this study only the extracellular domains of E-cadherins was mimicked by CRY2 and CIBN to induce cell-cell contacts; hence, there is no link to the actin cytoskeleton or any scaffold proteins that transmit signals inside the cells as happens upon native cell-cell contact formation. However, by addition of the cytosolic tail of cadherins to the blue light-induced heterodimerization system, this bridge to the actin cytoskeleton could be achieved and used for studying signaling mechanisms, cell migration and mechanotransduction upon cell-cell contact formation. Furthermore, the current 2D system can be transferred into 3D spheroid cultures to study cell-sorting behavior with and without link to the actin cytoskeleton in order to observe the impact of interfacial tension.

In the second part of the project, orthogonal blue and red light switchable cell-material interactions of multiple cell types were developed. The adhesion of cells expressing CRY2 or PhyB to the CIBN and PIF6-functionalized substrates was achieved depending on blue or red light illumination, respectively. This adhesion was reversed in the dark or under far-red light illumination. The time needed for cell attachment and detachment was also determined from the kinetic studies. It was also shown in this study that cell spreading area due to photoswitchable interactions was similar to the integrin mediated spreading area. The cells were only differing in their morphology; while the integrin mediated adhesions led to the rearrangements of the actin cytoskeleton, actin was homogeneously distributed in the cells that are adhered through photoswitchable interactions. Finally, depending on the wavelength of the light, adhesion of either CRY2 or PhyB, or both cell types to their substrate was also shown.

The CRY2/CIBN and PhyB/PIF6 mediated photoswitchable cell-material interactions have key features of native ones; hence, they are advantageous compared to the current platforms. First of all, the control with light makes provides high spatial and temporal resolution. The low intensities of blue and red light that triggers these cell-

material interactions are noninvasive for the cells. Additionally, these photoswitchable cell-material interactions are reversible; hence, it is possible to dynamically attach and detach a specific cell type. Finally, it was shown that this system is suitable for independent and wavelength selective cell adhesion of different cell types due to the orthogonality of the blue and red light responsive systems.

Here, both the ECM components and integrins were mimicked but once again there is not any link to the actin cytoskeleton. This study showed that PhyB and CRY2 cells could spread on their complementary protein functionalized substrates only without forming actin fibers. An actin link can be added by fusing cytosolic tail of the integrin β-subunit, which interacts with actin cytoskeleton through adaptor proteins, to CRY2 and PhyB and focal adhesions can be studied with high spatiotemporal resolution. This orthogonal blue and red light dependent heterodimerization system can also be integrated into hydrogel systems, where 3D ECM can be achieved, depending on the protein stability under the hydrogel preparation conditions.

Last but not least, there are more visible light responsive proteins engineered as optogenetic tools, which are used to control intracellular and receptor signaling pathways.[82,84,85,129,133] These tools can also be introduced to control cell-cell and cell-material contacts by visible light to open a new door for developments in tissue engineering and biomedicine, where dynamic and high spatiotemporal control over cell interactions is required.

Chapter 4

Materials and Methods

4. Materials and Methods

4.1 Equipment list

General laboratory equipment	
Amersham Imager 600	GE Healthcare Europe GmbH, Freiburg, Germany
Cell culture hood (Herasafe™)	Thermo Fisher Scientific Germany BV & Co KG, Braunschweig,Germany
Centrifuges	
5417R centrifuge	Eppendorf AG, Hamburg, Germany
5702R centrifuge	Eppendorf AG, Hamburg, Germany
Avanti J-26XP centrifuge (JA-10, JA-25.50 rotors)	Beckman Coulter Inc., Brea, USA
Rotina R380 centrifuge	Andreas Hettich GmbH & Co. KG, Tuttlingen, Germany
Electroporator (GenePulser Xcell™)	Bio-Rad Laborotories, Inc. Munich, Germany
Gel electrophoresis	Bio-Rad Laborotories, Inc. Munich, Germany
Agarose gel	
SDS gel	
GFL Water bath	ProfiLab24 GmbH, Berlin, Germany
Hemacytometer	Laboroptik Ltd., Lancing, United Kingdom
HiLoad™ 16/600 Superdex™ 200 pg	GE Healthcare Europe GmbH, Freiburg, Germany
HisTrap™ HP	GE Healthcare Europe GmbH, Freiburg, Germany
HPLC- ÄKTA Pure	GE Healthcare Europe GmbH, Freiburg, Germany
Incubators	
Cell culture incubator (culturing)	Thermo Fisher Scientific Germany BV & Co KG, Braunschweig,Germany
Cell culture incubator (experimental)	Thermo Fisher Scientific Germany BV & Co KG, Braunschweig,Germany
Excella E24R incubator shaker	New Brunswick Scientific Co., Inc., Enfield, USA
Minitron shaker	Infors AG, Bottmingen/Basel, Switzerland
Plate incubator	VWR International LLC., Radnor, PA, USA
Lamps	
Bulbs (red, blue and far-red), 15 Watts	Osram GmbH, Munich, Germany
FloraLED 230V/50Hz 2A Modell V10 with TS110-Controller	CLF PlantClimatics GmbH, Wertingen, Germany
ND 1000 Spectrophotometer	PEQLAB Biotechnologie GmbH,

Omni Sonic Ruptor 400 Ultrasonic homogenizer	Omni International Inc., Tulsa, USA
Pipette boy and micro pipettes	Eppendorf AG, Hamburg, Germany
Plasma system (100-E)	TePla, Kirchheim, Germany
Plate reader (Infinite M200)	Tecan Group Ltd., Männedorf, Switzerland
QCM-D Q-sense E4 SiO_2 QCM-D sensors (QSX 303)	Q-Sense, Västra Frölunda, Sweden
Rotary evaporator (Laborota 4000)	Heidolph Instruments GmbH & Co. KG, Schwabach, Germany
Sonication bath	BANDELIN electronic GmbH & Co. KG, Berlin, Germany
Thermocycler (T100™)	Bio-Rad Laboratories, Inc. Munich, Germany
UV-VIS spectrophotometer	Lambda25, Perkin Elmer, Germany
Vortex (Reax Top)	Heidolph Instruments GmbH & Co. KG, Schwabach, Germany

Microscopes

Bright field microscope	Carl Zeiss Microscopy GmbH, Jena, Germany
Zeiss Axiovert 40C 10x air lens objective (A-Plan 10X/0,25 Phase contrast) Digital Sight DS-2Mv Camera	Nikon GmbH, Düsseldorf, Germany
Confocal microscope Zeiss LSM 880 inverted microscope UV diode (405 nm), Ar laser (488 nm), HeNe laser (633 nm) ZEN black2.0 software 63x/1.4 oil-immersion objective	Carl Zeiss Microscopy GmbH, Jena, Germany
Delta Vision Olympus IX inverted microscope Delta Vision RT system Cooled CCD camera Resolve 3D software 20x air lens objective UPlanFI 20x/0.50 phase contrast	Olympus Deutschland GmbH, Hamburg, Germany Applied Precision Inc., Issaquah, USA Photometrics, Tucson, USA Applied Precision Inc., Issaquah, USA Carl Zeiss AG, Jena, Germany
Fluorescence microscope Leica DM6000B upright microscope EL6000 external light source with aliquid optical fiber DFC 365 FX camera LAS AF 3.1.0 software 10x air lens (HCX PL APO 10X/0.40)	Leica Microsystems GmbH, Wetzlar, Germany

20x air lens (HCX PL APO 20X/7)
40x air lens (HCX PL APO 40X/0.85)

Chemicals	
Acetic acid	J.T> Baker, Deventer, Netherlands
Agarose	Carl Roth GmbH &Co. KG, Karlsruhe, Germany
Antibiotics	
Ampicillin	Carl Roth GmbH &Co. KG, Karlsruhe, Germany
Geneticin (G418)	Gibco by Life Technologies, distributed by Thermo Fisher Scientific BV & Co KG, Braunschweig, Germany
Kanamycin	Carl Roth GmbH &Co. KG, Karlsruhe, Germany
Penicillin/Streptomycin	Gibco by Life Technologies, distributed by Thermo Fisher Scientific BV & Co KG, Braunschweig, Germany
Brilliant blue	Sigma Aldrich, Munich, Germany
Citric acid	Sigma Aldrich, Munich, Germany
Chloroform	Merck KGaA, Darmstadt, Germany
$CuSO_4.5H_2O$	Grüssing GmbH Analytika, Filsum, Germany
Diethylether	Sigma Aldrich, Munich, Germany
DMSO	Sigma Aldrich, Munich, Germany
DTT	Sigma Aldrich, Munich, Germany
EDTA	Sigma Aldrich, Munich, Germany
Ethanol	Carl Roth GmbH &Co. KG, Karlsruhe, Germany
Ethyl acetate	Merck KGaA, Darmstadt, Germany
Glycerol	Sigma Aldrich, Munich, Germany
Glycine	Sigma Aldrich, Munich, Germany
H_2O_2 (33 %)	AppliChem, GmbH, Darmstadt, Germany
H_2SO_4 (96%)	Merck KGaA, Darmstadt, Germany
Imidazole	Sigma Aldrich, Munich, Germany
L-Ascorbic acid	Sigma Aldrich, Munich, Germany
Methanol	Carl Roth GmbH &Co. KG, Karlsruhe, Germany
MTT	Sigma Aldrich, Munich, Germany
NaCl	Sigma Aldrich, Munich, Germany
$NaHCO_3$	Sigma Aldrich, Munich, Germany
$NiCl_2.6H_2O$	Sigma Aldrich, Munich, Germany
NTA alkyne	Synthesized by Julia Ricken[134,135]
Paraformaldehyde	Sigma Aldrich, Munich, Germany
PEG-N_3	Rapp Polymer GmbH, Tübingen, Germany
PMSF	Sigma Aldrich, Munich, Germany

Ponceau	Sigma Aldrich, Munich, Germany
SDS	Carl Roth GmbH &Co. KG, Karlsruhe, Germany
Toluene	Merck KGaA, Darmstadt, Germany
Triethyl amine	Sigma Aldrich, Munich, Germany
TRIS-base	Carl Roth GmbH &Co. KG, Karlsruhe, Germany
Triton X-100	Sigma Aldrich, Munich, Germany
Tween-20	Carl Roth GmbH &Co. KG, Karlsruhe, Germany

Biologicals

Antibodies	
Anti-mouse AlexaFluor 488 catalogue #: A-11029	Thermo Fisher Scientific Germany BV & Co KG, Braunschweig,Germany
anti-c-*myc* (catalogue #: DLN-07720)	Dianova GmbH,Hamburg, Germany
Bacterial medium Agar LB	Carl Roth GmbH &Co. KG, Karlsruhe, Germany
Cell culture medium DMEM: F12 DMEM:F12 without phenol red OPTI-MEM	Gibco by Life Technologies, distributed by Thermo Fisher Scientific BV & Co KG, Braunschweig, Germany
DAPI	Sigma Aldrich, Munich, Germany
DiI	Sigma Aldrich, Munich, Germany
DiO	Sigma Aldrich, Munich, Germany
DNA gel loading dye	Thermo Fisher Scientific BV & Co KG, Braunschweig, Germany
DNA ladder (0.1-10 kb)	NEB GmbH, Frankfurt am Main, Germany
DNA stain G	SERVA Electrophoresis GmbH, Heidelberg, Germany
Enzymes	
Accutase	Gibco by Life Technologies, distributed by Thermo Fisher Scientific BV & Co KG, Braunschweig, Germany
HF Phusion DNA polymerase	NEB GmbH, Frankfurt am Main, Germany
Restriction enzymes AscI, BglII, DpnI, NdeI, PstI-HF SacII, SalI, XhoI, XmaI	NEB GmbH, Frankfurt am Main, Germany
T4 DNA ligase	NEB GmbH, Frankfurt am Main, Germany
Trypsin-EDTA (0.05%)	Thermo Fisher Scientific BV & Co KG, Braunschweig, Germany
FAD	Sigma Aldrich, Munich, Germany
Kits	
Gel extraction	QIAGEN Inc., Hilden, Germany

Lipofectamine® 2000 Transfection Reagent	Thermo Fisher Scientific BV & Co KG, Braunschweig, Germany
MiniPrep	QIAGEN Inc., Hilden, Germany
PCR purification	QIAGEN Inc., Hilden, Germany
Site-directed mutagenesis	Agilent Technologies, Santa Clara, CA, USA
L-Glutamine (200 mM)	Gibco by Life Technologies, distributed by Thermo Fisher Scientific BV & Co KG, Braunschweig, Germany
MDA-MB-231 cell line	ATCC®, Wesel, Germany
Milk powder (low fat)	Carl Roth GmbH &Co. KG, Karlsruhe, Germany
Mowiol 488	Carl Roth GmbH &Co. KG, Karlsruhe, Germany
Novex™ Prestained Protein Standard	Thermo Fisher Scientific BV & Co KG, Braunschweig, Germany
NuPAGE® Antioxidants	Thermo Fisher Scientific BV & Co KG, Braunschweig, Germany
NuPAGE® LDS Sample buffer	Thermo Fisher Scientific BV & Co KG, Braunschweig, Germany
NuPAGE® MOPS SDS running buffer	Thermo Fisher Scientific BV & Co KG, Braunschweig, Germany
PBS tablets	Gibco by Life Technologies, distributed by Thermo Fisher Scientific BV & Co KG, Braunschweig, Germany
Plasmids	
pAL149 (22275)[115]	Addgene, Teddington, United Kingdom
pAL175 (22276)[115]	Addgene, Teddington, United Kingdom
pCIBN(deltaNLS)-pmGFP (26867)[91]	Addgene, Teddington, United Kingdom
pCRY2FL(deltaNLS)-mCherryN1 (26871)[91]	Addgene, Teddington, United Kingdom
pDisplay (V660-20)	Invitrogen by Life Technologies, distributed by Thermo Fisher Scientific BV & Co KG, Braunschweig, Germany
pDisplay-AP-CFP-TM (20861)[136]	Addgene, Teddington, United Kingdom
pDisplay-FLIPE-600n (13545)[137]	Addgene, Teddington, United Kingdom
pET21b (69741-3)	Novagen, EMD Chemical Inc., San Diego CA, USA
Phalloidin-TRITC	Sigma Aldrich, Munich, Germany
Primers	Integrated DNA Technologies Inc., Leuven, Belgium
Spirulina (for PCB isolation)	Rainforest Foods, Sheffield, UK

Disposables	
Amicon Ultra-15 centrifugal filter units 100K, 50 mL	Merck KGaA, Darmstadt, Germany
Cell culture flasks (25 and 75 cm^2)	Greiner CELLSTAR®, Sigma Aldrich, Munich, Germany

Cell scraper	Greiner CELLSTAR®, Sigma Aldrich, Munich, Germany
Cellulose filters (0.2 and 0.45 µm)	Carl Roth GmbH &Co. KG, Karlsruhe, Germany
Cover slips (20 x 20, 24 x 24 mm)	Carl Roth GmbH &Co. KG, Karlsruhe, Germany
Cryovials (2 mL)	Greiner CELLSTAR®, Sigma Aldrich, Munich, Germany
Electroporation cuvettes (1 mm)	Sigma Aldrich, Munich, Germany
Eppendorf tubes (0.5 mL, 1.5 mL, 2 mL)	Eppendorf AG, Hamburg, Germany
Falcon® tubes (15 mL, 50 mL)	Corning Inc., Kaiserlautern, Germany
Glass bottom dish (1.7 cm^2)	LabTek, Nalge Nunc. International, Rochester, NY, USA
Microscope slides	Carl Roth GmbH &Co. KG, Karlsruhe, Germany
Molecular sieves (3Å)	Carl Roth GmbH &Co. KG, Karlsruhe, Germany
Multi-well plates (6-well, 96-well)	Greiner CELLSTAR®, Sigma Aldrich, Munich, Germany
Petri dishes (10, 20, 60 cm^2)	Corning Inc., Kaiserlautern, Germany
Plastic pipettes (2 mL, 5 mL, 10 mL)	Greiner CELLSTAR®, Sigma Aldrich, Munich, Germany
UV-VIS semi-micro polystyrene cuvettes	Sigma Aldrich, Munich, Germany

Softwares
ChemDraw
EndNote X7
GraphPad Prism7
Image J 1.51f
Microsoft office (word, excel, power point)

4.2 Cloning

4.2.1 Vector design

For mammalian expression of proteins on the cell surface, pDisplay vector was chosen. pDisplay includes an N-terminal murine Igκ-chain leader sequence for secretion of the protein to the extracellular side of the plasma membrane and a C-terminal platelet derived growth factor receptor (PDFR) transmembrane (TM) domain, which anchors the protein to the plasma membrane. There is also a c-*myc* epitope expressed together with the recombinant proteins in pDisplay, which allows detection by immunofluorescence. For purification of proteins from bacteria, pET21b

vector was used. pET21b carries a C-terminal His_6-tag for protein purification and a *lac* operator for IPTG inducible protein expression.

All purchased plasmids were delivered in transformed *E. coli*. For plasmid isolation from bacteria, the cells were streaked on an LB agar plate containing 50 µg/ml ampicillin (for pAL149, pAL175, pDisplay and pET21b) or 35 µg/ml kanamycin (for pCRY2FL(deltaNLS)-mCherryN1 and pCIBN(deltaNLS)-pmGFP) and grown at 37^{o}C overnight. The colonies were grown in LB medium containing the corresponding antibiotics and plasmid DNAs were isolated with MiniPrep kit following the provider's instructions.

4.2.2 Polymerase chain reaction (PCR)

CRY2, CIBN, PhyB and PIF6 were PCR amplified with gene specific primers **(Table 4.1)** and inserted in pDisplay or in pET21b either by restriction enzyme digestion and following ligation or by Gibson assembly.

A general PCR protocol was as follows:

PCR mix (1x): total volume = 100 µl

Template (100 ng/µL)	0.5 µl
dNTPs (10 mM stock)	2 µl
Forwards primer (10 µM)	5 µl
Reverse primer (10 µM)	5 µl
HF phusion polymerase buffer (5x)	20 µl
HF phusion polymerase	1 µl
Distilled water	66.5 µl

PCR conditions:

Step 1) 95^{o}C, 1 min
Step 2) 95^{o}C, 30 sec
Step 3) 60^{o}C, 30 sec
Step 4) 72^{o}C, 30 sec-4 min (depending of the length of the insert, 1 min/kb)
Step 5) Go to step 2 (34 cycles)
Step 6) 72^{o}C, 10 min
Step 7) 4^{o}C, forever

All PCR mixtures were digested with 1 µl Dpn1 at 37^{o}C for 1 hr to degrade the template DNA and the PCR products were verified with agarose gel electrophoresis.

For this, 1% (w/v) agarose was prepared in TRIS-acetate-EDTA buffer (TAE buffer (1x): 40 mM TRIS base, 40 mM acetic acid, 1 mM EDTA, pH 8.3) and mixed with 4 µl of DNA stain G. Gel was run for 20 min at 120 volts.

Table 4.1 List of gene specific primers.

Gene	Primer	Vector
CRY2-mCherry (~2,5 kb)	FWD: 5'- CAGATCTCCCGCGATCCGCGGAATGAAGATGGACAAAAA GAC - 3'	pDisplay
	REV: 5'-GATGAGTTTTTGTTCGTCGACCTTGTACAGCTCGTCCAT GCC- 3'	
CIBN-GFP (~1 kb)	FWD: 5'- GATATACCCGGGATGAATGGAGCTATAGGAGG - 3'	pDisplay-FLIPE-600n
	REV: 5'- GATATAGTCGACCATAATTACACACTTTGTC - 3'	
PhyB (~3 kb)	FWD: 5'- CGGCCAGATCTCCCGGGATGGTTTCCGGAGTC - 3'	pDisplay
	REV: 5'- CGACCTGCAGCCGCGGGCTCGGGATTTGCAAG - 3'	
YFP (~0.5 kb)	FWD: 5'-ATCCCGAGCCCGCGGCAGTGCTGGTGTGAGCAAGGGCG - 3'	pDisplay
	REV: 5'-GTTCGTCGACCTGCAGCAGCTCGTCCATGCCGAG - 3'	
PIF6 (~0.5 kb)	Forward: 5'- GATATAAGATCTATGATGTTCTTACCAACCG - 3'	pDisplay-AP-CFP-TM
	Reverse: 5'- GATATAGGCGCGCCGTCAACATGTTTATTGCTT TC - 3'	
CIBN-GFP (~1 kb)	Forward: 5'- CACACACATATGATGAATGGAGCTATAG - 3'	pET21b
	Reverse: 5'- GGTGGTGGTGCTCGAGCGACATAATTACACACTTTG - 3'	
	Forward: 5'-CAAAGTGTGTAATTATGTCGCTCGAGCACCACCACC - 3'	Mutation primers
	Reverse: 5'- GGTGGTGGTGCTCGAGCGACATAATTACACACTTTG - 3'	
PIF6 (~0.5 kb)	Forward: 5'- CACACACATATGATGTTCTTACCAACCG - 3'	pET21b
	Reverse: 5'- CACACACTCGAGCTTGTACAGCTCGTC - 3'	

Site directed mutagenesis was done to remove the stop codon CIBN-GFP and His_6-tag. The PCR condition for mutagenesis was as follows:

PCR mix (1X): total volume = 50 µl

Template (100 ng/µL)	0.5 µl
dNTPs (10 mM stock)	1 µl
Forwards primer (10 µM)	1 µl
Reverse primer (10 µM)	1 µl
PFU buffer (10x)	5 µl
PFU	1 µl
Quick change solution	3 µl
Distilled water	37.5 µl

PCR conditions:

Step 1) 95^{o}C, 1 min
Step 2) 95^{o}C, 50 sec
Step 3) 60^{o}C, 50 sec
Step 4) 68^{o}C, 7 min
Step 5) Go to step 2 (18 cycles)
Step 6) 68^{o}C, 10 min
Step 7) 4^{o}C, forever

4.2.3 Restriction enzyme digestion and ligation

PCR products and vectors were double-digested with the restriction enzymes **(Table 4.2)**, then purified with PCR purification kit. For each digestion, 200 ng/µl substrate (PCR product or vector) was mixed with 1 µl of each enzyme and final volume was adjusted 50 µl with miliQ water.

Table 4.2 Restriction enzymes and digestion conditions

Substrates (insert/vector)	Enzymes	Conditions
CRY2-mCherry/pDisplay	SalI/SacII	1x Cut smart buffer, 37^{o}C, overnight
CIBN-GFP/pDisplay-FLIPE-600n	SalI/XmaI	1x Cut smart buffer, 37^{o}C, overnight
CIBN-GFP/pET21b	NdeI/XhoI	1x Cut smart buffer, 37^{o}C, overnight
PhyB/pDisplay	XmaI/SacII	1x Cut smart buffer, 37^{o}C, overnight
YFP/pDisplay-PhyB	SacII/PstI	1x Cut smart buffer, 37^{o}C, overnight
PIF6/pDisplay-AP-CFP-TM	BglII/AscI	1) 1x NEB Buffer 3.1 for BglII digestion, 37^{o}C, overnight 2) 1x Cut smart buffer, 37^{o}C, overnight
PIF6/pET21b	NdeI/XhoI	Cut smart buffer, 37^{o}C, overnight

After digestions, agarose gels were done to verify the products. The vectors pDisplay-FLIPE-600n and pDisplay-AP-CFP-TM were purified with gel extraction kit following the provider's instructions. The other digestion products were purified by using PCR purification kit due to the small size of the removed nucleotides. To determine the concentrations of digested products, absorbance was measured at 260 nm with a Nanodrop spectrometer.

CRY2-mCherry, PhyB and YFP were ligated into pDisplay plasmids following Gibson assembly protocol. For this, the purified digested vector and PCR products were mixed in a 1:2 (vector:insert) molar ratio with 5 µl Gibson assembly Master mix (2x) and incubated at 50^{o}C for 1 hr. A mixture without a PCR product was used as a negative control. CIBN-GFP and PIF6 were ligated into pDisplay and pET21b by following a general ligation protocol as follows. The digested vector and insert were mixed in a 1:3 and 1:5 (vector:insert) molar ratio with 0.5 µl and 1 µl T4 DNA ligase buffer (10x), and incubated 4^{o}C overnight. In both cases, final volume was adjusted to 10 µl with miliQ water.

4.2.4 Transformation into *E.coli* by electroporation

After all cloning steps were completed, the final ligated plasmids were transformed into *E. coli* DH5α by electroporation. For electroporation, 2 µl ligation or Gibson product was mixed with 48 µl electrocompetent *E. coli* DH5α on ice. This mixture was placed in the electroporation cuvettes and a pulse was given (1800 V, 25 µF, 200 Ω). Immediately after pulsing, 450 µl LB was added to the cells and the transformants were placed in a clean 1.5 ml tube. The cultures were incubated on a heating block for 1 h at 37 ^{o}C at 200 rpm. The transformants were plated on an LB agar plate with 50 µg/ml ampicillin at 37^{o}C overnight. The following day, colonies were picked and grown in 10 mL LB with 50 µg/ml ampicillin at 37 ^{o}C overnight. The next day, plasmids were isolated with miniprep kit and sent for sequencing with a T7 forward primer. The sequences of these constructs are shown in Section 6.1.

4.3 Cell Culture

4.3.1 Culturing and freezing medium

Complete medium was prepared by filtering Dulbecco's Modified Eagle Medium (DMEM)/F12 (1:1) with 10% FBS through 0.2 µm sterile cellulose filters and 1% penicillin/streptomycin was added after filtration. All cells were cultured in the complete medium and incubated at 37^{o}C and under 5% CO_2. For stable cell lines, 0.9 mg/ml Geneticin (G418) was added to the complete medium. For illumination experiments phenol-red free medium was used and 200 mM *L*-glutamine was added. FBS was excluded for the illumination experiments to control cell-material interactions. Cells were frozen for storage in liquid nitrogen in a 1:1 mixture of DMEM:FBS-DMSO (80%FBS and 20% DMSO) was used.

4.3.2 Generation of stable cell lines

To generate the stable cells lines, the cells were transfected with pDisplay-CRY2-mCherry, pDisplay-CIBN-GFP and pDisplay-PhyB-YFP plasmids by using Lipofectamine^{TM} LTX reagent following the instructions provided by the manufacturers as follows. MDA-MB-231 cells were seeded on 6-well polystyrene plates at a density of 6.25 x 10^4 cells/cm^2 and grown overnight. The next day, the cells were washed twice with warm PBS and fresh medium is added. For transfection,

2.5 µg DNA was mixed with 500 µl OPTI-MEM and 2.5 µl PLUS reagent. This DNA solution was incubated at room temperature for 15 min. 8.75 µl of LTX reagent was added to the solution and the mixture was incubated for 30 min at room temperature. Finally, 500 µl DNA-Lipofectamine solution was added to the cell medium drop-wise. After 24 hours, cells were cultured in medium with 0.9 mg/ml Geneticin (G418) for selection over 2 weeks and subsequently cell stocks were prepared. The resulting cell lines were named as MDA-CRY2-mCherry, MDA-CIBN-GFP and MDA-PhyB-YFP. These cell lines were used for illumination experiments up to the passage number 11.

4.3.3 Fixation, actin and nuclear staining

For fixation, the medium was removed, cells were washed twice with PBS and cells were incubated with 1 ml 4% paraformaldehyde (PFA) for 15 min at room temperature. Then, PFA was removed and the cells were washed twice with PBS. For actin staining, cells were permeabilized with 0.1 % Triton X-100 in PBS for 5 min at room temperature, stained with 0.5 µg/ml Phalloidin-TRITC in PBS for 30 min in dark to prevent bleaching. Finally, the samples were mounted with mowiole-488 containing 1 µg/ml DAPI for nuclear staining. For the unmounted samples, the cells were incubated with 1 µg/ml DAPI in PBS for one hour at room temperature in the dark.

4.3.4 Immunostaining

MDA-CRY2-mCherry and MDA-CIBN-GFP cells were seeded 24 mm x 24 mm cover slips, which were cleaned with 70% ethanol, at a density of 15000 cells/cm^2 and grown overnight. The next day, the cells were fixed with PFA. One set of cells was permeabilized whereas one set was kept impermeable for the primary antibody in order to stain only the proteins at the plasma membrane. The samples were blocked with 1% BSA in PBS for 10 min at room temperature. Meanwhile, the primary antibody, mouse anti-c-*myc*, was diluted 1:200 in 1% BSA-PBS. The coverslips were placed in a humid chamber and 150 µL of primary antibody solution was added drop-wise on the cells. The samples were incubated with the primary antibody for 1 hour at room temperature and then, the cells were washed three times with 1% BSA-PBS

solution for 2 min. The secondary antibody, goat anti-mouse AlexaFluor 488, was prepared with at 1:1000 dilution in 1% BSA-PBS and 150 µL of it was added drop-wise on the cells. The samples were incubated with the secondary antibody for 1 hour at room temperature in dark to prevent bleaching of the AlexaFluor488. After the secondary antibody staining, the cells were washed three times with 1% BSA-PBS solution for 2 min. The impermeable set of cells was permeabilized for actin staining after the secondary antibody staining. The cells were stained for actin with phalloidin-TRITC and mounted with mowiole:DAPI as described above. The samples were imaged with a Zeiss LSM 880 confocal microscope.

4.4 Isolation of PCB

Following the protocol from Müller *et al.,* PCB was isolated from *Spirulina* extract by methanolysis and organic extraction.[112] 25 g *Spirulina* extract was boiled in 250 ml methanol for 2 min under reflux. The green liquid was removed by vacuum filtration and the reflux and filtration steps were repeated 6-8 times until the flow through was colorless. At this step the powder could be stored overnight at 4^{o}C. The next day, the washed powder was boiled in methanol for 4 hours in reflux under the dim light. The liquid was vacuum filtrated and it was reduced to 15 ml with a rotary evaporator. The dark green solution was transferred into a thin separatory funnel and mixed with 35 ml diethyl ether and 50 ml of 1% (w/v) citric acid solution in water. The bottom aqueous phase was collected into a clean flask for re-extraction. The organic phase in the separatory funnel was mixed with 25 ml of 1% (w/v) $NaHCO_3$ and PCB was extracted from the newly formed organic phase. The aqueous phase from this extraction was transferred into a second separatory funnel, acidified by adding 5 ml, 1 M HCl. Protonated PCB was extracted with 25 ml chloroform. Chloroform was evaporated *in vacuo* and the product was dried on the vacuum line overnight. The dried PCB was dissolved in 1.5 ml DMSO and aliquots were stored at -20^{o}C. To determine the concentration of PCB, it was diluted 1:800 in methanol:HCl (95:5 (v/v)) and absorbance spectrum was measured between 300-800 nm (ε_{680} = 37900 $M^{-1}.cm^{-1}$; molecular weight: 586.7 g/mol):

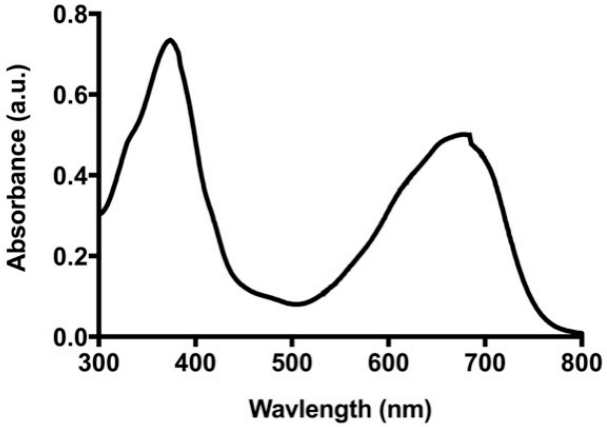

The concentration obtained from this purification was 36 mM. 5 µM PCB was added to the cell culture medium for illumination experiments with red light.

4.5 Protein purification and characterization

4.5.1 Protein expression

PIF6-CFP-His_6 and CIBN-GFP-His_6 were transformed chemically into *E. coli* BL21 using a standard protocol. In short, 2 µl plasmid was mixed with 48 µl chemicompetent *E. coli* BL21 on ice for 30 min. This mixture was placed in heating block for 45 sec at 42^{o}C and subsequently placed back on ice for a few minutes. Then, 450 µl LB was added and the cells were incubated on a heating block for 1 h at 37 ^{o}C at 200 rpm. The transformants were placed on an LB agar plate with 50 µg/ml ampicillin at 37^{o}C and grown overnight. The next day, a colony from each plate was selected and grown in 10 mL LB with 50 µg/ml ampicillin overnight at 37 ^{o}C at 200 rpm. The following day, the bacterial cultures were transferred into 1 l LB with 50 µg/ml ampicillin and were grown at 37 ^{o}C at 200 rpm until they reached a density of OD_{600} = 0.4-0.6. Protein expression was induced with 0.5 mM IPTG and the bacterial culture was incubated at 16^{o}C at 200 rpm overnight following the induction. The bacteria were harvested by centrifugation (6000 g, 8 min).

4.5.2 Affinity chromatography

For protein purification all the steps were performed on ice or at 4^{o}C. The bacterial pellet was resuspended in 20 ml Buffer A (50 mM TRIS at pH 7.4 and 300 mM NaCl) containing 1.25 mM PMSF (stock solution 100 mM in methanol) and 1.25 mM DTT. The bacterial suspension was homogenized using a rupture sonicator at 50%

frequency, 40% power for 10 min. The homogenized solution was centrifuged at 12000 rpm at 4^{o}C for 30 min. The supernatant was filtered through a 0.45 µm cellulose filter twice. His-trap^{TM} HP column (column volume is 5 ml) was equilibrated with 20 ml Buffer A containing 1.25 mM DTT. The filtered protein solution was passed over the column and the column was washed first with 10 ml Buffer A and then, with 50 ml Buffer A containing 12.5 mM imidazole. Finally, the protein was eluted with the elution buffer (Buffer A containing 250 mM imidazole). After the elution was completed, the His-Trap column was cleaned first with 50 ml elution buffer and then with 50 ml Buffer A. For long term storage, the column was washed with 20 ml water followed by 20 ml 20% ethanol and was left in ethanol to prevent bacterial growth.

4.5.3 Size exclusion chromatography

The His-trap purified proteins were further purified with size exclusion chromatography on an ÄKTA Pure system. For this, first the protein solution was concentrated to a final volume of 2 mL by 50 mL centrifugal filter units. The size exclusion column was equilibrated with Buffer A containing 1 mM DTT at a flow rate of 1 ml/min. The concentrated protein solution was injected into the sample loop, the column was run for 120 ml (1 column volume) and 1 ml fractions were collected. The purified protein was characterized with SDS-PAGE. The retention times for CIBN-GFP and PIF6-CFP were 50 min and 75 min, respectively. After the fractionation was complete, the column was cleaned first with 120 ml Buffer A, then 120 ml water and finally 120 ml 20 % ethanol for storage to prevent bacterial growth.

4.5.4 SDS-PAGE

20 µl from each fraction was mixed with 5 µl SDS sample buffer (4x) and incubated at 90^{o}C for 10 min for protein denaturation. Then, the denatured proteins were loaded in the SDS gels along with a pre-stained protein marker. The gel was run in MOPS buffer (50 mM MOPS, 50 mM TRIS-base, 0.1 (w/v) SDS, 1 mM EDTA, pH 7.7) for 50 min, at 220 volts and 120 mA. After the gel run was complete, the gel was stained with comassie for 1 hr at room temperature on roller. Then, the gel was placed in de-staining buffer (20% (v/v) methanol and 10 % (v/v) acetic acid in miliQ water) and imaged with Amersham 600 imager. The fractions with right sizes were combined,

concentrated in the centrifugal filter units and the final concentrations of proteins were determined by measuring the absorbance at 280 nm with a nanodrop spectrometer. The molecular masses and the molar extinction coefficients were theoretically calculated from an online tool (http://web.expasy.org/protparam/) and were as follows:

PIF6-CFP: 38.8 kDa, ε_{280} = 29300 $M^{-1}.cm^{-1}$

CIBN-GFP: 48.9 kDa, ε_{280} = 24890 $M^{-1}.cm^{-1}$

The concentrations were as follows: [CIBN-GFP-His_6] = 0.24 mM and
[PIF6-CFP-His_6] = 0.4 mM

4.6 Surface functionalization and protein immobilization

The surface modification scheme was adapted from Schenk *et al*.[132] In short, 20 mm x 20 mm cover slips were cleaned in piranha solution (3:1 H_2SO_4:H_2O_2) for 1 hr at room temperature, rinsed thoroughly with water and dried with N_2 stream. The substrates were immersed in a solution of 0.25 mM PEG-N_3 (PEG 3000 with a terminal azide and a terminal triethoxysilane group) and 25 µM triethylamine in dry toluene (dried over molecular sieves (3Å)) and held at 78°C overnight under a nitrogen atmosphere **(Section 6.2)**. The substrates were sonicated in ethylacetate for 5 min and then, sonicated in methanol for 5 min and dried in a stream of nitrogen. For copper catalyzed azide alkyne cycloaddition (CuAAC), the PEGylated substrates were incubated with a freshly prepared aqueous solution of 100 mM TRIS (pH 9.5), 100 mM *L*-ascorbic acid, 150 µM NTA-alkyne (synthesized by Julia Ricken)[134,135] and 1 mM $CuSO_4$ for 2 hours in a moisture chamber. Substrates were washed twice with a buffer (Buffer A), once with 50 mM EDTA and twice with Buffer A. The substrates were then incubated with 100 mM $NiCl_2$ for 5 min for Ni^{2+} coordination with NTA and then washed once with Buffer A. Finally, the Ni^{2+}-NTA functionalized surfaces were incubated with 10 µM His_6-tagged protein for 30 min at room temperature.

4.7 Quartz Crystal Microbalance with dissipation monitoring (QCM-D)

SiO_2 sensors were immersed in an aqueous solution of 2% (w/v) SDS overnight, washed with water thoroughly and dried in a nitrogen stream. The SiO_2 sensors were then cleaned and activated in an O_2 plasma (0.4 mbar, 150 W, 45 min). Subsequently,

the QCM-D crystals were functionalized with a PEG layer with a terminal Ni^{2+}-NTA group as described above. Then, the crystals were placed in the QCM-D closed module and a flow rate of 100 µl/min was used for all measurements. First, the crystals were washed with the same buffer (Buffer A) until a baseline was reached and then 10 µM His_6-tagged proteins were washed over the crystals, where the binding of proteins to the Ni^{2+}-NTA-functionalized surface was observed as a decrease in frequency. The crystals were washed once again with Buffer A to remove unspecifically bound proteins. Finally, they were washed with the elution buffer to remove all proteins, which are bound to the crystals through His_6-Ni^{2+}-NTA coordination.

4.8 Blue - light induced cell-cell contacts

4.8.1 Cell-cell contact formation and quantification

For illumination experiments, MDA-CRY2-mCherry and MDA-CIBN-GFP were seeded on 24 mm x 24 mm cover slips (cleaned with 70% ethanol) at a density of 5000 cells/cm^2 each in the presence of 0.5 µM FAD and kept in dark and under blue light (471 nm, 80 µW/cm^2) for 4 hours. After incubation, cells were fixed in dark and under blue light and stained for actin and nucleus. Fluorescence images in the TRITC and DAPI channels were acquired with a tile scan of an area of 1 cm^2 on an upright fluorescence microscope (Leica DM6000B) through a 10x air lens objective. All images were analyzed in ImageJ. The number of cells (nuclei as objects of 50-5000 µm^2) was determined with the analyze particles tool using images in the DAPI channel. The total area, the area of each object and the number of objects were determined for all cells (objects > 300 µm^2), single cells (objects of 300-3000 µm^2) and clusters (objects > 10000 µm^2) with the analyze particles tool using images in the TRITC channel. The % area that single cells or cell clusters occupy was calculated as the total area of single cells or clusters divided by the total area of all cells. All clustering experiments were done in technical duplicates with 2 replicates in each. Statistical analysis was performed using the unpaired t-test in GraphPad Prism and statistical significance is indicated on the figures.

4.8.2 Reversible cell-cell contacts

MDA-CRY2-mCherry cells were seeded on adhesive circular micropatterns (Cytoo chips) with 20 μm in diameter at a density of 10000 cells/cm^2 and cultured overnight. For live cell imaging an Olympus IX inverted microscope equipped with an incubation chamber (37^oC, under 5% CO_2) and a 20x air objective was used. A time lapse-movie was recorded at 1 frame/minute and illumination was done with a blue LED lamp (471 nm, 15 Watts) from the top of the cells. First images of MDA-CRY2-mCherry cells were acquired in the dark for 5 min, then under blue light for 5 min before adding MDA-CIBN-GFP cells. After the addition of MDA-CIBN-GFP cells (100 μl from 200 000 cells/ml), the imaging continued for 30 min under blue light and subsequently images were acquired in repeated dark/light for 20 min/cycle. Interacting cells were marked and the distance over time is measured in ImageJ.

4.8.3 Layer-by-layer tissue formation

MDA-CIBN-GFP and MDA-CRY2-mCherry cells were pre-stained with lipophilic tracers, DiO (3,3' - Dioctadecyloxacarbocyanine Perchlorate) and DiI (1,1' - dioctadecyl-3,3,3'3'-tetramethylindocarbocyanine perchlorate), respectively, by adding these dyes in the culture medium at final concentration of 6 μM DiO and 3 μM DiI. MDA-CIBN-GFP cells were then seeded on a glass bottom dish at a density of 300 cells/cm^2 and cultured overnight to confluency. The next day, MDA-CRY2-mCherry cells were added on top of CIBN expressing cells at a density of 300 cells/cm^2 and cultured in dark or under blue light illumination for 8 hours. After the incubation cells were washed, fixed and stained with DAPI. Confocal imaging was done to observe the tissue formation under blue light illumination.

4.9 Blue and red light induced cell – surface contacts

4.9.1 Blue and red light induced cell adhesion

PIF6-CFP-His_6 and CIBN-GFP-His_6 were immobilized on Ni^{2+}-NTA-functionalized glass substrates separately. MDA-CRY2-mCherry and MDA-PhyB-YFP cells were seeded on their complementary substrates at a density of 5000 cells/cm^2. The samples were incubated in dark, under blue light (471 nm, 80 μW/cm^2) or red light (673 nm, 55 μW/cm^2) for 2 hours in the presence of 0.5 μM FAD and 5 μM PCB for MDA-CRY2-

mCherry and MDA-PhyB-YFP cells, respectively. After incubation, cells were fixed and mounted with mowiole:DAPI. Fluorescence images in the DAPI channel was acquired with a tile scan of an area of 1 cm^2 on an upright fluorescence microscope (Leica DM6000B) through a 10x air lens objective. The number of cells (nuclei as objects of 50-5000 μm^2) was determined with the analyze particles tool on ImageJ.

4.9.2 Cell spreading by photoswitchable interactions

MDA-CRY2-mCherry and MDA-PhyB-YFP cells were seeded on substrates with their complementary partner proteins and on a bare glass surface (control) and incubated for 2 hours. Fixation, staining for actin and mounting were done as described above. Fluorescence images in the TRITC and DAPI channels were acquired with a tile scan of an area of 1 cm^2 on an upright fluorescence microscope (Leica DM6000B) through a 10x air lens objective. All images were analyzed in ImageJ. The spreading area of the cells on the protein functionalized substrates and on the glass surfaces was calculated using the Cell outliner tool in ImageJ. For comparison of cell morphology when they were on protein and on the glass substrates, confocal imaging was done with Zeiss LSM 880 microscope. The cells were fixed and stained for actin; however, they were not mounted. In order to detect mCherry signal from MDA-CRY2-mCherry stable cell line, a Phalloidin-FITC conjugate was used for actin staining.

4.9.3 Adhesion and reversion kinetics

For the adhesion kinetics, cells were incubated on substrates with their complementary interaction partners under blue light for MDA-CRY2-mCherry cells and under red light for MDA-PhyB-YFP cells for 30, 60, 90 and 120 min and in dark for 120 min. At each time point a triplicate set of samples were fixed. For reversion kinetics cells were first incubated on substrates with their complementary interaction partners under light for 60 min as described above, and then placed in dark for 30, 60, 90 and 120 min. At each time point a triplicate set of samples were fixed. For MDA-PhyB-YFP cells on PIF6 immobilized substrates, the samples were also incubated under far-red light (750 nm, 50 $\mu W/cm^2$) for 5, 15 and 30 min following 1 h red light illumination. At each time point a triplicate set of samples were fixed. Fluorescence images in the DAPI channel was acquired with a tile scan of an area of 1

cm^2 on an upright fluorescence microscope (Leica DM6000B) through a 10x air lens objective. All images were analyzed in ImageJ. The number of cells (nuclei as objects of 50-5000 μm^2) was determined with the analyze particles tool.

4.9.4 Orthogonal switching of cell adhesion

PhyB and CRY2 expressing cells were pre-stained with lipophilic tracers, DiO and DiI, respectively, as described above. 10 µM PIF6-CFP-His_6 and 10 µM CIBN-GFP-His_6 were incubated with Ni^{2+}-NTA-functionalized glass surfaces to co-immobilize the two proteins. The pre-stained PhyB and CRY2 expressing cells were seeded at 5000 cells/cm^2 each as described. The cells were incubated in dark, just under red or blue light or under co-illumination of blue and red light for 2 hours, fixed and mounted as described above. Fluorescence images in the FITC (MDA-PhyB-YFP cells), TRITC (MDA-CRY2-mCherry cells) and DAPI channels were acquired with a tile scan of an area of 1 cm^2 on an upright fluorescence microscope (Leica DM6000B) through a 10x air lens objective. The number of PhyB and CRY2 expressing cells was determined with the analyze particles tool using images in the FITC and TRITC channel, respectively.

4.10 Cell viability assay

MTT (3-(4,5-dimethylthiazol-2-yl)-2,5-diphenyltetrazolium bromide) assay was used to measure phototoxicity under blue light illumination. 5 mg MTT was dissolved in 1 ml PBS to obtain 12 mM MTT. MDA-MB-231 cells were seeded in a flat-bottom 96-well plate at a density of 150 000 cells/cm^2 in duplicates. Cells were incubated in dark and under 80 µW/cm^2, 800 µW/cm^2 and 8000 µW/cm^2 blue light for 4 hours. Then, 10 µl of 12 mM MTT was added and cells were incubated 4 hours in dark. Finally, 50 µl DMSO was added and incubated for 10 min in dark. Absorbance at 540 nm was measured using a microplate reader Infinite 200M controlled by i-control 1.9. All the absorbance values were normalized to the absorbance values of the dark samples.

4.11 Confocal imaging

Confocal images were acquired on a LSM 880 Zeiss confocal microscope equipped with a UV diode (405 nm), Ar laser (488 nm), HeNe laser (633 nm) and a 63x oil-immersion objective to detect mCherry and GFP signals from the stable cell lines, for

immunostainings and for the microtissue formed layer-by-layer. z-stacks were obtained from samples and images were shown from xy, xz and yz axeses.

Chapter 5

Bibliography

5. Bibliography

1 Nagafuchi, A. & Takeichi, M. Transmembrane control of cadherin-mediated cell adhesion: a 94 kDa protein functionally associated with a specific region of the cytoplasmic domain of E-cadherin. *Cell Regul.* **1**, 37-44 (1989).

2 Shapiro, L. & Weis, W. I. Structure and biochemistry of cadherins and catenins. *Cold Spring Harb Perspect Biol.* **1**, a003053, doi:10.1101/cshperspect.a003053 (2009).

3 Gumbiner, B. M. Cell adhesion: the molecular basis of tissue architecture and morphogenesis. *Cell* **84**, 345-357 (1996).

4 Aplin, A. E., Howe, A., Alahari, S. K. & Juliano, R. L. Signal transduction and signal modulation by cell adhesion receptors: the role of integrins, cadherins, immunoglobulin-cell adhesion molecules, and selectins. *Pharmacol. Rev.* **50**, 197-263 (1998).

5 Gall, T. M. & Frampton, A. E. Gene of the month: E-cadherin (CDH1). *J. Clin. Pathol.* **66**, 928-932, doi:10.1136/jclinpath-2013-201768 (2013).

6 Duguay, D., Foty, R. A. & Steinberg, M. S. Cadherin-mediated cell adhesion and tissue segregation: qualitative and quantitative determinants. *Dev. Biol.* **253**, 309-323 (2003).

7 Foty, R. A. & Steinberg, M. S. The differential adhesion hypothesis: a direct evaluation. *Dev. Biol.* **278**, 255-263, doi:10.1016/j.ydbio.2004.11.012 (2005).

8 Steinberg, M. S. Reconstruction of tissues by dissociated cells. Some morphogenetic tissue movements and the sorting out of embryonic cells may have a common explanation. *Science* **141**, 401-408 (1963).

9 Brodland, G. W. The Differential Interfacial Tension Hypothesis (DITH): a comprehensive theory for the self-rearrangement of embryonic cells and tissues. *J. Biomech. Eng.* **124**, 188-197 (2002).

10 Harris, A. K. Is Cell sorting caused by differences in the work of intercellular adhesion? A critique of the Steinberg hypothesis. *J. Theor. Biol.* **61**, 267-285 (1976).

11 Fagotto, F. The cellular basis of tissue separation. *Development* **141**, 3303-3318, doi:10.1242/dev.090332 (2014).

12 Manning, M. L., Foty, R. A., Steinberg, M. S. & Schoetz, E. M. Coaction of intercellular adhesion and cortical tension specifies tissue surface tension. *Proc. Natl. Acad. Sci. USA* **107**, 12517-12522, doi:10.1073/pnas.1003743107 (2010).

13 Moore, R., Tao, W., Meng, Y., Smith, E. R. & Xu, X. X. Cell adhesion and sorting in embryoid bodies derived from N- or E-cadherin deficient murine embryonic stem cells. *Biol. Open* **3**, 121-128, doi:10.1242/bio.20146254 (2014).

14 Maitre, J. L. *et al.* Adhesion functions in cell sorting by mechanically coupling the cortices of adhering cells. *Science* **338**, 253-256, doi:10.1126/science.1225399 (2012).

15 Lecuit, T. & Yap, A. S. E-cadherin junctions as active mechanical integrators in tissue dynamics. *Nat. Cell. Biol.* **17**, 533-539, doi:10.1038/ncb3136 (2015).
16 Maitre, J. L. & Heisenberg, C. P. Three functions of cadherins in cell adhesion. *Curr. Biol.* **23**, R626-633, doi:10.1016/j.cub.2013.06.019 (2013).
17 Borghi, N. *et al.* E-cadherin is under constitutive actomyosin-generated tension that is increased at cell-cell contacts upon externally applied stretch. *Proc. Natl. Acad. Sci. USA* **109**, 12568-12573, doi:10.1073/pnas.1204390109 (2012).
18 Ng, M. R., Besser, A., Brugge, J. S. & Danuser, G. Mapping the dynamics of force transduction at cell-cell junctions of epithelial clusters. *Elife* **3**, e03282, doi:10.7554/eLife.03282 (2014).
19 Anastasiadis, P. Z. p120-ctn: A nexus for contextual signaling via Rho GTPases. *Biochim. Biophys. Acta* **1773**, 34-46, doi:10.1016/j.bbamcr.2006.08.040 (2007).
20 Nelson, W. J. & Nusse, R. Convergence of Wnt, beta-catenin, and cadherin pathways. *Science* **303**, 1483-1487, doi:10.1126/science.1094291 (2004).
21 Howard, S., Deroo, T., Fujita, Y. & Itasaki, N. A positive role of cadherin in Wnt/beta-catenin signalling during epithelial-mesenchymal transition. *PLoS One* **6**, e23899, doi:10.1371/journal.pone.0023899 (2011).
22 Moon, R. T., Kohn, A. D., De Ferrari, G. V. & Kaykas, A. WNT and beta-catenin signalling: diseases and therapies. *Nat. Rev. Genet.* **5**, 691-701, doi:10.1038/nrg1427 (2004).
23 Lamouille, S., Xu, J. & Derynck, R. Molecular mechanisms of epithelial-mesenchymal transition. *Nat Rev Mol. Cell Biol.* **15**, 178-196, doi:10.1038/nrm3758 (2014).
24 Li, W. & Kang, Y. Probing the Fifty Shades of EMT in Metastasis. *Trends Cancer* **2**, 65-67, doi:10.1016/j.trecan.2016.01.001 (2016).
25 Campbell, I. D. & Humphries, M. J. Integrin structure, activation, and interactions. *Cold Spring Harb Perspect. Biol.* **3**, doi:10.1101/cshperspect.a004994 (2011).
26 Giancotti, F. G. & Ruoslahti, E. Integrin signaling. *Science* **285**, 1028-1032 (1999).
27 Albelda, S. M. & Buck, C. A. Integrins and other cell adhesion molecules. *FASEB J.* **4**, 2868-2880 (1990).
28 Hynes, R. O. Integrins: versatility, modulation, and signaling in cell adhesion. *Cell* **69**, 11-25 (1992).
29 Shattil, S. J., Kim, C. & Ginsberg, M. H. The final steps of integrin activation: the end game. *Nat. Rev. Mol. Cell Biol.* **11**, 288-300, doi:10.1038/nrm2871 (2010).
30 Wu, C. Focal adhesion: a focal point in current cell biology and molecular medicine. *Cell Adh. Migr.* **1**, 13-18 (2007).
31 Millard, M., Odde, S. & Neamati, N. Integrin targeted therapeutics. *Theranostics* **1**, 154-188 (2011).
32 Athanasiou, K. A., Eswaramoorthy, R., Hadidi, P. & Hu, J. C. Self-organization and the self-assembling process in tissue engineering. *Annu. Rev. Biomed. Eng.* **15**, 115-136, doi:10.1146/annurev-bioeng-071812-152423 (2013).

33 Jakab, K. *et al.* Tissue engineering by self-assembly and bio-printing of living cells. *Biofabrication* **2**, 022001, doi:10.1088/1758-5082/2/2/022001 (2010).
34 Nichol, J. W. & Khademhosseini, A. Modular Tissue Engineering: Engineering Biological Tissues from the Bottom Up. *Soft Matter* **5**, 1312-1319, doi:10.1039/b814285h (2009).
35 Lu, T., Li, Y. & Chen, T. Techniques for fabrication and construction of three-dimensional scaffolds for tissue engineering. *Int. J. Nanomedicine* **8**, 337-350, doi:10.2147/IJN.S38635 (2013).
36 Mironov, V. *et al.* Organ printing: tissue spheroids as building blocks. *Biomaterials* **30**, 2164-2174, doi:10.1016/j.biomaterials.2008.12.084 (2009).
37 Kaji, H., Camci-Unal, G., Langer, R. & Khademhosseini, A. Engineering systems for the generation of patterned co-cultures for controlling cell-cell interactions. *Biochim. Biophys. Acta* **1810**, 239-250, doi:10.1016/j.bbagen.2010.07.002 (2011).
38 Liu, J. S. & Gartner, Z. J. Directing the assembly of spatially organized multicomponent tissues from the bottom up. *Trends Cell Biol.* **22**, 683-691, doi:10.1016/j.tcb.2012.09.004 (2012).
39 Elbert, D. L. Bottom-up tissue engineering. *Curr. Opin. Biotechnol.* **22**, 674-680, doi:10.1016/j.copbio.2011.04.001 (2011).
40 Nieman, M. T., Prudoff, R. S., Johnson, K. R. & Wheelock, M. J. N-cadherin promotes motility in human breast cancer cells regardless of their E-cadherin expression. *J. Cell Biol.* **147**, 631-644 (1999).
41 Guglielmi, G., Falk, H. J. & De Renzis, S. Optogenetic Control of Protein Function: From Intracellular Processes to Tissue Morphogenesis. *Trends Cell Biol.* **26**, 864-874, doi:10.1016/j.tcb.2016.09.006 (2016).
42 Dutta, D., Pulsipher, A., Luo, W. & Yousaf, M. N. Synthetic chemoselective rewiring of cell surfaces: generation of three-dimensional tissue structures. *J. Am. Chem. Soc.* **133**, 8704-8713, doi:10.1021/ja2022569 (2011).
43 O'Brien, P. J., Luo, W., Rogozhnikov, D., Chen, J. & Yousaf, M. N. Spheroid and Tissue Assembly via Click Chemistry in Microfluidic Flow. *Bioconjug. Chem.* **26**, 1939-1949, doi:10.1021/acs.bioconjchem.5b00376 (2015).
44 Koo, H. *et al.* Bioorthogonal Click Chemistry-Based Synthetic Cell Glue. *Small* **11**, 6458-6466, doi:10.1002/smll.201502972 (2015).
45 De Bank, P. A. *et al.* Accelerated formation of multicellular 3-D structures by cell-to-cell cross-linking. *Biotechnol. Bioeng.* **97**, 1617-1625, doi:10.1002/bit.21343 (2007).
46 Gartner, Z. J. & Bertozzi, C. R. Programmed assembly of 3-dimensional microtissues with defined cellular connectivity. *Proc. Natl. Acad. Sci. USA* **106**, 4606-4610, doi:10.1073/pnas.0900717106 (2009).
47 Wang, J. *et al.* Chemical remodeling of cell-surface sialic acids through a palladium-triggered bioorthogonal elimination reaction. *Angew. Chem. Int. Ed.* **54**, 5364-5368, doi:10.1002/anie.201409145 (2015).
48 Gabrielse, K. *et al.* Reversible re-programing of cell-cell interactions. *Angew. Chem. Int. Ed.* **53**, 5112-5116, doi:10.1002/anie.201310645 (2014).

49 Wang, B. *et al.* Multicellular assembly and light-regulation of cell-cell communication by conjugated polymer materials. *Adv. Mater.* **26**, 2371-2375, doi:10.1002/adma.201304593 (2014).
50 Teramura, Y., Chen, H., Kawamoto, T. & Iwata, H. Control of cell attachment through polyDNA hybridization. *Biomaterials* **31**, 2229-2235, doi:10.1016/j.biomaterials.2009.11.098 (2010).
51 Todhunter, M. E. *et al.* Programmed synthesis of three-dimensional tissues. *Nat. Methods* **12**, 975-981, doi:10.1038/nmeth.3553 (2015).
52 Shi, P. *et al.* Host–guest recognition on photo-responsive cell surfaces directs cell–cell contacts. *Materials Today* **20**, 16-21, doi:10.1016/j.mattod.2016.12.006 (2017).
53 Shi, P. *et al.* Spatiotemporal control of cell-cell reversible interactions using molecular engineering. *Nat. Commun.* **7**, 13088, doi:10.1038/ncomms13088 (2016).
54 Luo, W., Pulsipher, A., Dutta, D., Lamb, B. M. & Yousaf, M. N. Remote control of tissue interactions via engineered photo-switchable cell surfaces. *Sci. Rep.* **4**, 6313, doi:10.1038/srep06313 (2014).
55 Robertus, J., Browne, W. R. & Feringa, B. L. Dynamic control over cell adhesive properties using molecular-based surface engineering strategies. *Chem. Soc. Rev.* **39**, 354-378, doi:10.1039/b906608j (2010).
56 Li, W., Wang, J., Ren, J. & Qu, X. Near-infrared- and pH-responsive system for reversible cell adhesion using graphene/gold nanorods functionalized with i-motif DNA. *Angew. Chem. Int. Ed.* **52**, 6726-6730, doi:10.1002/anie.201302048 (2013).
57 Rechenmacher, F. *et al.* A molecular toolkit for the functionalization of titanium-based biomaterials that selectively control integrin-mediated cell adhesion. *Chemistry* **19**, 9218-9223, doi:10.1002/chem.201301478 (2013).
58 Rechenmacher, F. *et al.* Functionalizing alphavbeta3- or alpha5beta1-selective integrin antagonists for surface coating: a method to discriminate integrin subtypes in vitro. *Angew. Chem. Int. Ed.* **52**, 1572-1575, doi:10.1002/anie.201206370 (2013).
59 Custodio, C. A., Frias, A. M., del Campo, A., Reis, R. L. & Mano, J. F. Selective cell recruitment and spatially controlled cell attachment on instructive chitosan surfaces functionalized with antibodies. *Biointerphases* **7**, 65, doi:10.1007/s13758-012-0065-3 (2012).
60 Chandra, R. A., Douglas, E. S., Mathies, R. A., Bertozzi, C. R. & Francis, M. B. Programmable cell adhesion encoded by DNA hybridization. *Angew. Chem. Int. Ed.* **45**, 896-901, doi:10.1002/anie.200502421 (2006).
61 Douglas, E. S., Chandra, R. A., Bertozzi, C. R., Mathies, R. A. & Francis, M. B. Self-assembled cellular microarrays patterned using DNA barcodes. *Lab Chip* **7**, 1442-1448, doi:10.1039/b708666k (2007).
62 Leroy, L. *et al.* Photothermal effect for localized desorption of primary lymphocytes arrayed on an antibody/DNA-based biochip. *Lab Chip* **14**, 1987-1990, doi:10.1039/c4lc00336e (2014).
63 Custodio, C. A. *et al.* Photopatterned antibodies for selective cell attachment. *Langmuir* **30**, 10066-10071, doi:10.1021/la502688h (2014).

64 Guasch, J. *et al.* Segregation versus colocalization: orthogonally functionalized binary micropatterned substrates regulate the molecular distribution in focal adhesions. *Adv. Mater.* **27**, 3737-3747, doi:10.1002/adma.201500900 (2015).
65 Lee, T. T. *et al.* Light-triggered in vivo activation of adhesive peptides regulates cell adhesion, inflammation and vascularization of biomaterials. *Nat. Mater.* **14**, 352-360, doi:10.1038/nmat4157 (2015).
66 Salierno, M. J., García, A. J. & del Campo, A. Photo-Activatable Surfaces for Cell Migration Assays. *Advanced Functional Materials* **23**, 5974-5980, doi:10.1002/adfm.201300902 (2013).
67 Petersen, S. *et al.* Phototriggering of cell adhesion by caged cyclic RGD peptides. *Angew. Chem. Int. Ed.* **47**, 3192-3195, doi:10.1002/anie.200704857 (2008).
68 Auernheimer, J., Dahmen, C., Hersel, U., Bausch, A. & Kessler, H. Photoswitched cell adhesion on surfaces with RGD peptides. *J. Am. Chem. Soc.* **127**, 16107-16110, doi:10.1021/ja053648q (2005).
69 Kadem, L. F. *et al.* Rapid Reversible Photoswitching of Integrin-Mediated Adhesion at the Single-Cell Level. *Adv. Mater.* **28**, 1799-1802, doi:10.1002/adma.201504394 (2016).
70 Liu, D., Xie, Y., Shao, H. & Jiang, X. Using azobenzene-embedded self-assembled monolayers to photochemically control cell adhesion reversibly. *Angew. Chem. Int. Ed.* **48**, 4406-4408, doi:10.1002/anie.200901130 (2009).
71 Li, W., Wang, J., Ren, J. & Qu, X. Near-infrared upconversion controls photocaged cell adhesion. *J. Am. Chem. Soc.* **136**, 2248-2251, doi:10.1021/ja412364m (2014).
72 Li, W. *et al.* Noninvasive and Reversible Cell Adhesion and Detachment via Single-Wavelength Near-Infrared Laser Mediated Photoisomerization. *J. Am. Chem. Soc.* **137**, 8199-8205, doi:10.1021/jacs.5b03872 (2015).
73 Muhlhauser, W. W., Fischer, A., Weber, W. & Radziwill, G. Optogenetics - Bringing light into the darkness of mammalian signal transduction. *Biochim. Biophys. Acta* **1864**, 280-292, doi:10.1016/j.bbamcr.2016.11.009 (2017).
74 Muller, K. & Weber, W. Optogenetic tools for mammalian systems. *Mol. Biosyst.* **9**, 596-608, doi:10.1039/c3mb25590e (2013).
75 Boyden, E. S., Zhang, F., Bamberg, E., Nagel, G. & Deisseroth, K. Millisecond-timescale, genetically targeted optical control of neural activity. *Nat. Neurosci.* **8**, 1263-1268, doi:10.1038/nn1525 (2005).
76 Bruegmann, T. *et al.* Optogenetic control of heart muscle in vitro and in vivo. *Nat. Methods* **7**, 897-900, doi:10.1038/nmeth.1512 (2010).
77 Doroudchi, M. M. *et al.* Virally delivered channelrhodopsin-2 safely and effectively restores visual function in multiple mouse models of blindness. *Mol. Ther.* **19**, 1220-1229, doi:10.1038/mt.2011.69 (2011).
78 Tsai, H. C. *et al.* Phasic firing in dopaminergic neurons is sufficient for behavioral conditioning. *Science* **324**, 1080-1084, doi:10.1126/science.1168878 (2009).
79 Cho, Y. K. & Li, D. Optogenetics: Basic Concepts and Their Development. *Methods Mol. Biol.* **1408**, 1-17, doi:10.1007/978-1-4939-3512-3_1 (2016).
80 Tischer, D. & Weiner, O. D. Illuminating cell signalling with optogenetic tools. *Nat. Rev. Mol. Cell Biol.* **15**, 551-558, doi:10.1038/nrm3837 (2014).

81 Crefcoeur, R. P., Yin, R., Ulm, R. & Halazonetis, T. D. Ultraviolet-B-mediated induction of protein-protein interactions in mammalian cells. *Nat. Commun.* **4**, 1779, doi:10.1038/ncomms2800 (2013).
82 Niopek, D. *et al.* Engineering light-inducible nuclear localization signals for precise spatiotemporal control of protein dynamics in living cells. *Nat. Commun.* **5**, 4404, doi:10.1038/ncomms5404 (2014).
83 Quejada, J. R. *et al.* Optimized light-inducible transcription in mammalian cells using Flavin Kelch-repeat F-box1/GIGANTEA and CRY2/CIB1. *Nucleic Acids Res.*, doi:10.1093/nar/gkx804 (2017).
84 Guntas, G. *et al.* Engineering an improved light-induced dimer (iLID) for controlling the localization and activity of signaling proteins. *Proc. Natl. Acad. Sci. USA* **112**, 112-117, doi:10.1073/pnas.1417910112 (2015).
85 Liao, Z., Kasirer-Friede, A. & Shattil, S. J. Optogenetic interrogation of integrin alphaVbeta3 function in endothelial cells. *J. Cell Sci.* **130**, 3532-3541, doi:10.1242/jcs.205203 (2017).
86 Day, R. N. & Davidson, M. W. The fluorescent protein palette: tools for cellular imaging. *Chem. Soc. Rev.* **38**, 2887-2921, doi:10.1039/b901966a (2009).
87 Habuchi, S. *et al.* Reversible single-molecule photoswitching in the GFP-like fluorescent protein Dronpa. *Proc. Natl. Acad. Sci. USA* **102**, 9511-9516, doi:10.1073/pnas.0500489102 (2005).
88 Ando, R., Mizuno, H. & Miyawaki, A. Regulated fast nucleocytoplasmic shuttling observed by reversible protein highlighting. *Science* **306**, 1370-1373, doi:10.1126/science.1102506 (2004).
89 Zhou, X. X., Chung, H. K., Lam, A. J. & Lin, M. Z. Optical control of protein activity by fluorescent protein domains. *Science* **338**, 810-814, doi:10.1126/science.1226854 (2012).
90 Liu, H., Liu, B., Zhao, C., Pepper, M. & Lin, C. The action mechanisms of plant cryptochromes. *Trends Plant Sci.* **16**, 684-691, doi:10.1016/j.tplants.2011.09.002 (2011).
91 Kennedy, M. J. *et al.* Rapid blue-light-mediated induction of protein interactions in living cells. *Nat. Methods* **7**, 973-975, doi:10.1038/nmeth.1524 (2010).
92 Muhlhauser, W. W., Horner, M., Weber, W. & Radziwill, G. Light-Regulated Protein Kinases Based on the CRY2-CIB1 System. *Methods Mol. Biol.* **1596**, 257-270, doi:10.1007/978-1-4939-6940-1_16 (2017).
93 Taslimi, A. *et al.* Optimized second-generation CRY2-CIB dimerizers and photoactivatable Cre recombinase. *Nat. Chem. Biol.* **12**, 425-430, doi:10.1038/nchembio.2063 (2016).
94 Che, D. L., Duan, L., Zhang, K. & Cui, B. The Dual Characteristics of Light-Induced Cryptochrome 2, Homo-oligomerization and Heterodimerization, for Optogenetic Manipulation in Mammalian Cells. *ACS Synth. Biol.* **4**, 1124-1135, doi:10.1021/acssynbio.5b00048 (2015).
95 Bugaj, L. J., Choksi, A. T., Mesuda, C. K., Kane, R. S. & Schaffer, D. V. Optogenetic protein clustering and signaling activation in mammalian cells. *Nat. Methods* **10**, 249-252, doi:10.1038/nmeth.2360 (2013).
96 Kim, N. *et al.* Spatiotemporal control of fibroblast growth factor receptor signals by blue light. *Chem. Biol.* **21**, 903-912, doi:10.1016/j.chembiol.2014.05.013 (2014).

97 Taslimi, A. *et al.* An optimized optogenetic clustering tool for probing protein interaction and function. *Nat. Commun.* **5**, 4925, doi:10.1038/ncomms5925 (2014).
98 Idevall-Hagren, O., Dickson, E. J., Hille, B., Toomre, D. K. & De Camilli, P. Optogenetic control of phosphoinositide metabolism. *Proc. Natl. Acad. Sci. USA* **109**, E2316-2323, doi:10.1073/pnas.1211305109 (2012).
99 Idevall-Hagren, O. & Decamilli, P. Manipulation of plasma membrane phosphoinositides using photoinduced protein-protein interactions. *Methods Mol. Biol.* **1148**, 109-128, doi:10.1007/978-1-4939-0470-9_8 (2014).
100 Xu, Y., Nan, D., Fan, J., Bogan, J. S. & Toomre, D. Optogenetic activation reveals distinct roles of PIP3 and Akt in adipocyte insulin action. *J. Cell Sci.* **129**, 2085-2095, doi:10.1242/jcs.174805 (2016).
101 Valon, L., Marin-Llaurado, A., Wyatt, T., Charras, G. & Trepat, X. Optogenetic control of cellular forces and mechanotransduction. *Nat. Commun.* **8**, 14396, doi:10.1038/ncomms14396 (2017).
102 Duan, L. *et al.* Optogenetic control of molecular motors and organelle distributions in cells. *Chem. Biol.* **22**, 671-682, doi:10.1016/j.chembiol.2015.04.014 (2015).
103 Sinnen, B. L. *et al.* Optogenetic Control of Synaptic Composition and Function. *Neuron* **93**, 646-660 e645, doi:10.1016/j.neuron.2016.12.037 (2017).
104 Deb Roy, A. *et al.* Optogenetic activation of Plexin-B1 reveals contact repulsion between osteoclasts and osteoblasts. *Nat. Commun.* **8**, 15831, doi:10.1038/ncomms15831 (2017).
105 Polstein, L. R. & Gersbach, C. A. A light-inducible CRISPR-Cas9 system for control of endogenous gene activation. *Nat. Chem. Biol.* **11**, 198-200, doi:10.1038/nchembio.1753 (2015).
106 Choudhury, S. R. *et al.* Optogenetic regulation of site-specific subtelomeric DNA methylation. *Oncotarget* **7**, 50380-50391, doi:10.18632/oncotarget.10394 (2016).
107 Krishnamurthy, V. V. *et al.* Reversible optogenetic control of kinase activity during differentiation and embryonic development. *Development* **143**, 4085-4094, doi:10.1242/dev.140889 (2016).
108 Duan, L. *et al.* Understanding CRY2 interactions for optical control of intracellular signaling. *Nat. Commun.* **8**, 547, doi:10.1038/s41467-017-00648-8 (2017).
109 Guglielmi, G. & De Renzis, S. Optogenetic inhibition of apical constriction during Drosophila embryonic development. *Methods Cell Biol.* **139**, 167-186, doi:10.1016/bs.mcb.2016.10.007 (2017).
110 Li, J., Li, G., Wang, H. & Wang Deng, X. Phytochrome signaling mechanisms. *Arabidopsis Book* **9**, e0148, doi:10.1199/tab.0148 (2011).
111 Castillon, A., Shen, H. & Huq, E. Phytochrome Interacting Factors: central players in phytochrome-mediated light signaling networks. *Trends Plant Sci.* **12**, 514-521, doi:10.1016/j.tplants.2007.10.001 (2007).
112 Muller, K., Zurbriggen, M. D. & Weber, W. Control of gene expression using a red- and far-red light-responsive bi-stable toggle switch. *Nat. Protoc.* **9**, 622-632, doi:10.1038/nprot.2014.038 (2014).

113 Muller, K. *et al.* Synthesis of phycocyanobilin in mammalian cells. *Chem. Commun. (Camb.)* **49**, 8970-8972, doi:10.1039/c3cc45065a (2013).
114 Uda, Y. *et al.* Efficient synthesis of phycocyanobilin in mammalian cells for optogenetic control of cell signaling. *Proc. Natl. Acad. Sci. USA* **114**, 11962-11967, doi:10.1073/pnas.1707190114 (2017).
115 Levskaya, A., Weiner, O. D., Lim, W. A. & Voigt, C. A. Spatiotemporal control of cell signalling using a light-switchable protein interaction. *Nature* **461**, 997-1001, doi:10.1038/nature08446 (2009).
116 Hughes, R. M., Bolger, S., Tapadia, H. & Tucker, C. L. Light-mediated control of DNA transcription in yeast. *Methods* **58**, 385-391, doi:10.1016/j.ymeth.2012.08.004 (2012).
117 Pittman, A. M. *et al.* Rapid profiling of disease alleles using a tunable reporter of protein misfolding. *Genetics* **192**, 831-842, doi:10.1534/genetics.112.143750 (2012).
118 Shimizu-Sato, S., Huq, E., Tepperman, J. M. & Quail, P. H. A light-switchable gene promoter system. *Nat. Biotechnol.* **20**, 1041-1044, doi:10.1038/nbt734 (2002).
119 Tyszkiewicz, A. B. & Muir, T. W. Activation of protein splicing with light in yeast. *Nat. Methods* **5**, 303-305, doi:10.1038/nmeth.1189 (2008).
120 Pathak, G. P., Strickland, D., Vrana, J. D. & Tucker, C. L. Benchmarking of optical dimerizer systems. *ACS Synth. Biol.* **3**, 832-838, doi:10.1021/sb500291r (2014).
121 Toettcher, J. E., Weiner, O. D. & Lim, W. A. Using optogenetics to interrogate the dynamic control of signal transmission by the Ras/Erk module. *Cell* **155**, 1422-1434, doi:10.1016/j.cell.2013.11.004 (2013).
122 Yu, G. *et al.* Optical manipulation of the alpha subunits of heterotrimeric G proteins using photoswitchable dimerization systems. *Sci. Rep.* **6**, 35777, doi:10.1038/srep35777 (2016).
123 Juillot, S. *et al.* Signalling to the nucleus under the control of light and small molecules. *Mol. Biosyst.* **12**, 345-349, doi:10.1039/c5mb00763a (2016).
124 Muller, K. *et al.* A red/far-red light-responsive bi-stable toggle switch to control gene expression in mammalian cells. *Nucleic Acids Res.* **41**, e77, doi:10.1093/nar/gkt002 (2013).
125 Gomez, E. J., Gerhardt, K., Judd, J., Tabor, J. J. & Suh, J. Light-Activated Nuclear Translocation of Adeno-Associated Virus Nanoparticles Using Phytochrome B for Enhanced, Tunable, and Spatially Programmable Gene Delivery. *ACS Nano* **10**, 225-237, doi:10.1021/acsnano.5b05558 (2016).
126 Goglia, A. G., Wilson, M. Z., DiGiorno, D. B. & Toettcher, J. E. Optogenetic Control of Ras/Erk Signaling Using the Phy-PIF System. *Methods Mol. Biol.* **1636**, 3-20, doi:10.1007/978-1-4939-7154-1_1 (2017).
127 Johnson, H. E. *et al.* The Spatiotemporal Limits of Developmental Erk Signaling. *Dev. Cell* **40**, 185-192, doi:10.1016/j.devcel.2016.12.002 (2017).
128 Buckley, C. E. *et al.* Reversible Optogenetic Control of Subcellular Protein Localization in a Live Vertebrate Embryo. *Dev. Cell* **36**, 117-126, doi:10.1016/j.devcel.2015.12.011 (2016).
129 Reichhart, E., Ingles-Prieto, A., Tichy, A. M., McKenzie, C. & Janovjak, H. A Phytochrome Sensory Domain Permits Receptor Activation by Red Light. *Angew. Chem. Int. Ed.* **55**, 6339-6342, doi:10.1002/anie.201601736 (2016).

130 Hopkins, S. L. *et al.* An in vitro cell irradiation protocol for testing photopharmaceuticals and the effect of blue, green, and red light on human cancer cell lines. *Photochem. Photobiol. Sci.* **15**, 644-653, doi:10.1039/c5pp00424a (2016).
131 Rogozhnikov, D., O'Brien, P. J., Elahipanah, S. & Yousaf, M. N. Scaffold Free Bio-orthogonal Assembly of 3-Dimensional Cardiac Tissue via Cell Surface Engineering. *Sci. Rep.* **6**, 39806, doi:10.1038/srep39806 (2016).
132 Schenk, F. C., Boehm, H., Spatz, J. P. & Wegner, S. V. Dual-functionalized nanostructured biointerfaces by click chemistry. *Langmuir* **30**, 6897-6905, doi:10.1021/la500766t (2014).
133 Niopek, D., Wehler, P., Roensch, J., Eils, R. & Di Ventura, B. Optogenetic control of nuclear protein export. *Nat. Commun.* **7**, 10624, doi:10.1038/ncomms10624 (2016).
134 Li, Y. *et al.* Patterning of proteins into nanostripes on Si-wafer over large areas: a combination of Langmuir–Blodgett patterning and orthogonal surface chemistry. *Soft Matter* **7**, 861-863, doi:10.1039/c0sm00994f (2011).
135 Luo, Y., Knuckley, B., Bhatia, M., Pellechia, P. J. & Thompson, P. R. Activity-based protein profiling reagents for protein arginine deiminase 4 (PAD4): synthesis and in vitro evaluation of a fluorescently labeled probe. *J. Am. Chem. Soc.* **128**, 14468-14469, doi:10.1021/ja0656907 (2006).
136 Okumoto, S. *et al.* Detection of glutamate release from neurons by genetically encoded surface-displayed FRET nanosensors. *Proc. Natl. Acad. Sci. USA* **102**, 8740-8745, doi:10.1073/pnas.0503274102 (2005).
137 Howarth, M., Takao, K., Hayashi, Y. & Ting, A. Y. Targeting quantum dots to surface proteins in living cells with biotin ligase. *Proc. Natl. Acad. Sci. USA* **102**, 7583-7588, doi:10.1073/pnas.0503125102 (2005).

Chapter 6

Appendix

6. Appendix

6.1 DNA and aminoacid sequences of cloned constructs

6.1.1 pDisplay-CRY2-mCherry

DNA sequence:

Ig-κ leader sequence-HA-SacII-CRY2-mCherry-SalI-myc epitope-TM domain

ATGGAGACAGACACACTCCTGCTATGGGTACTGCTGCTCTGGGTTCCAGGTTCCACTGGTGA
CTATCCATATGATGTTCCAGATTATGCTGGGGCCCAGCCGGCCAGATCTCCCGGGATCCGCG
GAATGAAGATGGACAAAAAGACTATAGTTTTGTTTAGAAGAGACCTAAGGATTGAGGATAA
TCCTGCATTAGCAGCAGCTGCTCACGAAGGATCTGTTTTTCCTGTCTTCATTTGGTGTCCTGA
AGAAGAAGGACAGTTTTATCCTGGAAGAGCTTCAAGATGGTGGATGAAACAATCACTTGCT
CACTTATCTCAATCCTTGAAGGCTCTTGGATCTGACCTCACTTTAATCAAAACCCACAACACG
ATTTCAGCGATCTTGGATTGTATCCGCGTTACCGGTGCTACAAAAGTCGTCTTTAACCACCTC
TATGATCCTGTTTCGTTAGTTCGGGACCATACCGTAAAGGAGAAGCTGGTGGAACGTGGGA
TCTCTGTGCAAAGCTACAATGGAGATCTATTGTATGAACCGTGGGAGATATACTGCGAAAAG
GGCAAACCTTTTACGAGTTTCAATTCTTACTGGAAGAAATGCTTAGATATGTCGATTGAATCC
GTTATGCTTCCTCCTCCTTGGCGGTTGATGCCAATAACTGCAGCGGCTGAAGCGATTTGGGC
GTGTTCGATTGAAGAACTAGGGCTGGAGAATGAGGCCGAGAAACCGAGCAATGCGTTGTTA
ACTAGAGCTTGGTCTCCAGGATGGAGCAATGCTGATAAGTTACTAAATGAGTTCATCGAGAA
GCAGTTGATAGATTATGCAAAGAACAGCAAGAAAAGTTGTTGGGAATTCTACTTCACTACTT
TCTCCGTATCTCCATTTCGGGGAAATAAGCGTCAGACACGTTTTCCAGTGTGCCCGGATGAA
ACAAATTATATGGGCAAGAGATAAGAACAGTGAAGGAGAAGAAAGTGCAGATCTTTTTCTT
AGGGGAATCGGTTTAAGAGAGTATTCTCGGTATATATGTTTCAACTTCCCGTTTACTCACGAG
CAATCGTTGTTGAGTCATCTTCGGTTTTTCCCTTGGGATGCTGATGTTGATAAGTTCAAGGCC
TGGAGACAAGGCAGGACCGGTTATCCGTTGGTGGATGCCGGAATGAGAGAGCTTTGGGCT
ACCGGATGGATGCATAACAGAATAAGAGTGATTGTTTCAAGCTTTGCTGTGAAAGTTTCTTC
TCCTTCCATGGAAATGGGGAATGAAGTATTTCTGGGATACACTTTTGGATGCTGATTTGGAA
TGTGACATCCTTGGCTGGCAGTATATCTCTGGGAGTATCCCCGATGGCCACGAGCTTGATCG
CTTGGACAATCCCGCGTTACAAGGCGCCAAATATGACCCAGAAGGTGAGTACATAAGGCAA
TGGCTTCCCGAGCTTGCGAGATTGCCAACTGAATGGATCCATCATCCATGGACGCTCCTTTAA
CCGTACTCAAAGCTTCTGGTGTGGAACTCGGAACAAACTATGCGAAACCCATTGTAGACATC

GACACAGCTCGTGAGCTACTAGCTAAAGCTATTTCAAGAACCCGTGAAGCACAGATCATGAT
CGGAGCAGCACCTGATGAGATTGTAGCAGATAGCTTCGAGGCCTTAGGGGCTAATACCATT
ACCGAACCTGGTCTTTGCCCATCTGTGTCTTCTAATGACCAACAAGTACCTTCGGCTGTTCGT
TACAACGGGTCAGCGGCAGTGAAACCTGAGGAAGAAGAAGAGAGAGACATGAAGAAATCT
AGGGGATTCGATGAAAGGGAGTTGTTTTCGACTGCTGAATCTTCTTCTTCTTCGAGTGTGTTT
TTCGTTTCGCAGTCTTGCTCGTTGGCATCAGAAGGGAAGAATCTGGAAGGTATTCAAGATTC
ATCTGATCAGATTACTACAAGTTTGGGAAAAAATGGTTGCAAAGCCCGGGATCCACCGGTCG
CCACCATGGTGAGCAAGGGCGAGGAGGATAACATGGCCATCATCAAGGAGTTCATGCGCTT
CAAGGTGCACATGGAGGGCTCCGTGAACGGCCACGAGTTCGAGATCGAGGGCGAGGGCGA
GGGCCGCCCCTACGAGGGCACCCAGACCGCCAAGCTGAAGGTGACCAAGGGTGGCCCCCT
GCCCTTCGCCTGGGACATCCTGTCCCCTCAGTTCATGTACGGCTCCAAGGCCTACGTGAAGC
ACCCCGCCGACATCCCCGACTACTTGAAGCTGTCCTTCCCCGAGGGCTTCAAGTGGGAGCGC
GTGATGAACTTCGAGGACGGCGGCGTGGTGACCGTGACCCAGGACTCCTCCCTGCAGGACG
GCGAGTTCATCTACAAGGTGAAGCTGCGCGGCACCAACTTCCCCTCCGACGGCCCCGTAATG
CAGAAGAAGACCATGGGCTGGGAGGCCTCCTCCGAGCGGATGTACCCCGAGGACGGCGCC
CTGAAGGGCGAGATCAAGCAGAGGCTGAAGCTGAAGGACGGCGGCCACTACGACGCTGAG
GTCAAGACCACCTACAAGGCCAAGAAGCCCGTGCAGCTGCCCGGCGCCTACAACGTCAACA
TCAAGTTGGACATCACCTCCCACAACGAGGACTACACCATCGTGGAACAGTACGAACGCGCC
GAGGGCCGCCACTCCACCGGCGGCATGGACGAGCTGTACAAGGTCGACGAACAAAAACTCA
TCTCAGAAGAGGATCTGAATGCTGTGGGCCAGGACACGCAGGAGGTCATCGTGGTGCCACA
CTCCTTGCCCTTTAAGGTGGTGGTGATCTCAGCCATCCTGGCCCTGGTGGTGCTCACCATCAT
CTCCCTTATCATCCTCATCATGCTTTGGCAGAAGAAGCCACGTTAG

Aminoacid sequence: Ig-κ leader sequence-HA-CRY2-mCherry-myc epitope-TM domain

Met E T D T L L L W V L L L W V P G S T G D Y P Y D V P D Y A G A Q P A R S P G I R G M
K M D K K T I V W F R R D L R I E D N P A L A A A A H E G S V F P V F I W C P E E E G Q F
Y P G R A S R W W M K Q S L A H L S Q S L K A L G S D L T L I K T H N T I S A I L D C I R V
T G A T K V V F N H L Y D P V S L V R D H T V K E K L V E R G I S V Q S Y N G D L L Y E P W
E I Y C E K G K P F T S F N S Y W K K C L D M S I E S V M L P P P W R L M P I T A A A E A I
W A C S I E E L G L E N E A E K P S N A L L T R A W S P G W S N A D K L L N E F I E K Q L I
D Y A K N S K K V V G N S T S L L S P Y L H F G E I S V R H V F Q C A R M K Q I I W A R D K

N S E G E E S A D L F L R G I G L R E Y S R Y I C F N F P F T H E Q S L L S H L R F F P W D A

D V D K F K A W R Q G R T G Y P L V D A G M R E L W A T G W M H N R I R V I V S S F A

V K F L L L P W K W G M K Y F W D T L L D A D L E C D I L G W Q Y I S G S I P D G H E L D

R L D N P A L Q G A K Y D P E G E Y I R Q W L P E L A R L P T E W I H H P W D A P L T V L

K A S G V E L G T N Y A K P I V D I D T A R E L L A K A I S R T R E A Q I M I G A A P D E I V

A D S F E A L G A N T I K E P G L C P S V S S N D Q Q V P S A V R Y N G S A A V K P E E E E

E R D M K K S R G F D E R E L F S T A E S S S S S S V F F V S Q S C S L A S E G K N L E G I Q

D S S D Q I T T S L G K N G C K A R D P P V A T M V S K G E E D N M A I I K E F M R F K V

H M E G S V N G H E F E I E G E G E G R P Y E G T Q T A K L K V T K G G P L P F A W D I L

S P Q F M Y G S K A Y V K H P A D I P D Y L K L S F P E G F K W E R V M N F E D G G V V T

V T Q D S S L Q D G E F I Y K V K L R G T N F P S D G P V M Q K K T M G W E A S S E R M

Y P E D G A L K G E I K Q R L K L K D G G H Y D A E V K T T Y K A K K P V Q L P G A Y N V

N I K L D I T S H N E D Y T I V E Q Y E R A E G R H S T G G M D E L Y K V D E Q K L I S E E

D L N A V G Q D T Q E V I V V P H S L P F K V V V I S A I L A L V V L T I I S L I I L I M L W Q

K K P R –

6.1.2 pDisplay-CIBN-GFP

DNA sequence:

Ig-κ leader sequence-HA-SalI-CIBN-GFP-XmaI-myc epitope-TM domain

ATGGAGACAGACACACTCCTGCTATGGGTACTGCTGCTCTGGGTTCCAGGTTCCACTGGTGA

CTATCCATATGATGTTCCAGATTATGCTGGGGCCCAGCCGGCCAGATCTCCCGGGATGAATG

GAGCTATAGGAGGTGACCTTTTGCTCAATTTTCCTGACATGTCGGTCCTAGAGCGCCAAAGG

GCTCACCTCAAGTACCTCAATCCCACCTTTGATTCTCCTCTCGCCGGCTTCTTTGCCGATTCTTC

AATGATTACCGGCGGCGAGATGGACAGCTATCTTTCGACTGCCGGTTTGAATCTTCCGATGA

TGTACGGTGAGACGACGGTGGAAGGTGATTCAAGACTCTCAATTTCGCCGGAAACGACGCT

TGGGACTGGAAATTTCAAGGCAGCGAAGTTTGATACAGAGACTAAGGATTGTAATGAGGCG

GCGAAGAAGATGACGATGAACAGAGATGACCTAGTAGAAGAAGGAGAAGAAGAGAAGTC

GAAAATAACAGAGCAAAACAATGGGAGCACAAAAAGCATCAAGAAGATGAAACACAAAGC

CAACGAAACAAGAGAACAATTTCTCTAATGATTCATCTAAAGTGACGAAGGAATTGGAGAA

AACGGATTATATTCATGTACCGGTCGCCACCATGGTGAGCAAGGGCGAGGAGCTGTTCACC

GGGGTGGTGCCCATCCTGGTCGAGCTGGACGGCGACGTAAACGGCCACAAGTTCAGCGTGT

CCGGCGAGGGCGAGGGCGATGCCACCTACGGCAAGCTGACCCTGAAGTTCATCTGCACCAC
CGGCAAGCTGCCCGTGCCCTGGCCCACCCTCGTGACCACCCTGACCTACGGCGTGCAGTGCT
TCAGCCGCTACCCCGACCACATGAAGCAGCACGACTTCTTCAAGTCCGCCATGCCCGAAGGC
TACGTCCAGGAGCGCACCATCTTCTTCAAGGACGACGGCAACTACAAGACCCGCGCCGAGG
TGAAGTTCGAGGGCGACACCCTGGTGAACCGCATCGAGCTGAAGGGCATCGACTTCAAGGA
GGACGGCAACATCCTGGGGCACAAGCTGGAGTACAACTACAACAGCCACAACGTCTATATC
ATGGCCGACAAGCAGAAGAACGGCATCAAGGTGAACTTCAAGATCCGCCACAACATCGAGG
ACGGCAGCGTGCAGCTCGCCGACCACTACCAGCAGAACACCCCCATCGGCGACGGCCCCGT
GCTGCTGCCCGACAACCACTACCTGAGCACCCAGTCCGCCCTGAGCAAAGACCCCAACGAGA
AGCGCGATCACATGGTCCTGCTGGAGTTCGTGACCGCCGCCGGGATCACTCTCGGCATGGA
CGAGCTGTATAAGGGTAAAAAGAAGAAAAAGAAGTCAAAGACAAGTGTAATTATGGTCGA
CGAACAAAAACTCATCTCAGAAGAGGATCTGAATGCTGTGGGCCAGGACACGCAGGAGGTC
ATCGTGGTGCCACACTCCTTGCCCTTTAAGGTGGTGGTGATCTCAGCCATCCTGGCCCTGGT
GGTGCTCACCATCATCTCCCTTATCATCCTCATCATGCTTTGGCAGAAGAAGCCACGTTAG

Aminoacid sequence: Ig-κ leader sequence-HA-CIBN-GFP-myc epitope-TM domain

M E T D T L L L W V L L L W V P G S T G D Y P Y D V P D Y A G A Q P A R S P G M N G A I
G G D L L L N F P D M S V L E R Q R A H L K Y L N P T F D S P L A G F F A D S S M I T G G
E M D S Y L S T A G L N L P M M Y G E T T V E G D S R L S I S P E T T L G T G N F K A A K F
D T E T K D C N E A A K K M T M N R D D L V E E G E E E K S K I T E Q N N G S T K S I K K
M K H K A K K E E N N F S N D S S K V T K E L E K T D Y I H V P V A T M V S K G E E L F T
G V V P I L V E L D G D V N G H K F S V S G E G E G D A T Y G K L T L K F I C T T G K L P V
P W P T L V T T L T Y G V Q C F S R Y P D H M K Q H D F F K S A M P E G Y V Q E R T I F F
K D D G N Y K T R A E V K F E G D T L V N R I E L K G I D F K E D G N I L G H K L E Y N Y N
S H N V Y I MA D K Q K N G I K V N F K I R H N I E D G S V Q L A D H Y Q Q N T P I G D G
P V L L P D N H Y L S T Q S A L S K D P N E K R D H M V L L E F V T A A G I T L G M D E L Y
K G K K K K K K S K T K C V I M V D E Q K L I S E E D L N A V G Q D T Q E V I V V P H S L P
F K V V V I S A I L A L V V L T I I S L I I L I M L W Q K K P R -

6.1.3 pDisplay-PhyB-YFP

DNA sequence:

Ig-κ leader sequence-HA-SacII-PhyB-PstI- linker-YFP-SalI-myc epitope-TM domain

ATGGAGACAGACACACTCCTGCTATGGGTACTGCTGCTCTGGGTTCCAGGTTCCACTGGTGA
CTATCCATATGATGTTCCAGATTATGCTGGGGCCCAGCCGGCCAGATCTCCCGGGATGGTTTC
CGGAGTCGGGGGTAGTGGCGGTGGCCGTGGCGGTGGCCGTGGCGGAGAAGAAGAACCGTCGTCAA
GTCACACTCCTAATAACCGAAGAGGAGGAGAACAAGCTCAATCGTCGGGAACGAAATCTCTCAGACC
AAGAAGCAACACTGAATCAATGAGCAAAGCAATTCAACAGTACACCGTCGACGCAAGACTCCACGCC
GTTTTCGAACAATCCGGCGAATCAGGGAAATCATTCGACTACTCACAATCACTCAAAACGACGACGTA
CGGTTCCTCTGTACCTGAGCAACAGATCACAGCTTATCTCTCTCGAATCCAGCGAGGTGGTTACATTCA
GCCTTTCGGATGTATGATCGCCGTCGATGAATCCAGTTTCCGGATCATCGGTTACAGTGAAAACGCCA
GAGAAATGTTAGGGATTATGCCTCAATCTGTTCCTACTCTTGAGAAACCTGAGATTCTAGCTATGGGA
ACTGATGTGAGATCTTTGTTCACTTCTTCGAGCTCGATTCTACTCGAGCGTGCTTTCGTTGCTCGAGAG
ATTACCTTGTTAAATCCGGTTTGGATCCATTCCAAGAATACTGGTAAACCGTTTTACGCCATTCTTCAT
AGGATTGATGTTGGTGTTGTTATTGATTTAGAGCCAGCTAGAACTGAAGATCCTGCGCTTTCTATTGC
TGGTGCTGTTCAATCGCAGAAACTCGCGGTTCGTGCGATTTCTCAGTTACAGGCTCTTCCTGGTGGAG
ATATTAAGCTTTTGTGTGACACTGTCGTGGAAAGTGTGAGGGACTTGACTGGTTATGATCGTGTTATG
GTTTATAAGTTTCATGAAGATGAGCATGGAGAAGTTGTAGCTGAGAGTAAACGAGATGATTTAGAGC
CTTATATTGGACTGCATTATCCTGCTACTGATATTCCTCAAGCGTCAAGGTTCTTGTTTAAGCAGAACC
GTGTCCGAATGATAGTAGATTGCAATGCCACACCTGTTCTTGTGGTCCAGGACGATAGGCTAACTCAG
TCTATGTGCTTGGTTGGTTCTACTCTTAGGGCTCCTCATGGTTGTCACTCTCAGTATATGGCTAACATG
GGATCTATTGCGTCTTTAGCAATGGCGGTTATAATCAATGGAAATGAAGATGATGGGAGCAATGTAG
CTAGTGGAAGAAGCTCGATGAGGCTTTGGGGTTTGGTTGTTTGCCATCACACTTCTTCTCGCTGCATA
CCGTTTCCGCTAAGGTATGCTTGTGAGTTTTTGATGCAGGCTTTCGGTTTACAGTTAAACATGGAATTG
CAGTTAGCTTTGCAAATGTCAGAGAAACGCGTTTTGAGAACGCAGACACTGTTATGTGATATGCTTCT
GCGTGACTCGCCTGCTGGAATTGTTACACAGAGTCCCAGTATCATGGACTTAGTGAAATGTGACGGT
GCAGCATTTCTTTACCACGGGAAGTATTACCCGTTGGGTGTTGCTCCTAGTGAAGTTCAGATAAAAGA
TGTTGTGGAGTGGTTGCTTGCGAATCATGCGGATTCAACCGGATTAAGCACTGATAGTTTAGGCGAT
GCGGGGTATCCCGGTGCAGCTGCGTTAGGGGATGCTGTGTGCGGTATGGCAGTTGCATATATCACAA
AAAGAGACTTTCTTTTTTGGTTTCGATCTCACACTGCGAAAGAAATCAAATGGGGAGGCGCTAAGCAT
CATCCGGAGGATAAAGATGATGGGCAACGAATGCATCCTCGTTCGTCCTTTCAGGCTTTTCTTGAAGT
TGTTAAGAGCCGGAGTCAGCCATGGGAAACTGCGGAAATGGATGCGATTCACTCGCTCCAGCTTATT
CTGAGAGACTCTTTTAAAGAATCTGAGGCGGCTATGSACTCTAAAGTTGTGGATGGTGTGGTTCAGCC

ATGTAGGGATATGGCGGGGGAACAGGGGATTGATGAGTTAGGTGCAGTTGCAAGAGAGATGGTTA
GGCTCATTGAGACTGCAACTGTTCCTATATTCGCTGTGGATGCCGGAGGCTGCATCAATGGATGGAA
CGCTAAGATTGCAGAGTTGACAGGTCTCTCAGTTGAAGAAGCTATGGGGAAGTCTCTGGTTTCTGATT
TAATATACAAAGAGAATGAAGCAACTGTCAATAAGCTTCTTTCTCGTGCTTTGAGAGGGGACGAGGA
AAAGAATGTGGAGGTTAAGCTGAAAACTTTCAGCCCCGAACTACAAGGGAAAGCAGTTTTTGTGGTT
GTGAATGCTTGTTCCAGCAAGGACTACTTGAACAACATTGTCGGCGTTTGTTTTGTTGGACAAGACGT
TACTAGTCAGAAAATCGTAATGGATAAGTTCATCAACATACAAGGAGATTACAAGGTATTGTACATAG
CCCAAACCCTCTAATCCCGCCAATTTTTGCTCCTGACGAGAACACGTGCTGCCTGGAATGGAACATGG
CGATGGAAAAGCTTACGGGTTGGTCTCGCAGTGAAGTGATTGGGAAAATGATTGTCGGGGAAGTGT
TTGGGAGCTGTTGCATGCTAAAGGGTCCTGATGCTTTAACCAAGTTCATGATTGTATTGCATAATGCG
ATTGGTGGCCAAGATACGGATAAGTTCCCTTTCCCATTCTTTGACCGCAATGGGAAGTTTGTTCAGGC
TCTATTGACTGCAAACAAGCGGGTTAGCCTCGAGGGAAAGGTTATTGGGGCTTTCTGTTTCTTGCAAA
TCCCGAGCCCGCGGAGTGCTGGTGCAGTGAGCAAGGGCGAGGAGCTGTTCACCGGGGTGGT
GCCCATCCTGGTCGAGCTGGACGGCGACGTAAACGGCCACAAGTTCAGCGTGTCCGGCGAG
GGCGAGGGCGATGCCACCTACGGCAAGCTGACCCTGAAGTTCATCTGCACCACCGGCAAGC
TGCCCGTGCCCTGGCCCACCCTCGTGACCACCTTCGGCTACGGCCTGCAGTGCTTCGCCCGCT
ACCCCGACCACATGAAGCAGCACGACTTCTTCAAGTCCGCCATGCCCGAAGGCTACGTCCAG
GAGCGCACCATCTTCTTCAAGGACGACGGCAACTACAAGACCCGCGCCGAGGTGAAGTTCG
AGGGCGACACCCTGGTGAACCGCATCGAGCTGAAGGGCATCGACTTCAAGGAGGACGGCA
ACATCCTGGGGCACAAGCTGGAGTACAACTACAACAGCCACAACGTCTATATCATGGCCGAC
AAGCAGAAGAACGGCATCAAGGTGAACTTCAAGATCCGCCACAACATCGAGGACGGCAGC
GTGCAGCTCGCCGACCACTACCAGCAGAACACCCCCATCGGCGACGGCCCCGTGCTGCTGCC
CGACAACCACTACCTGAGCTACCAGTCCGCCCTGAGCAAAGACCCCAACGAGAAGCGCGAT
CACATGGTCCTGCTGGAGTTCGTGACCGCCGCCGGGATCACTCTCGGCATGGACGAGCTGCT
GCAGGTCGACGAACAAAAACTCATCTCAGAAGAGGATCTGAATGCTGTGGGCCAGGACACG
CAGGAGGTCATCGTGGTGCCACACTCCTTGCCCTTTAAGGTGGTGGTGATCTCAGCCATCCT
GGCCCTGGTGGTGCTCACCATCATCTCCCTTATCATCCTCATCATGCTTTGGCAGAAGAAGCC
ACGTTAG

Aminoacid sequence: Ig-κ leader sequence-PhyB-YFP-myc epitope-TM domain

M E T D T L L L W V L L L W V P G S T G D Y P Y D V P D Y A G A Q P A R S P G M V S G V
G G S G G G R G G G R G G E E E P S S S H T P N N R R G G E Q A Q S S G T K S L R P R S
N T E S M S K A I Q Q Y T V D A R L H A V F E Q S G E S G K S F D Y S Q S L K T T T Y G S S

VPEQQITAYLSRIQRGGYIQPFGCMIAVDESSFRIIGYSENARE MLG
IMPQSVPTLEKPEILAMGTDVRSLFTSSSSILLERAFVAREITLLNPV
WIHSKNTGKPFYAILHRIDVGVVIDLEPARTEDPALSIAGAVQSQKL
AVRAISQLQALPGGDIKLLCDTVVESVRDLTGYDRVMVYKFHEDEH
GEVVAESKRDDLEPYIGLHYPATDIPQASRFLFKQNRVRMIVDCNA
TPVLVVQDDRLTQSMCLVGSTLRAPHGCHSQYMANMGSIASLAM
AVIINGNEDDGSNVASGRSSMRLWGLVVCHHTSSRCIPFPLRYAC
EFLMQAFGLQLNMELQLALQMSEKRVLRTQTLLCDMLLRDSPAGI
VTQSPSIMDLVKCDGAAFLYHGKYYPLGVAPSEVQIKDVVEWLLA
NHADSTGLSTDSLGDAGYPGAAALGDAVCGMAVAYITKRDFLFWF
RSHTAKEIKWGGAKHHPEDKDDGQRMHPRSSFQAFLEVVKSRSQ
PWETAEMDAIHSLQLILRDSFKESEAAMNSKVVDGVVQPCRDMA
GEQGIDELGAVAREMVRLIETATVPIFAVDAGGCINGWNAKIAELT
GLSVEEAMGKSLVSDLIYKENEATVNKLLSRALRGDEEKNVEVKLK
TFSPELQGKAVFVVVNACSSKDYLNNIVGVCFVGQDVTSQKIVMD
KFINIQGDYKAIVHSPNPLIPPIFAADENTCCLEWNMAMEKLTGW
SRSEVIGKMIVGEVFGSCCMLKGPDALTKFMIVLHNAIGGQDTDK
FPFPFFDRNGKFVQALLTANKRVSLEGKVIGAFCFLQIPSPRSAGA
VSKGEELFTGVVPILVELDGDVNGHKFSVSGEGEGDATYGKLTLKF
ICTTGKLPVPWPTLVTTFGYGLQCFARYPDHMKQHDFFKSAMPEG
YVQERTIFFKDDGNYKTRAEVKFEGDTLVNRIELKGIDFKEDGNILG
HKLEYNYNSHNVYIMADKQKNGIKVNFKIRHNIEDGSVQLADHYQ
QNTPIGDGPVLLPDNHYLSYQSALSKDPNEKRDHMVLLEFVTAAGI
TLGMDELLQVDEQKLISEEDLNAVGQDTQEVIVVPHSLPFKVVVIS
AILALVVLTIISLIILIMLWQKKPR–

6.1.4 pDisplay-PIF6-CFP

DNA sequence:

Ig-κ leader sequence-HA-BglII-PIF6-AscI-CFP-myc epitope-TM domain

ATGGAGACAGACACACTCCTGCTATGGGTACTGCTGCTCTGGGTTCCAGGTTCCACTGGTGA
CTATCCATATGATGTTCCAGATTATGCTGGGGCCCAGCCGGCCAGATCTATGATGTTCTTACC
AACCGATTATTGTTGCAGGTTAAGCGATCAAGAGTATATGGAGCTTGTGTTTGAGAATGGCC
AGATTCTTGCAAAGGGCCAAAGATCCAACGTTTCTCTGCATAATCAACGTACCAAATCGATC
ATGGATTTGTATGAGGCAGAGTATAACGAGGATTTCATGAAGAGTATCATCCATGGTGGTG
GTGGTGCCATCACAAATCTCGGGGACACGCAGGTTGTTCCACAAAGTCATGTTGCTGCTGCC
CATGAAACAAACATGTTGGAAAGCAATAAACATGTTGACGGCGCGCCGATGGTGAGCAAGG
GCGAGGAGCTGTTCACCGGGGTGGTGCCCATCCTGGTCGAGCTGGACGGCGACGTAAACG
GCCACAAGTTCAGCGTGTCCGGCGAGGGCGAGGGCGATGCCACCTACGGCAAGCTGACCCT
GAAGTTCATCTGCACCACCGGCAAGCTGCCCGTGCCCTGGCCCACCCTGGTGACCACCCTGA
CCTGGGGCGTGCAGTGCTTCAGCCGCTACCCCGACCACATGAAGCAGCACGACTTCTTCAAG
TCCGCCATGCCCGAAGGCTACGTCCAGGAGCGCACCATCTTCTTCAAGGACGACGGCAACTA
CAAGACCCGCGCCGAGGTGAAGTTCGAGGGCGACACCCTGGTGAACCGCATCGAGCTGAA
GGGCATCGACTTCAAGGAGGACGGCAACATCCTGGGGCACAAGCTGGAGTACAACTACATC
AGCCACAACGTCTATATCACCGCCGACAAGCAGAAGAACGGCATCAAGGCCAACTTCAAGA
TCCGCCACAACATCGAGGACGGCAGCGTGCAGCTCGCCGACCACTACCAGCAGAACACCCC
CATCGGCGACGGCCCCGTGCTGCTGCCCGACAACCACTACCTGAGCACCCAGTCCGCCCTGA
GCAAAGACCCCAACGAGAAGCGCGATCACATGGTCCTGCTGGAGTTCGTGACCGCCGCCGG
GATCACTCTCGGCATGGACGAGCTGTACAAGCGGCCGCGGCTGCAGGTCGACGAACAAAAC
TCATCTCAGAAGAGGATCTGAATGCTGTGGGCCAGGACACGCAGGAGGTCATCGTGGTGCC
ACACTCCTTGCCCTTTAAGGTGGTGGTGATCTCAGCCATCCTGGCCCTGGTGGTGCTCACCAT
CATCTCCCTTATCATCCTCATCATGCTTTGGCAGAAGAAGCCACGTTAG

Aminoacid sequence: Ig-κ leader sequence-HA-PIF6-CFP-myc epitope-TM domain

METDTLLLWVLLLWVPGSTGDYPYDVPDYAGAQPARSMMFLPTDYCCRLSDQEYMELVFENG
QILAKGQRSNVSLHNQRTKSIMDLYEAEYNEDFMKSIIHGGGGAITNLGDTQVVPQSHVAAAHE
TNMLESNKHVDGAPMVSKGEELFTGVVPILVELDGDVNGHKFSVSGEGEGDATYGKLTLKFICT
TGKLPVPWPTLVTTLTWGVQCFSRYPDHMKQHDFFKSAMPEGYVQERTIFFKDDGNYKTRAEV

KFEGDTLVNRIELKGIDFKEDGNILGHKLEYNYISHNVYITADKQKNGIKANFKIRHNIEDGSVQLA
DHYQQNTPIGDGPVLLPDNHYLSTQSALSKDPNEKRDHMVLLEFVTAAGITLGMDELYKRPRLQ
VDEQKLISEEDLNAVGQDTQEVIVVPHSLPFKVVVISAILALVVLTIISLIILIMLWQKKPR-

6.1.5 pET21b-CIBN-GFP

DNA sequence: NdeI- CIBN-GFP-XhoI-His_6

CATATGATGAATGGAGCTATAGGAGGTGACCTTTTGCTCAATTTTCCTGACATGTCGGTCCTA
GAGCGCCAAAGGGCTCACCTCAAGTACCTCAATCCCACCTTTGATTCTCCTCTCGCCGGCTTC
TTTGCCGATTCTTCAATGATTACCGGCGGCGAGATGGACAGCTATCTTTCGACTGCCGGTTTG
AATCTTCCGATGATGTACGGTGAGACGACGGTGGAAGGTGATTCAAGACTCTCAATTTCGCC
GGAAACGACGCTTGGGACTGGAAATTTCAAGGCAGCGAAGTTTGATACAGAGACTAAGGAT
TGTAATGAGGCGGCGAAGAAGATGACGATGAACAGAGATGACCTAGTAGAAGAAGGAGAA
GAAGAGAAGTCGAAAATAACAGAGCAAAACAATGGGAGCACAAAAAGCATCAAGAAGATG
AAACACAAAGCCAACGAAACAAGAGAACAATTTCTCTAATGATTCATCTAAAGTGACGAAG
GAATTGGAGAAAACGGATTATATTCATGTACCGGTCGCCACCATGGTGAGCAAGGGCGAGG
AGCTGTTCACCGGGGTGGTGCCCATCCTGGTCGAGCTGGACGGCGACGTAAACGGCCACAA
GTTCAGCGTGTCCGGCGAGGGCGAGGGCGATGCCACCTACGGCAAGCTGACCCTGAAGTTC
ATCTGCACCACCGGCAAGCTGCCCGTGCCCTGGCCCACCCTCGTGACCACCCTGACCTACGG
CGTGCAGTGCTTCAGCCGCTACCCCGACCACATGAAGCAGCACGACTTCTTCAAGTCCGCCA
TGCCCGAAGGCTACGTCCAGGAGCGCACCATCTTCTTCAAGGACGACGGCAACTACAAGAC
CCGCGCCGAGGTGAAGTTCGAGGGCGACACCCTGGTGAACCGCATCGAGCTGAAGGGCAT
CGACTTCAAGGAGGACGGCAACATCCTGGGGCACAAGCTGGAGTACAACTACAACAGCCAC
AACGTCTATATCATGGCCGACAAGCAGAAGAACGGCATCAAGGTGAACTTCAAGATCCGCC
ACAACATCGAGGACGGCAGCGTGCAGCTCGCCGACCACTACCAGCAGAACACCCCCATCGG
CGACGGCCCCGTGCTGCTGCCCGACAACCACTACCTGAGCACCCAGTCCGCCCTGAGCAAAG
ACCCCAACGAGAAGCGCGATCACATGGTCCTGCTGGAGTTCGTGACCGCCGCCGGGATCAC
TCTCGGCATGGACGAGCTGTATAAGGGTAAAAAGAAGAAAAAGAAGTCAAAGACAAGTGT
AATTATGCTCGAGCACCACCACCACCACCACTGA

Aminoacid sequence: NdeI-CIBN-GFP-XhoI-His_6

H M M N G A I G G D L L L N F P D M S V L E R Q R A H L K Y L N P T F D S P L A G F F A D

S S M I T G G E M D S Y L S T A G L N L P M M M Y G E T T V E G D S R L S I S P E T T L G T G

N F K A A K F D T E T K D C N E A A K K M T M N R D D L V E E G E E E K S K I T E Q N N G

S T K S I K K M K H K A K K E E N N F S N D S S K V T K E L E K T D Y I H V P V A T M V S K

G E E L F T G V V P I L V E L D G D V N G H K F S V S G E G E G D A T Y G K L T L K F I C T

T G K L P V P W P T L V T T L T Y G V Q C F S R Y P D H M K Q H D F F K S A M P E G Y V

Q E R T I F F K D D G N Y K T R A E V K F E G D T L V N R I E L K G I D F K E D G N I L G H K

L E Y N Y N S H N V Y I MA D K Q K N G I K V N F K I R H N I E D G S V Q L A D H Y Q Q N

T P I G D G P V L L P D N H Y L S T Q S A L S K D P N E K R D H M V L L E F V T A A G I T L

G M D E L Y K G K K K K K S K T K C V I L E H H H H H H –

6.1.6 pET21b-PIF6-CFP

DNA sequence: NdeI- PIF6-CFP-XhoI-His_6

CATATGATGATGTTCTTACCAACCGATTATTGTTGCAGGTTAAGCGATCAAGAGTATATGGA

GCTTGTGTTTGAGAATGGCCAGATTCTTGCAAAGGGCCAAAGATCCAACGTTTCTCTGCATA

ATCAACGTACCAAATCGATCATGGATTTGTATGAGGCAGAGTATAACGAGGATTTCATGAAG

AGTATCATCCATGGTGGTGGTGGTGCCATCACAAATCTCGGGGACACGCAGGTTGTTCCACA

AAGTCATGTTGCTGCTGCCCATGAAACAAACATGTTGGAAAGCAATAAACATGTTGACGGCG

CGCCGATGGTGAGCAAGGGCGAGGAGCTGTTCACCGGGGTGGTGCCCATCCTGGTCGAGC

TGGACGGCGACGTAAACGGCCACAAGTTCAGCGTGTCCGGCGAGGGCGAGGGCGATGCCA

CCTACGGCAAGCTGACCCTGAAGTTCATCTGCACCACCGGCAAGCTGCCCGTGCCCTGGCCC

ACCCTGGTGACCACCCTGACCTGGGGCGTGCAGTGCTTCAGCCGCTACCCCGACCACATGAA

GCAGCACGACTTCTTCAAGTCCGCCATGCCCGAAGGCTACGTCCAGGAGCGCACCATCTTCT

TCAAGGACGACGGCAACTACAAGACCCGCGCCGAGGTGAAGTTCGAGGGCGACACCCTGG

TGAACCGCATCGAGCTGAAGGGCATCGACTTCAAGGAGGACGGCAACATCCTGGGGCACAA

GCTGGAGTACAACTACATCAGCCACAACGTCTATATCACCGCCGACAAGCAGAAGAACGGC

ATCAAGGCCAACTTCAAGATCCGCCACAACATCGAGGACGGCAGCGTGCAGCTCGCCGACC

ACTACCAGCAGAACACCCCCATCGGCGACGGCCCCGTGCTGCTGCCCGACAACCACTACCTG

AGCACCCAGTCCGCCCTGAGCAAAGACCCCAACGAGAAGCGCGATCACATGGTCCTGCTGG

AGTTCGTGACCGCCGCCGGGATCACTCTCGGCATGGACGAGCTGTACAAGCTCGAGCACCA

CCACCACCACCACTGA

Aminoacid sequence: NdeI- PIF6-CFP-XhoI-His_6

HMMMFLPTDYCCRLSDQEYMELVFENGQILAKGQRSNVSLHNQRTKSIMDLYEAEYNEDFMK
SIIHGGGGAITNLGDTQVVPQSHVAAAHETNMLESNKHVDGAPMVSKGEELFTGVVPILVELDG
DVNGHKFSVSGEGEGDATYGKLTLKFICTTGKLPVPWPTLVTTLTWGVQCFSRYPDHMKQHDF
FKSAMPEGYVQERTIFFKDDGNYKTRAEVKFEGDTLVNRIELKGIDFKEDGNILGHKLEYNYISHN
VYITADKQKNGIKANFKIRHNIEDGSVQLADHYQQNTPIGDGPVLLPDNHYLSTQSALSKDPNEK
RDHMVLLEFVTAAGITLGMDELYK L EH H H H H H H –

7.1 Click reaction scheme

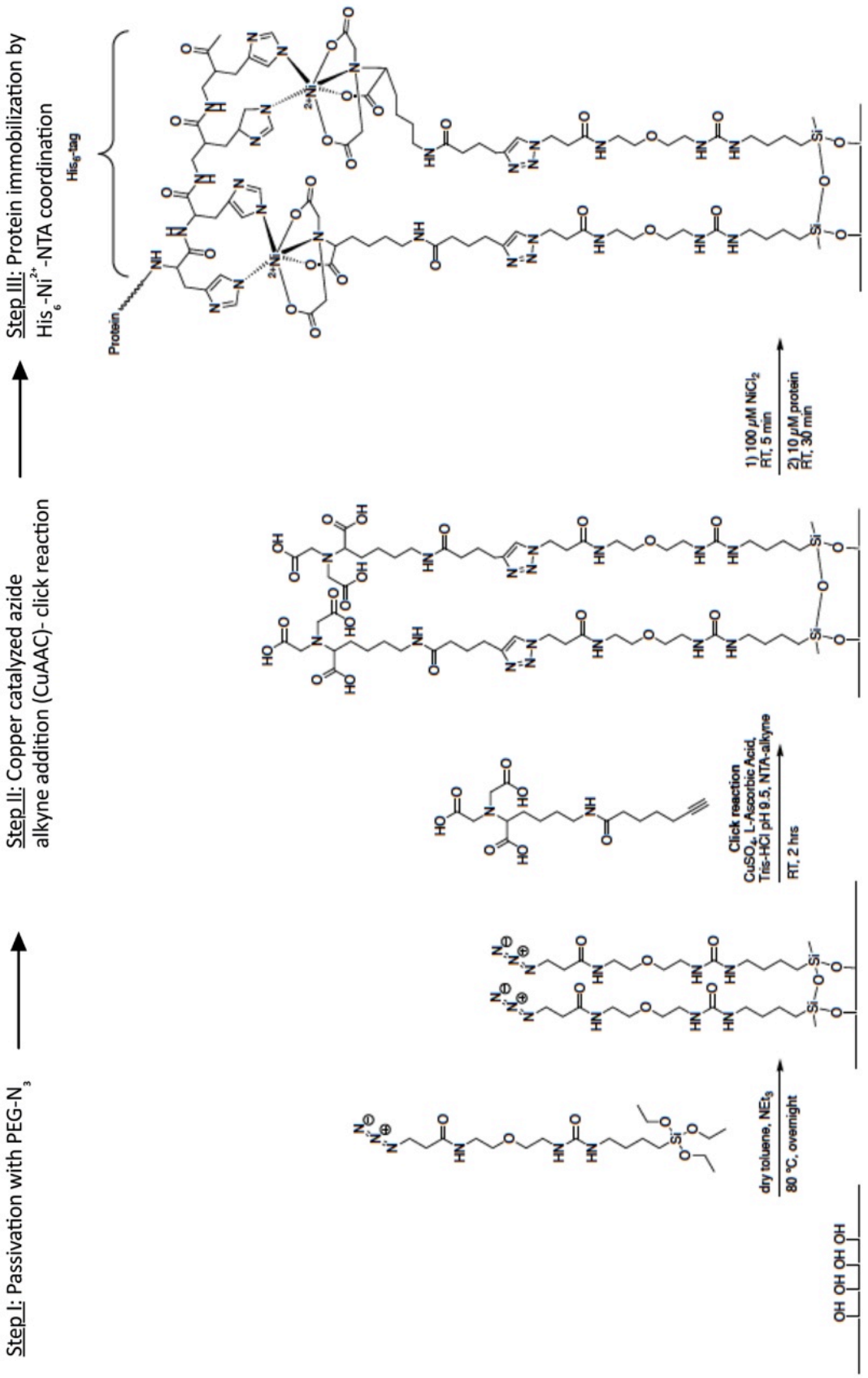

requires no external energy **(Figure 1.9)**.[32] The spontaneous organization in the self-assembling process occurs as a result of minimization of free energy by maximizing cell-cell contacts.[32]

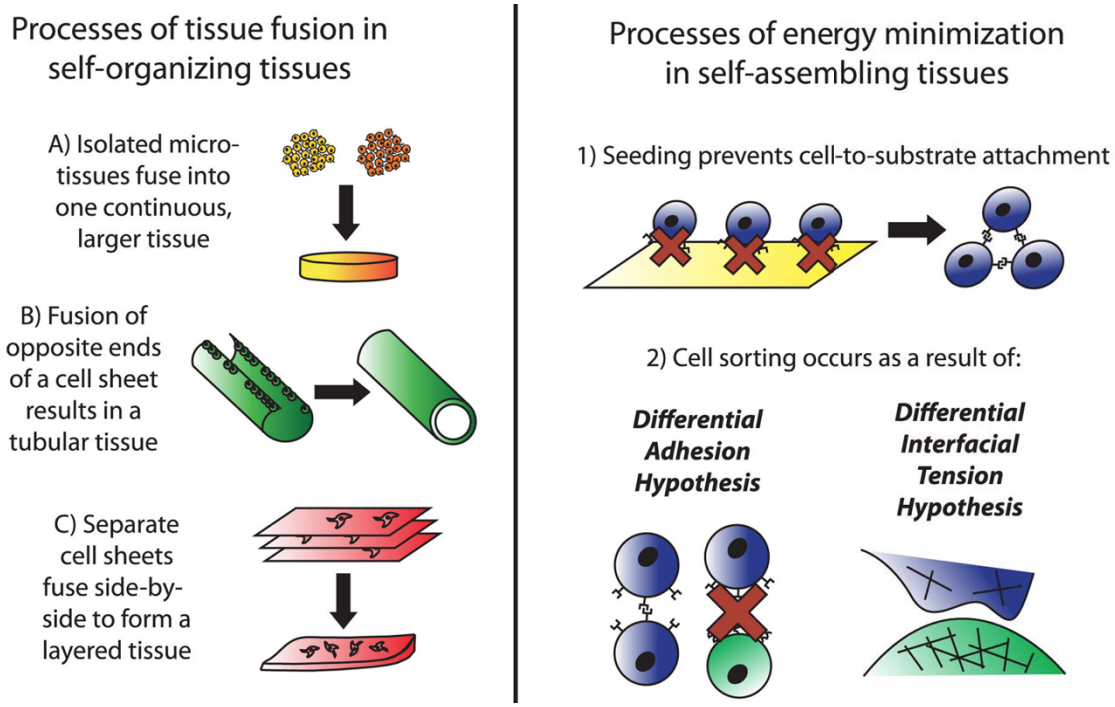

Figure 1.9 Self-organization and self-assembling processes in bottom-up tissue engineering. Tissue fusion takes place in both self-organizing and self-assembling processes. Tissue fusion includes cell-cell, cell-to-matrix and matrix-to-matrix contacts. Adapted from Athanasiou *et al*.[32]

Self-organization can be achieved by several techniques such as cell-encapsulating (or cell-laden) hydrogels (microgels), cell-sheet generation and cell printing **(Figure 1.8B)**.[32,35] Cell-laden hydrogels are used to create robust microtissues from the cells, which are not able to produce sufficient ECM. Commonly cells are embedded in photopolymerizable polymers such as polyethyleneglycol (PEG), temperature sensitive hydrogels or self-assembling peptide gels.[34] Cell-sheet technology involves the generation of sheets of cells under conditions that stimulate ECM production. Stacking these cell-sheets layer-by-layer leads to the formation of mechanically robust tissues.[34] In cell-printing technique, cells are deposited in small groups to engineer tissues with a variety of properties and geometries.[34]

Generation of cell aggregates is a self-assembly process. It involves use of a non-adherent substrate so that the cells will form aggregates or spheroids by minimizing the tissue free energy **(Figure 1.9)**.[32] This is achieved by maximizing cell-cell contacts,